

## **Historic, Archive Document**

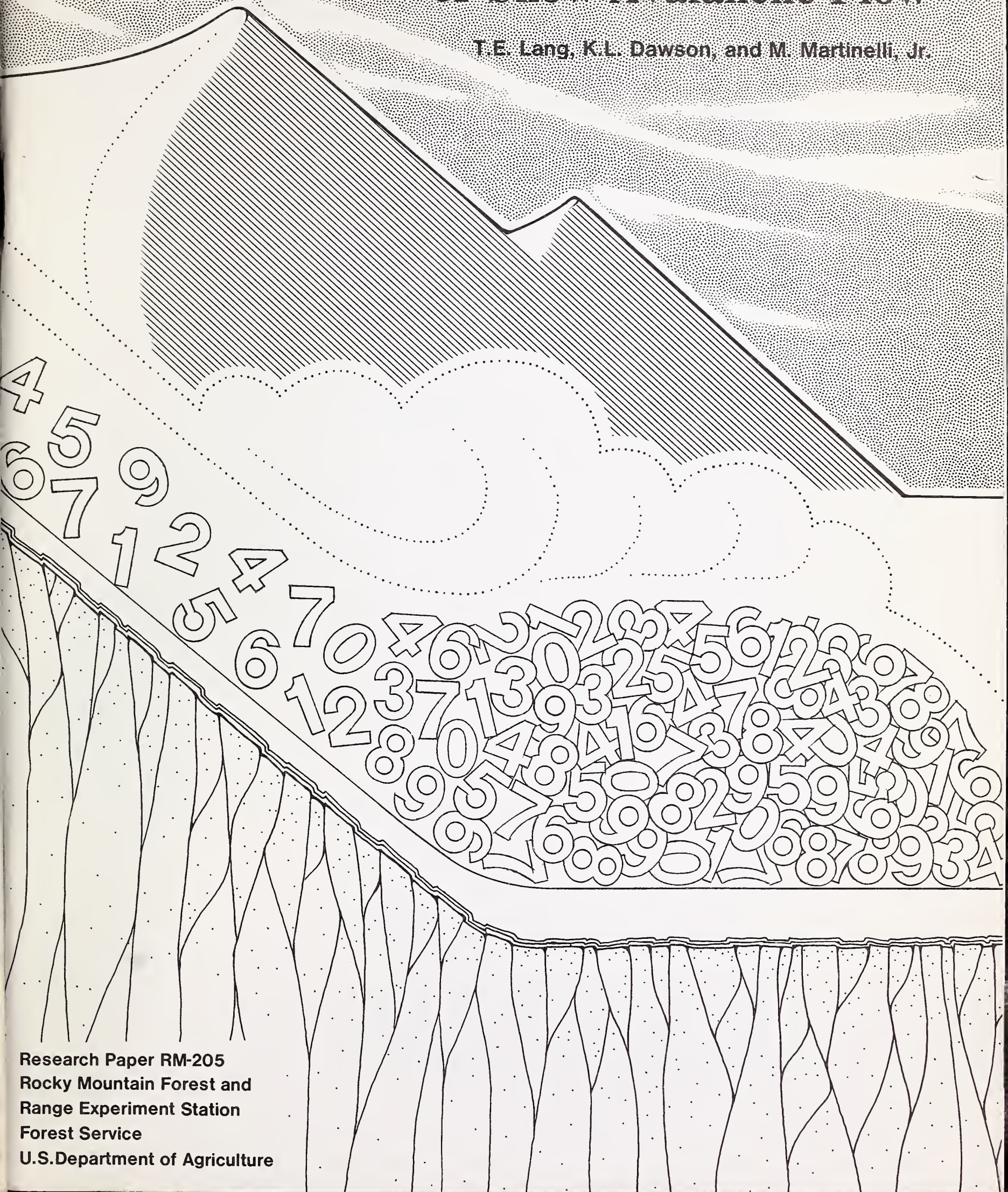
Do not assume content reflects current scientific knowledge, policies, or practices.



A99.9  
F76324  
cop. 2

# Numerical Simulation of Snow Avalanche Flow

T.E. Lang, K.L. Dawson, and M. Martinelli, Jr.



Research Paper RM-205  
Rocky Mountain Forest and  
Range Experiment Station  
Forest Service  
U.S. Department of Agriculture

### **Abstract**

A numerical, finite difference computer program based on the Navier-Stokes equations is modified to give avalanche runout distance, velocity of the leading edge of the avalanche and depth of debris in the runout zone. The program requires a longitudinal profile of the avalanche path, thickness of the snow in the starting zone, and two friction coefficients. Kinematic viscosity (or coefficient of internal friction) is expressed as an average for the entire avalanche path. Slope inclinations and coefficient of surface friction can be varied for every 10- to 20-m increment of the avalanche path. The program can be modified to allow for variable width of flow and for snow entrainment during flow. In test cases, the program predicted results consistent with observations for a number of avalanche events.

# **Numerical Simulation of Snow Avalanche Flow <sup>1</sup>**

**T.E. Lang, Professor  
Montana State University**

**K.L. Dawson, Graduate Student <sup>2</sup>  
Montana State University**

**M. Martinelli, Jr., Principal Meteorologist  
Rocky Mountain Forest and Range Experiment Station <sup>3</sup>**

<sup>1</sup> *This paper reports findings of research done under Cooperative Agreement 16-627CA between the USDA Forest Service and Montana State University.*

<sup>2</sup> *Dawson is now Research Engineer, Boeing Aircraft Company, Seattle, Wash.*

<sup>3</sup> *Central headquarters is maintained in Fort Collins, Colo. in cooperation with Colorado State University.*

## Contents

	Page
Management Implications.....	1
Introduction.....	1
Description of the Avalanche Computer Code.....	2
Basic Features of the SOLASURF Code .....	2
Modification of the SOLASURF Code .....	3
Characteristics of the Fluid Modeling Equations .....	6
Avalanche Models, and Evaluations Using Program	
AVALNCH.....	7
Intent of Case Studies .....	7
Ironton Park Avalanche Path.....	7
Pallavicini Avalanche Path.....	10
Hematite Gulch Avalanche Path.....	13
Stanley Avalanche Path .....	14
Number 3 East Avalanche off Max's Mountain,	
Alyeska Ski Area, Girdwood, Alaska .....	16
Imogene Avalanche Path.....	17
Numerical Studies with Program AVALNCH .....	19
Equilibrium Flow Calculation .....	19
Variable Width Option for Program AVALNCH.....	19
Sensitivity of Runout Distance to Various Parameters .....	22
Leading Edge Snow Entrainment Modeling.....	24
Discussion and Summary .....	25
Literature Cited .....	28
Appendices	
A — Input Data Format .....	29
B — FORTRAN Listing of AVALNCH .....	31
C — Listing of Output Data from AVALNCH for Ironton Park Avalanche .....	37
D — Listing of Program AVALNCH with Variable Width Option .....	45

# Numerical Simulation of Snow Avalanche Flow

T.E. Lang, K.L. Dawson, and M. Martinelli, Jr.

## Management Implications

Many homes, lodges, and other structures are now being built in steep, snow-covered areas of the western U.S. Snow avalanches are a threat at many of these sites. Land managers, county commissioners, and other local authorities need information on the location of avalanche paths and the frequency and intensity of avalanches to safeguard the public and still permit orderly growth of mountain communities.

Potential development sites should be examined and avalanche zoning maps prepared before land values and political pressures increase. To do this, a reliable and objective way is needed to predict the runout distance, impact force, and return interval of avalanches of various sizes on specific avalanche

paths. From these data, avalanche areas can be mapped on the basis of the "50-year" or "100-year" avalanche in the same way floodplains are mapped for the "100-year" flood.

This paper presents a new technique for estimating runout distance and debris depths for specific avalanche paths based on terrain and snow conditions. Impact forces and return intervals will not be discussed.

Numerous approaches to avalanche dynamics have been undertaken in the past, and new or modified approaches will undoubtedly continue to be developed to give better solutions to the complex problems associated with avalanche movement.

---

## Introduction

The prediction of runout distance is an important factor in establishing avalanche zoning restrictions in many mountain regions. An approximate, strongly empirical, hydrodynamic method for predicting runout distance developed by Voellmy (1964) has been used as a basis for avalanche zoning in Switzerland for several years. The method is based on uniform, open-channel-flow hydrodynamics, which relates flow velocity to channel slope and dimensions and to surface roughness. The condition of equilibrium flow restricts the application of this approach to slowly varying changes in the governing parameters. The two basic parameters appearing in the velocity equation are a turbulence coefficient and a surface friction coefficient. These parameters are varied to take into account surface friction, slope irregularity, object intrusions (e.g., trees and rock outcrops), flow depth changes, and other phenomena of the flow that are characteristic of avalanches. In general, avalanche dynamists agree that the successful application of Voellmy's equations requires a great deal of professional judgment which can only be gained by repeated use of the equations.

Recognizing the transient behavior of the flow, and the need to separate changes in path geometry from the flow parameters, a numerical approach appears to be a better way to represent actual avalanche

motion history than the open channel flow technique. The basic flow parameters can then be varied at each increment along the fluid path adding flexibility to the model. The Los Alamos Scientific Laboratory has considerable experience in transient flow using finite differencing of mass and momentum transfer equations (Amsden and Harlow 1970, Welch et al. 1966, Hirt, Nichols and Romero 1975). The recently reported simplified fluid dynamics code, SOLA, (Hirt, Nichols and Romero 1975) has the essential features needed to model avalanche flow. These include capability to represent a free surface geometry (SOLASURF), to incorporate nonzero fluid viscosity, and to model a varying lower boundary profile. Major questions that are not answerable from cases considered in the Los Alamos references include whether or not long-duration flow, such as in an avalanche, remains stable, and whether an avalanche can be economically modeled and analyzed. This paper examines these questions and modifies the SOLA code to permit the modeling of avalanche runout distance.

This report also describes in detail modifications to the SOLASURF code to adapt it to the avalanche runout problem. The modified code is then applied to a number of avalanche cases to establish bounds on the kinematic (internal) viscosity and the surface friction coefficient.

## Description of the Avalanche Computer Code

### Basic Features of the SOLASURF Code

The governing equations of motion incorporated in the SOLASURF code in finite difference form are the Navier-Stokes equations:

$$\frac{Du}{Dt} = g_x - \frac{1}{\rho} \frac{\partial p}{\partial x} + \nu \nabla^2 u \quad [1]$$

$$\frac{Dv}{Dt} = g_y - \frac{1}{\rho} \frac{\partial p}{\partial y} + \nu \nabla^2 v.$$

In equation [1],  $u$  and  $v$  are velocity components;  $g_x$  and  $g_y$  are gravity components;  $\rho$  is the density of the incompressible fluid and is combined with pressure,  $p$ , to become the actual term solved for in the code and referred to as "pressure;"  $\nu$  is the kinematic viscosity (or internal friction). The two linear operators of equation [1] are

$$\frac{D}{Dt} = \frac{\partial}{\partial t} + u \frac{\partial}{\partial x} + v \frac{\partial}{\partial y}$$

and

$$\nabla^2 = \frac{\partial^2}{\partial x^2} + \frac{\partial^2}{\partial y^2} \quad [2]$$

Additionally, we impose the condition of conservation of mass for an incompressible fluid given by

$$\frac{\partial u}{\partial x} + \frac{\partial v}{\partial y} = 0. \quad [3]$$

Consistent with the usual finite difference approach, the fluid domain is divided into a uniform grid of rectangular cells, surrounded by a single-cell thickness of boundary cells. The notations associated with the grid layout are shown in figure 1.

In the code  $IBAR^4$  and  $JBAR$  are the number of flow domain cells in the  $x$  and  $y$  directions, respectively, and  $IMAX$  and  $JMAX$  are the corresponding number of cells including the boundary cells. Five 2-dimensional arrays with the dimensions  $IMAX$  by  $JMAX$ , establish the major memory allocation. The arrays are the current velocity components  $u$  and  $v$ , the updated velocity components  $u_n$  and  $v_n$ , and the pressure,  $p$ , in each cell. Limiting the size of these arrays is the primary method of controlling running time on the computer.

<sup>4</sup>Names in capital letters refer to parameters used in the SOLASURF code.

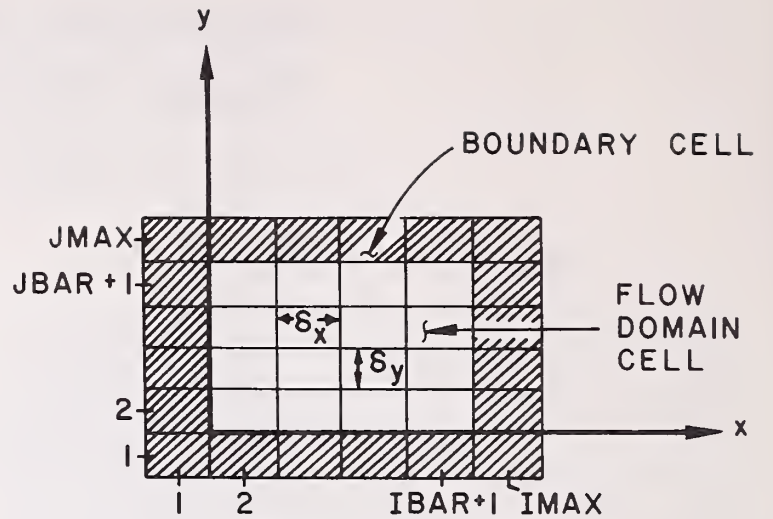


Figure 1.—Grid layout.

The algorithm starts with an initial distribution of fluid in the domain and computes a pressure and velocity distribution using a finite difference version of equation [1]. In general, the computed velocity components do not satisfy equation [3], so that small adjustments of cell pressure are required to achieve a zero-divergence condition to a prescribed level of accuracy controlled by parameters EPSI and DZRO (Hirt, Nichols and Romero 1975). The initial calculation of velocity and pressure using equation [1] is the start of a cycle (CYCLE) of calculations, and each small adjustment of parameters in one sweep of the cells is an iteration (ITER).

In the SOLASURF code, a choice between four types of boundary conditions is given for each boundary. In the modified version, a single type of boundary condition is imposed along each edge. The left wall, considered the crown face of the avalanche, is designated a rigid, slip-free boundary in the notation of Hirt, Nichols and Romero (1975). The right wall, which is placed beyond the runout terminus, is a continuative outflow boundary, as is the top boundary. The bottom boundary is modified from the rigid no-slip or free-slip options given in SOLASURF to model different friction conditions that might be encountered in an avalanche flow. Details of the various aspects of the modified program are given in the next section.

Output from SOLASURF includes two types of data, depending upon user preference. The more complete output at the end of an integral number of cycles, as controlled by the parameter CWPRT, is a listing of the velocity and pressure in each cell. At the end of cycles for which the complete printout is not requested, a single line is printed which includes the cycle number (CYCLE), number of iterations in that cycle (ITER), time increment (DELTA), total time into

flow (TIME), fluid volume (FVOL), maximum slope-parallel velocity in the flow (UMAX), leading edge slope-parallel velocity (UEDG), and cell number of the leading edge of the avalanche (LDEG).

An additional input parameter is TWFIN, which is the time estimate for the avalanche flow. Normally, this is set at a large value to be sure the complete avalanche flow is represented in a run. However, it may also be used to terminate computations, in which case an extended printout of the flow distribution is output.

Remaining input parameters needed for program execution are detailed in the next section, since they are associated directly with major modifications made to the code. A complete description and an example of the input data required are given in Appendix A.

The name adapted for the modified version of SOLASURF for the simulation of avalanche flow and runout distance is program AVALNCH, which will be used in subsequent references to the code.

The program is set up to use a specific set of units. All linear dimensions are expressed in meters, and time in seconds. Velocity has the units m/s; the pressure/density ratio has the units  $\text{m}^2/\text{s}^2$ ; the kinematic viscosity has units  $\text{m}^2/\text{s}$ , and acceleration due to gravity is set at  $9.80 \text{ m/s}^2$ .

### Modifications of the SOLASURF Code

There are several limitations to developing a numerical model for avalanche runout prediction. First, material properties must be expressed in nominal values, since point values of the properties as a function of slope, position and time are unknown. Second, the calculations should be low-cost, because computer and manpower resources are often limited. Third, representation of the flow should be simple and not require complex interpretation of parameter types and ranges. These three constraints have been met in the AVALNCH code with the imposition of several major modifications that are described below.

If a grid array, based upon the original requirements of SOLASURF, is fit to an avalanche slope profile, it appears as shown in figure 2. This involves a sizable number of elements in the y direction, since at no location can the slope exceed the ratio  $\delta_y/\delta_x$ . With this restriction,  $\delta_y$  is of the same order as  $\delta_x$  (10 to 30 m) for slopes of from 30 to 50 degrees, so that an avalanche 2 m high occupies only a small fraction of

one cell. An improvement on the grid of figure 2 is that shown in figure 3. The primary difficulty is the sensitivity of the governing equations in AVALNCH to height changes between successive cells along the path. This is not remedied by the grid of figure 3. The final grid layout, which appears most adaptable to the avalanche problem, is shown in figure 4, and is the one currently programmed. For each cell, the value of  $\Delta H$  (fig. 3) is input, from which gravity components are calculated by the equations

$$g_x = g \sin \phi, \quad \sin \phi = \frac{\Delta H}{\text{DELX}} \quad [4]$$

$$g_y = g \cos \phi, \quad \cos \phi = \sqrt{1 - \sin^2 \phi}.$$

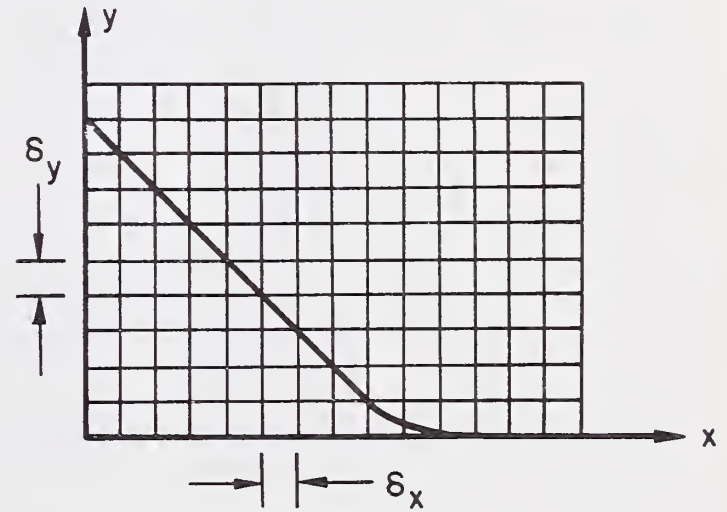


Figure 2.—Avalanche profile and grid.

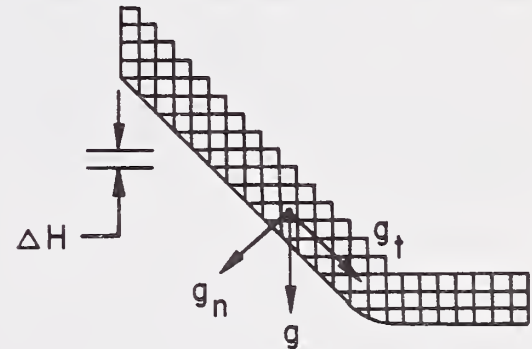


Figure 3.—Improved grid layout.

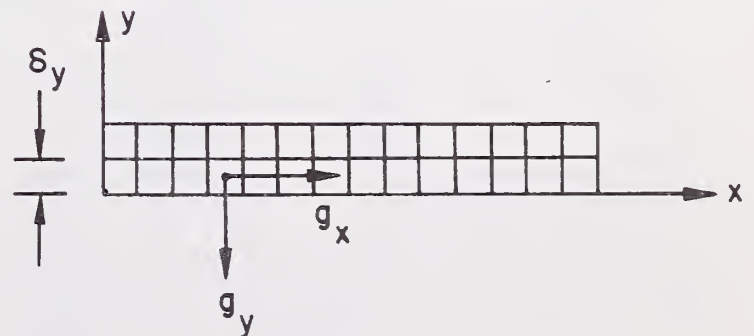


Figure 4.—Equivalent grid layout for avalanche flow.

Angle  $\phi$  is the average angle of the slope at the cell being specified. With this arrangement,  $\delta y$  can be selected independent from  $\delta x$ , where  $\delta x$ , is the slope-parallel increment along the avalanche path. For local intrusions, such as a level road bed, we set  $\Delta H=0$  for the cells in the road cut. In some cases a road cut may also cause an increase in the airborne component of a flowing avalanche by deflecting flow upward and entraining air. This can be represented in program AVALNCH by reducing the values of  $v$  and  $f$  (the coefficient of friction at the lower boundary) on the basis of available physical data.

The complex flow associated with a vertical drop is not representable in the present formulation. The  $g_x$  and  $g_y$  values enter the governing equations in AVALNCH at the stage of preliminary calculation of the velocity and pressure distribution at the start of each cycle. The ratio  $\delta y/\delta x$  enters later when boundary conditions are imposed, and when the updated flow height is computed. By numerical experimentation, it is determined that, whereas the limit of  $\delta y/\delta x < 1.0$  is a sensitive parameter to numerical stability, values of  $g_y/g_x > 1.0$  are readily handled. The difference is that rapid variation in velocity between cells is permissible, but rapid variation in boundary height is not. The values of  $\Delta H(HN(I))$  for each cell are input as a one-dimensional array following specification of the snow height,  $H(I)$ , also a one-dimensional array.

Velocity at the lower boundary,  $u_s$ , is determined by linear interpolation between the corresponding velocities in the boundary cell,  $u_1$ , and the lowest flow-domain cell  $u_2$ , (fig. 5) in which velocity  $u_1$  is expressed in terms of velocity  $u_2$ . We generalize this relationship from that of the SOLASURF code by specifying that

$$u_1 = u_2 (1 - 2f) \quad [5]$$

which is equivalent to a surface velocity given by

$$u_s = u_2 (1 - f) \quad [6]$$

For  $f = 0$ ,  $u_1 = u_2$ , and the surface is slip-free, and for  $f = 1$ ,  $u_1 = -u_2$ , so that  $u_s = 0$  a no-slip condition. For intermediate values of  $f$ , the boundary is a partial slip wall. Since  $f$  reflects friction at the boundary, we refer to this as the "friction coefficient," which is one of two basic parameters that must be sized for the avalanche runout problem.

Two options for input of  $f$  are given in AVALNCH. If  $f$  is constant over the entire path, then this value is input by specifying parameter, FRK. If  $f$  is a variable over the path, then a one-dimensional array, FRC(I), is specified, and  $FRK = 0.0$ . If the friction is actually to equal zero, it must be input by the array. If, in a particular application, values of  $f > 1.0$  are used, this can be interpreted as a penetration of the surface roughness into the flow. The surface roughness where  $u_s = 0.0$  is defined by

$$r = \frac{f - 1}{2f} \quad (f \geq 1) \quad [7]$$

as denoted in figure 5. There is an artificial aspect to this interpretation in that the quantity of flowing fluid is not reduced correspondingly due to  $r > 0$ . Thus, the analogy that perhaps most closely represents the case  $f > 1.0$  is sparsely spaced rock protrusions or tree trunks that slow the flow significantly, but do not trap large fractions of it. The variation in  $r$  for different values of  $f$ , as predicted by equation [7], is shown in figure 6.

The other parameter in AVALNCH requiring specification is the kinematic viscosity,  $\nu$  (NU). It is input as a single constant over the entire flow path, since information on possible variation of this parameter is generally lacking. When we learn enough to be able to specify changes in this variable down the path, program AVALNCH, as written, can easily accommodate this.

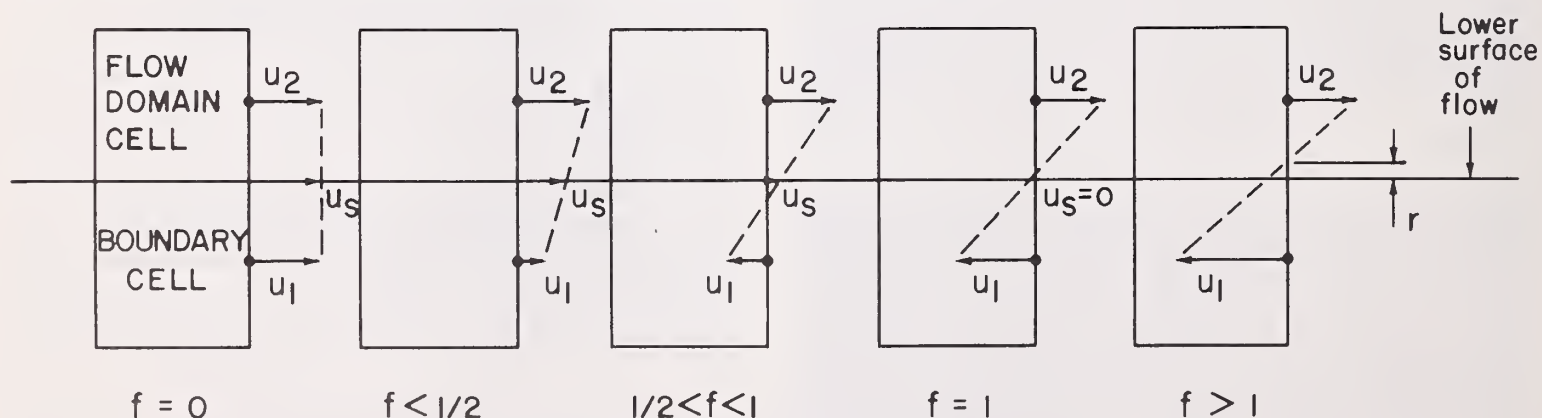


Figure 5.—Effect of friction on boundary flow.

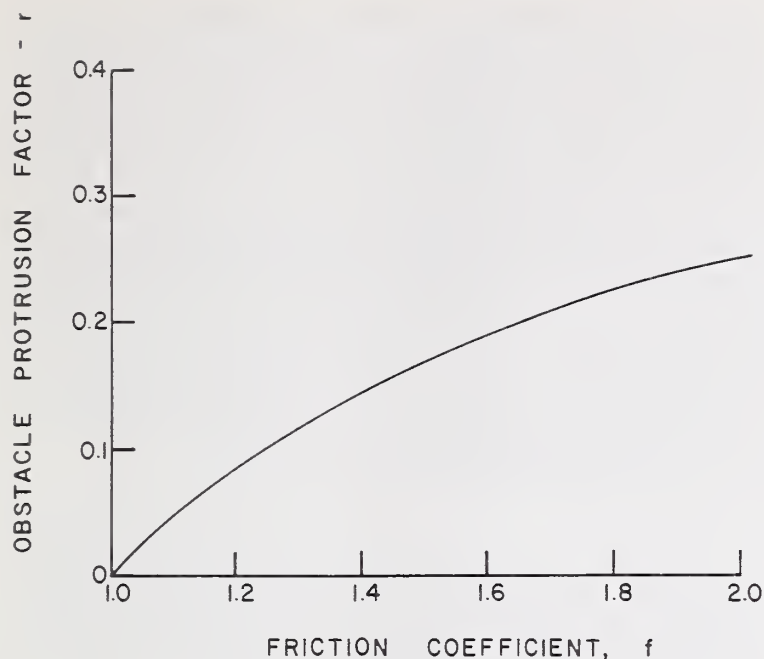


Figure 6.—Obstacle protrusion factor,  $r$ , versus friction coefficient  $f \geq 1.0$ .

From case studies it has been determined that the internal circulation in a flow is a function of the number of cells used in the  $y$  direction, for a fixed number of cells in the  $x$  direction. Since values for  $f$  and  $v$  must be established from case studies rather than from controlled experiments, their absolute values are not important. Thus, to standardize the cell geometry for all avalanche runs, a single cell height of the same dimension as the maximum thickness<sup>5</sup> of the fracture face is used. Flow height<sup>5</sup> as given by program AVALNCH, is the height of the "core material" and not of the snowdust cloud that accompanies mixed flow and powder avalanches. Actual field observations of "core height" are very difficult because, in most cases, only the dust cloud can be seen or photographed. A second flow domain cell is assumed above the avalanche cell, so that  $JBAR = 2$  for all cases. Based upon this selection of a flow domain geometry,  $f$  and  $v$  are sized from a number of modeled avalanche runs.

Besides numerical stability problems associated with the variable boundary option in SOLASURF, another difficulty is flow of mass through the boundary. Initial avalanche runs showed gradual disappearance of mass until, at some point downstream, the avalanche left the flow domain completely. This problem is reduced by using the standardized grid of figure 4, and is eliminated by inserting a multiplica-

tive factor equal to the ratio of original volume to current volume in the height update section (4000 section) of the code (Appendix B). This ratio is close to unity, so that the correction on each cycle is small, but sufficient to eliminate the monotonic divergence observed without the correction.

One difficulty of the circulating flow condition is in obtaining an accurate value for the average advance or "group" velocity of the fluid. (A "group" velocity is needed rather than a particle velocity.) The particle velocity, which reflects circulation as well as translation, listed in the expanded output of the flow profile is the maximum value of particle velocity (UMAX) and is used to predict the next time increment (DELTA) in AVALNCH. To obtain the "group" velocity in a mathematically rigorous manner requires a lengthy calculation. Instead, an approximate calculation utilizing the cell number of the leading (LDEG) and trailing (KTEG) edges of the avalanche is used. These cells are designated as the first occurring from opposite directions in which the flow height is 1% (or less) of the original avalanche height. Once the leading edge is located, the time change for advance of this edge to the next cell divided into the cell length is one estimate of the avalanche slope-parallel velocity (UEDG). Since fraction distance into the cells is not known, a nominal velocity estimate must be based upon averaging the values of UEDG over several (three to five) cells. Furthermore, UEDG can not be computed until the leading edge has left the cell, so that the listed values of UEDG must actually be associated with the cell previous to the current leading edge cell (LDEG).

A condition observed in early runs on avalanches was a tendency of the flow to reach a near steady-state shallow flow, not unlike equilibrium open channel flow, and to run out for considerable distances. Since this is not observed in most avalanches, a velocity dependent surface friction law is incorporated in the code (6000 section) in which the friction coefficient is increased exponentially with decrease in speed. The relationship established between  $f$  and  $u$  is:

$$f = f_0 (1 + 20e^{-1.25u}) \quad [8]$$

where  $f_0$  is the initial value selected for  $f$ . This surface friction-velocity relationship is written into the program to be operable anytime after the primary acceleration phase of the avalanche flow. A plot of equation [8] showing the variation in  $f/f_0$  versus  $u$  is given in figure 7. Although an actual quantitative physical basis for this phenomenon is not known, this

<sup>5</sup>The term "thickness" is used to designate the dimension of a snow layer perpendicular to the sliding surface. When speaking of the flowing snow, however, the term "flow height" is used to describe the dimension perpendicular to the slope to avoid using the term "flow thickness," which could be misunderstood as relating to the viscosity of the flowing snow.

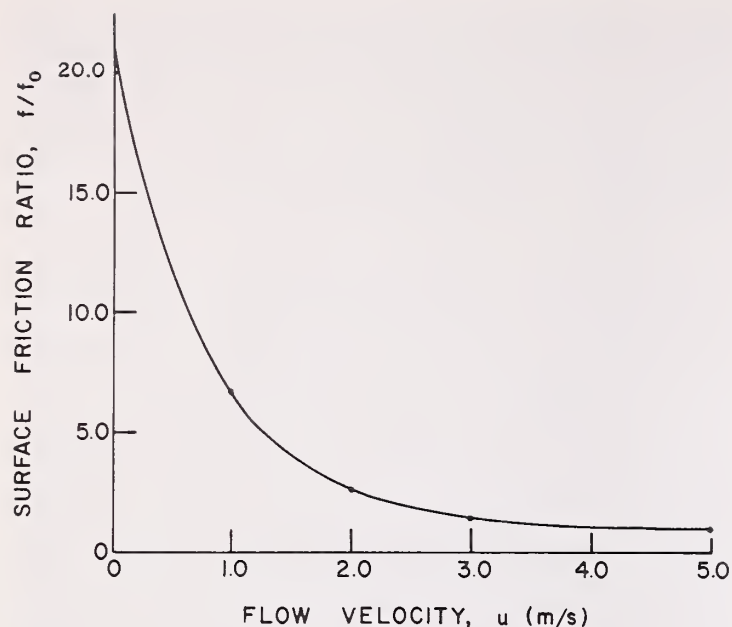


Figure 7.—Surface friction coefficient ratio as a function of flow velocity for “Fast-Stop” option in AVALNCH.

“fast-stop” option is a better representation for most avalanche flows than what is observed without it.

Apart from user program limits, there are five default conditions within AVALNCH which can terminate calculations. They are:

1. Number of iterations (ITER) within a cycle reaches 500.
2. Duration of avalanche flow exceeds time specified (TWFIN).
3. Leading edge flow velocity (UEDG) drops to less than 5% of maximum flow velocity achieved during the flow.
4. Leading edge of flow reaches lower limit of grid.
5. Leading edge of flow does not advance to a new cell in 50 cycles.

Parameter overflow occurs for condition 1. For conditions 2 through 5, the flow distribution is printed and an end statement is given prior to termination.

These are the major modifications incorporated in program AVALNCH. Other minor modifications have been made that can be identified by comparing the listing of AVALNCH (Appendix B) to that of SOLASURF (Hirt, Nichols and Romero 1975).

### Characteristics of Fluid Modeling Equations

Having reviewed the various features that have been incorporated in program AVALNCH, we consider the physical conditions that are modeled in the

computer formulation. The Navier-Stokes equations are equations of motion for laminar fluid flow. If internal viscosity is greater than zero, then, the flow is also considered to be rotational. In laminar, rotational flow fluid particles tend to follow curved paths along streamlines, and circulation patterns are evident. In contrast, particle motion in turbulent flow is completely random, and streamlines or flow path lines are not evident. From the study of numerous avalanche films, our conclusion is that for flowing and mixed motion avalanches the flow is often rotational and laminar. See Perla and Martinelli (1976) for description of avalanche motion.

At the extremes of avalanche motion are the cases of sliding rigid-blocks (sliding motion) for which internal viscosity is large, and turbulent flow (powder avalanches) for which viscosity is low. The low viscosity of turbulent flow is attributable to a large air-fraction in the flow and small snow particles, which produces the snow dust clouds surrounding the larger mixed motion avalanches. However, even in this case, there is a core of denser snow within the snow dust cloud that acts as a piston to drive or propel the airborne component. For this type of avalanche, program AVALNCH can be used, but it models only the flow of the core material, not the snow dust cloud. Once the snow is in motion, subsequent flow height predicted by the program is the height of the core material, not that of the snow dust cloud.

Most field observations of the flow height of this type of avalanche are to the top of the snow dust cloud, which gives no information on the type of flow that the core exhibits. However, based upon evidence from debris, the assumption of laminar rotational flow of the core material appears reasonable in many cases.

Program AVALNCH traces the snow flow starting from the initial, at-rest conditions of the release slab in the starting zone. Specification of the distribution of snow slab in the starting zone is, thus, a necessary part of the input. Any slab distribution may be input, the only restrictions are the following:

1. Only one height per slope-parallel cell may be specified; this height is assumed to be constant over the entire cell and is measured perpendicular to the slope.
2. Cell height is then set equal to the maximum slab thickness specified in the starting zone cells.

Snow entrainment as flow propagates down the slope is common in avalanche flow. To model this phenomenon, it is not accurate to specify snow thickness in downslope cells in the same way that starting zone material is specified. However, the modeling of snow entrainment is possible with program AVALNCH and is considered in detail in the section headed "Leading Edge Snow Entrainment Modeling."

## Avalanche Models, and Evaluations Using Program AVALNCH

### Intent of Case Studies

This part of the paper outlines a number of specific, recorded avalanche incidents to establish ranges for kinematic viscosity,  $\nu$ , and surface friction,  $f$ . Ideally, these ranges would be established using detailed information from many avalanches based on the following factors: fracture thickness, slope-parallel cross section of the initially released slab, type of surface layer of snow on slope, velocity of flow, actual runout distance,<sup>6</sup> and distribution of terminal debris. Since such detailed data are seldom available, we used case studies to size  $f$  and  $\nu$  to model overall runout response. Such a general approach is thought to have greater utility than one requiring highly accurate point variations in parameters because of the difficulty in obtaining such data for a wide range of snow and slope conditions.

Any, and ideally all of the above parameters, if measured, could be used to better quantify the values of  $\nu$  and  $f$ . However, the tremendous variation in snow and slope conditions that occur throughout a winter season preclude the utility of a specific slope analysis taking into account point variations in parameters. In fact a program requiring this accuracy would not be of general applicability for runout prediction, since specification of parameters is seldom accurate except under very specialized conditions.

### Ironton Park Avalanche Path

Location: San Juan Mountains, Red Mountain Pass North; southeast slope of Hayden Mountain, Colorado.

<sup>6</sup>The term "runout distance" is used to indicate the horizontal distance from the start of the runout zone to the most distant end of the avalanche debris. In this paper, the term "travel distance" is used to mean the horizontal distance from the fracture face in the starting zone to the most distant end of the avalanche debris.

Starting Zone: Wide, uniform slope below Half Moon Basin, below timberline; elevation 3,230 to 3,450 m.

Track: The entire slope; vertical drop 350 m; length 1,000 m.

Runout Zone: Level bottom of Ironton Park and frozen lake.

Avalanches: Large dry snow avalanche in 1958 crossed the road and left a debris pile approximately 1.5 m high on the road. No information is known on the starting zone fracture thickness or extent, nor on the type of snow constituting the flow.

Profile: Ironton Quadrangle, Colorado (7.5').

Length (m)	Elevation (m)	
0	354	
70	293	
174	232	
265	171	
326	110	
418	49	
509	0	
814	0	Location of road (Cell 93)
997	0	Opposite side of flat
1,073	49	

The profile constructed from these data points is shown in figure 8. The data needed from this profile is obtained by first marking off the increment distance  $\delta_x$  along the profile. This is selected to be 10 m slope distance in this case in order to describe the profile accurately and still keep the number of cells to less than the limit of 200 for AVALNCH. The change in elevation in each cell is taken directly from figure 8. For the present example only, the values of the elevation and change in elevation for each cell are listed in table 1. It should be noted that positive values of  $\Delta H$  correspond to decreases in elevation across cells, and negative values of  $\Delta H$  correspond to increases in elevation across cells (adverse slope). The values shown in table 1 for  $\Delta H$ , carried out to tenths of a meter, were obtained by interpolation, and reflect an accuracy not necessary for meaningful avalanche prediction. In subsequent runs, whole number values for  $\Delta H$  were used successfully, with much less time spent in data preparation. However, gross round-off of  $\Delta H$  to the point of masking 5- to 20-m length

perturbations in slope geometry is not recommended, as this order-of-magnitude perturbation can have a significant effect on the flow. Some of these conditions will be pointed out in the following avalanche cases.

In the case of the Ironton Park slope, little information is known about specific avalanches. Since the track is an open uniform slope, this example was used to examine the effect of varying the values of the kinematic viscosity,  $\nu$ , and surface friction,  $f$ . A summary of the values of  $\nu$  and  $f$  used for different travel distances is given in table 2. For most of the runs the initial slab thickness is set at 2 m for a downslope distance of 50 m, then a linear decrease in thickness out to 90 m, which is considered a large initial release. Other runs reported in table 2 for initial slab thickness other than the 2 m are vertically scaled modifications of the 2-m slab distribution.

The avalanche, which occurred in late December 1958 and deposited 1.5 m of snow on the road, is considered rare. Unfortunately, fracture line information is lacking. Occurrence of the avalanche in late December suggests moderate midwinter snow. On the basis of an initial slab thickness of 2 m, computer runs that characterize avalanche termination in the vicinity of the road are those for which values of  $\nu$  and  $f$  sum to 1.0 to 1.1. For example, for  $\nu = f = 0.5$ , the avalanche leading edge is 60 m beyond the road, and the debris on the road is nominally 1.9 m deep (Appendix C). For  $\nu = 0.4$ ,  $f = 0.7$ , the leading edge of the avalanche reaches the road, and for  $\nu = 0.5$ ,  $f$

$= 0.6$ , the leading edge is 20 m short of the road. It is apparent that by modifying  $\nu$  and  $f$  by relatively small amounts a wide variety of snow conditions can be modeled. We further note from the results in table 2 the near correspondence of results when the values of  $\nu$  and  $f$  are exchanged. That is, for  $\nu = 0.4$  and  $f = 0.7$ , travel distance is approximately the same as for  $\nu = 0.7$  and  $f = 0.4$ . Similar results are obtained for all other cases where  $\nu$  is not equal to  $f$  reported in table 2. This indicates the nearly equal influence of these two parameters in determining travel distance when using the units of measure selected for these studies. Thus, in the present case, we consider  $\nu = f = 0.5$  as representative of the flow, and adapt the practice of selecting  $\nu = f$ , except when physical conditions clearly indicate different values for  $\nu$  and  $f$  are warranted.

The computer listing of the input and output data for the case  $\nu = f = 0.5$  and a slab thickness of 2 m is shown in Appendix C. The listing includes the eight discrete input parameters, followed by the flow height, elevation change per cell, and the boundary friction coefficients, for the purpose of data verification. Finally, the gravity components,  $g_x$  and  $g_y$ , are printed for reference purposes. Any adverse grade in the slope profile shows up with negative values in the array for  $g_x$ . The values of  $g_y$  should always be negative. This completes printout of all input data needed for AVALNCH.

Outputs are the single line printouts of the avalanche flow status given after each cycle of calculation. By scanning the column of numbers labeled

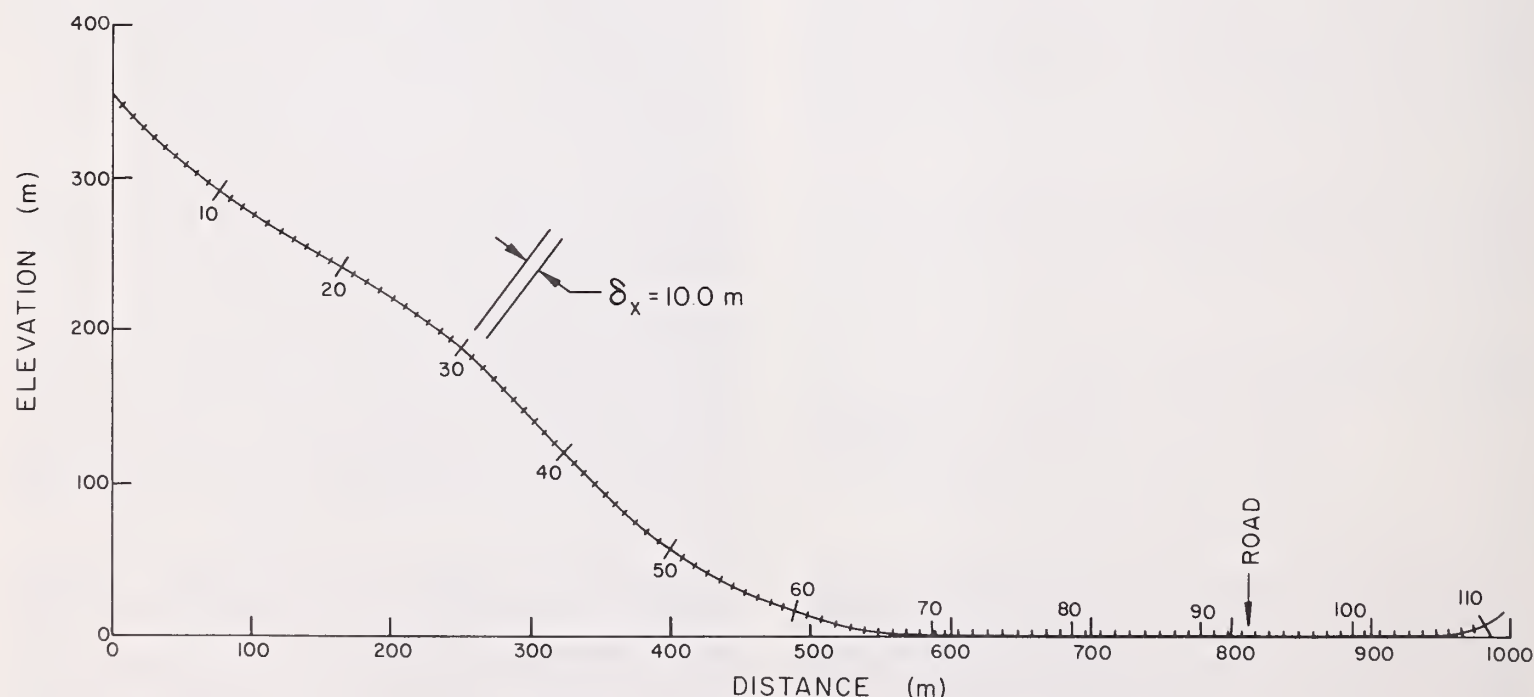


Figure 8.—Longitudinal profile of Ironton Park avalanche path.

Table 1. — Ironton Park profile elevation data

Station	Elevation (m)	$\Delta H$ (m)	Station	Elevation (m)	$\Delta H$ (m)	Station	Elevation (m)	$\Delta H$ (m)	Station	Elevation (m)	$\Delta H$ (m)	Station	Elevation (m)	$\Delta H$ (m)
0	357.0		23	226.2	4.6	46	81.4	6.0	69	2.0	0.9	92	0.0	0.0
1	350.5	6.5	24	221.4	4.8	47	75.4	6.0	70	1.3	0.7	93	0.0	0.0
2	344.3	6.2	25	216.4	5.0	48	69.8	5.6	71	0.8	0.5	94	0.0	0.0
3	338.1	6.2	26	211.2	5.2	49	64.6	5.2	72	0.4	0.4	95	0.0	0.0
4	331.9	6.2	27	205.8	5.4	50	59.4	5.2	73	0.1	0.3	96	0.0	0.0
5	325.4	6.5	28	200.2	5.6	51	54.4	5.0	74	0.0	0.1	97	0.0	0.0
6	319.2	6.2	29	194.4	5.8	52	49.8	4.6	75	0.0	0.0	98	0.0	0.0
7	313.0	6.2	30	188.2	6.2	53	45.6	4.2	76	0.0	0.0	99	0.0	0.0
8	306.8	6.2	31	182.0	6.2	54	41.4	4.2	77	0.0	0.0	100	0.0	0.0
9	300.3	6.5	32	175.8	6.2	55	37.4	4.0	78	0.0	0.0	101	0.0	0.0
10	293.8	6.5	33	169.6	6.2	56	33.4	4.0	79	0.0	0.0	102	0.0	0.0
11	287.6	6.2	34	163.1	6.5	57	29.8	3.6	80	0.0	0.0	103	0.0	0.0
12	281.8	5.8	35	156.3	6.8	58	26.2	3.6	81	0.0	0.0	104	0.0	0.0
13	275.8	6.0	36	148.9	7.4	59	22.8	3.4	82	0.0	0.0	105	0.0	0.0
14	270.0	5.8	37	141.7	7.2	60	19.4	3.4	83	0.0	0.0	106	0.0	0.0
15	264.4	5.6	38	134.5	7.2	61	16.4	3.0	84	0.0	0.0	107	1.0	-1.0
16	258.8	5.6	39	127.4	7.1	62	13.6	2.8	85	0.0	0.0	108	2.0	-1.0
17	253.6	5.2	40	120.4	7.0	63	11.1	2.5	86	0.0	0.0	109	4.0	-2.0
18	249.0	4.6	41	113.4	7.0	64	8.9	2.2	87	0.0	0.0	110	7.0	-3.0
19	244.8	4.2	42	106.4	7.0	65	7.1	1.8	88	0.0	0.0			
20	240.6	4.2	43	99.8	6.6	66	5.5	1.6	89	0.0	0.0			
21	236.0	4.6	44	93.6	6.2	67	4.1	1.4	90	0.0	0.0			
22	230.8	5.2	45	87.4	6.2	68	2.9	1.2	91	0.0	0.0			

Table 2. — Ironton Park avalanche travel distance for different values of viscosity and surface friction coefficients

Run No.	Viscosity ( $m^2/s$ )	Friction coeff.	Initial slab thickness (m)	Travel Distance <sup>1</sup> (m)	U max (m/s)	Cell No.	Comments
1	0.3	0.3	2.0	—	63/71		Avalanche flows out of grid at 25 m/s.
2	0.3	0.5	2.0	—	54/65		Avalanche flows out of grid at 16 m/s.
3	0.4	0.4	2.0	—	53/64		Avalanche flows out of grid at 15 m/s.
4	0.4	0.5	2.0	—	47/60		Avalanche flows out of grid at 8 m/s.
5	0.4	0.7	2.0	820	39/58		Avalanche stops on road. Max. debris depth: 2.4 m.
6	0.45	0.45	2.0	—	47/62		Avalanche flows out of grid at 8 m/s.
7	0.45	0.5	2.0	—	44/59		Avalanche flows out of grid at 2.5 m/s.
8	0.5	0.5	2.0	880	42/58		Avalanche stops 60 m beyond road. Max. debris depth 2.2 m.
9	0.5	0.6	2.0	790			Avalanche stops 20 m in front of road.
10	0.5	0.7	2.0	740	33/55		Avalanche stops 70 m in front of road. Max. debris depth 2.1 m.
11	0.6	0.5	2.0	790	37/56		Avalanche stops 20 m in front of road. Max. debris depth 2.2 m.
12	0.6	0.6	2.0	730	33/55		Avalanche stops 80 m in front of road. Max. debris depth 2.2 m.
13	0.6	0.7	2.0	700	33/55		Avalanche stops 110 m in front of road. Max. debris depth 2.0 m.
14	0.7	0.4	2.0	820	39/63		Avalanche stops on road. Max. debris depth 2.0 m.
15	0.7	0.5	2.0	740	39/55		Avalanche stops 70 m in front of road. Max. debris depth 2.7 m.
16	0.7	0.6	2.0	710	29/54		Avalanche stops 100 m in front of road. Max. debris depth 2.0 m.
17	0.4	0.4	1.5	820	39/63		Avalanche stops on road. Max. debris depth 1.5 m.
18	0.45	0.45	0.5	720	33/56		Avalanche stops 90 m in front of road. Max. debris depth 2.4 m.
19	0.5	0.5	1.5	690	20/51		Avalanche stops 120 m in front of road.
20	0.5	0.5	1.0	640	14/50		Avalanche stops 50 m onto flat. Max. debris depth 1.4 m.
21	0.5	0.5	0.75	160			After initial transient, avalanche decelerates continuously and stops on a bench of the slope.

<sup>1</sup> Travel distance is the horizontal distance from the crown of the avalanche to the leading edge of the terminal debris

UEDG and averaging over several cells, we see that the maximum velocity achieved by the avalanche is about 42 m/s in the vicinity of cell 64. This corresponds to a distance approximately 530 m (fig. 8), which is the start of the runout zone. The avalanche stops in cell 99, one cell short of the grid limit. The final listing of data is the extended output. By scanning the column labeled H (Appendix C), we find the final position of debris to extend from cell 91 (about 20 m in front of road), where the depth of debris is 0.8 m, to cell 99 where the debris depth is 0.02 m (Appendix C). Although velocity components persist in columns for  $u$  and  $v$ , these must be considered components of the circulation and are assumed to be negligible. Values for velocities and pressure outside the range of the flow domain can be ignored.

Holding  $\nu$  and  $f$  constant at 0.5, the thickness of the initial slab is varied from 0.5 to 2.0 m, and travel distance is noted as shown in figure 9. These results show a nonlinear dependence of runout distance with slab height with the "fast-stop" option having a significant effect on flow of the shallower avalanches.

An avalanche with a 2-m average slab thickness is considered unusual. What is perhaps more realistic is a thickness of 1.5 m, for which  $\nu = f = 0.4$  in order that the debris reach the road (table 2, run 17). Thus, we conclude that sensitive parameters that influence avalanche travel distance are the viscosity and fric-

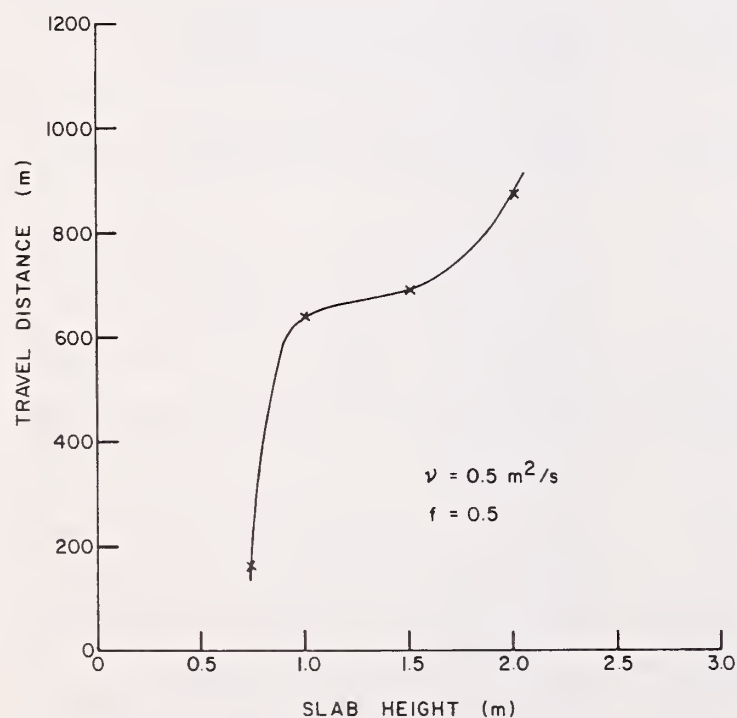


Figure 9.—Avalanche travel distances versus initial slab height for the Ironton Park path, holding viscosity and friction coefficients constant.

tion coefficients and initial slab thickness. Correlation between these parameters is expected as additional avalanche occurrences are evaluated.

The principal conclusions we obtain from this study of the Ironton Park profile are:

1. Values of  $\nu$  and  $f$  in the range 0.4 to 0.5 represent nominal values for early winter, dry hardpack snow in thick-slab avalanches.
2. Cell lengths of the order of tens-of-meters in the slope-parallel direction, coupled with cell heights of 1 to 2 m in the slope-normal direction, can be selected to reasonably model the avalanche flow.
3. Parameters that are identified to strongly influence avalanche travel distance are the kinematic viscosity, friction coefficient, and initial slab thickness. Ranges of values for these parameters should be established as additional case studies of specific avalanche paths are modeled.

### Pallavicini Avalanche Path

- Location:** Front range of Colorado Rockies; north slope of summit point 3,700 m southwest of Arapaho Basin ski area.
- Starting Zone:** Bowl-shaped depression in the north facing slope; above and below timberline; elevation 3,415 to 3,660 m.
- Track:** Wide opening in the heavily timbered slope; vertical drop 390 m; length 823 m.
- Runout Zone:** Flat bottom of the Snake River Valley; under severe conditions the avalanche may run across the 152-m-wide valley and reach the highway on the opposite slope.
- Avalanches:** The starting zone is controlled intensively by explosives and protective skiing, so that large avalanches are unlikely unless deposition occurs from a prolonged storm.
- Profile:** By a process described in detail for the Ironton Park avalanche path, the profile for the Pallavicini path is computed as shown in figure 10. Of particular note is the steep 80 m starting zone, in which the avalanche-

ing slab initially spans the upper 50 m. A second noteworthy characteristic of the profile is the adverse slope beyond the creek (cell 96) of 20% average grade.

The primary consideration in evaluating the Pallavicini path is to obtain qualitative information on the effect of the adverse grade in slowing and stopping avalanches. Good field data show that, in this path, only deep dry-snow slab avalanches with a significant airborne fraction ever reach the road. Most small midwinter avalanches stop between the grade change at about 400 m (cell 48) and the creek (cell 96), (fig. 10). The path is divided into 10-m increments or cells, and the avalanche starting zone is assumed to be 50 m long. Table 3 summarizes the computer runs made using the Pallavicini profile.

An avalanche of 0.75 m thickness stops quickly when viscosity and friction are set equal to 0.55. What might be considered nominal flow for an avalanche 0.75 m in thickness occurs when viscosity and friction are reduced to 0.5. In this case, the debris stops in cell 53, which is a bench in the lower part of the track (fig. 10). Flow of a 2-m avalanche with  $\nu$  and  $f$  at 0.5 (table 3, Run 8) ends 40 m beyond the creek, but does not reach the road. It is necessary to drop  $\nu$  and  $f$  to 0.4 for a 2-m avalanche to reach the road (Run 10). This indicates that a deep, dry avalanche with an airborne phase is modeled for  $\nu$  and  $f$  in the range of 0.4. Since many avalanches with an average fracture

face height of 2 m on the Pallavicini Path are known to stop in the vicinity of the creek, a value of 0.6 seems reasonable for  $\nu$  and  $f$ .

The 20% adverse slope beyond the creek in the Pallavicini Path is an effective mechanism for stopping avalanches that flow into this region, and mounding of the debris is noted in the AVALNCH prediction (table 3). Reynolds number,  $Re$ , which accounts for both inertial and viscous effects, is computed at the point of first occurrence of zero slope in the avalanche path, and is plotted in figure 11 versus runout distance for two of the paths analyzed. For Ironton Park, runout is across a frozen lake of zero slope. The 20% adverse slope of the Pallavicini path results in a 3.5 reduction of runout distance for  $Re = 240$ , and up to a 5.7 reduction at  $Re = 560$ . These results are based upon a nominal flow depth of  $H = 2$  m. Reynolds number,  $Re$ , defined as

$$Re = \frac{UH^*}{\nu}$$

was computed using  $U$  = the velocity of the avalanche leading edge at the instant it enters the runout zone,  $H^* = 4H$  and  $\nu$  is the kinematic viscosity which is usually near 0.5.

So far we have concentrated on the large avalanche that flows onto the adverse grade. For the smaller avalanche that stops in the track, flow height is a sensitive parameter that controls the distance of flow. Comparing Runs 1 and 2 in table 3, the

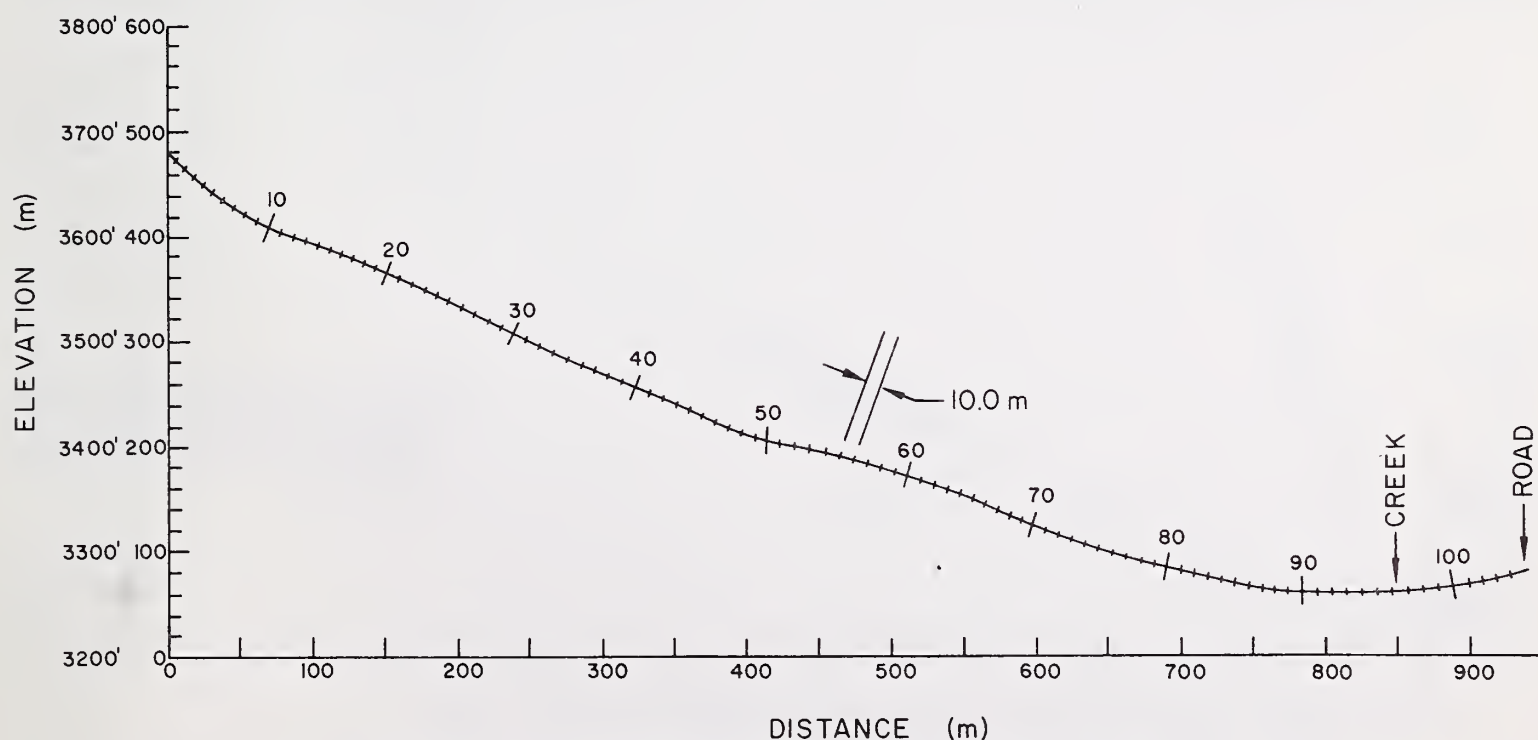


Figure 10.—Longitudinal profile of Pallavicini avalanche path.

Table 3. — Travel distance for the Pallavicini Avalanche for specified flow conditions

Run No.	Viscosity ( $m^2/s$ )	Friction Coeff.	Initial Thickness of slab (m)	Travel Distance (m)	Comments
1	0.55	0.55	0.75	130	Avalanche stops in cell 17. Maximum debris depth is 0.7 m and covers 80 m of slope.
2	0.50	0.50	0.75	440	Avalanche stops in cell 53. Maximum debris depth is 0.6 m and covers 130 m of slope.
3	0.5	0.5	1.00	780	Avalanche stops at cell 90. Maximum depth, 1.0 m; extent 100 m. Initial slab 40 m extent.
4	0.6	0.6	1.00	710	Avalanche stops in cell 82. Maximum debris depth is 0.8 m and covers 170 m of slope.
5	0.5	0.5	1.50	860	Avalanche stops at cell 97, 10 m beyond creek maximum depth 3.0 m, extent 40 m.
6	0.6	0.6	1.50	850	Avalanche stops at creek (cell 96). Maximum debris depth is 1.5 m and covers 60 m of slope.
7	0.6	0.6	2.00	870	Avalanche stops at cell 98 just beyond creek. Maximum debris depth 7.4 m. Avalanche covers 40 m of slope.
8	0.5	0.5	2.00	890	Avalanche stops at cell 100. Maximum depth 3.6 m, extent 40 m. Adverse slope is effective.
9	0.45	0.45	2.00	910	Avalanche stops at cell 102. Maximum depth 9.0 m; extent 40 m.
10	0.4	0.4	2.00	—	Avalanche leaves grid at cell 105 with velocity of 5.0 m/s.

sensitivity of travel distance to the values of  $\nu$  and  $f$  is pronounced. This indicates that the mechanisms to stop the small avalanche on a positive slope are the surface friction and kinematic viscosity coupled with local variation in slope profile. Since friction and viscosity are not well defined for different snow conditions, it is unlikely that programming for the small avalanche will be systematically correct for all avalanche incidents.

The major conclusions we draw from this analysis of the Pallavicini avalanche path are:

1. For the deep-slab, high air content avalanche flow, values of  $\nu$  and  $f$  of the order 0.4 yield results consistent with observed avalanche behavior on this slope.
2. The dominant characteristic of adverse slope in halting avalanches is noted, which substantiates long standing physical evidence. The effectiveness of adverse slopes of different angles and heights to stop avalanches is considered in greater detail in the section headed "Sensitivity of Runout Distance to Various Parameters."

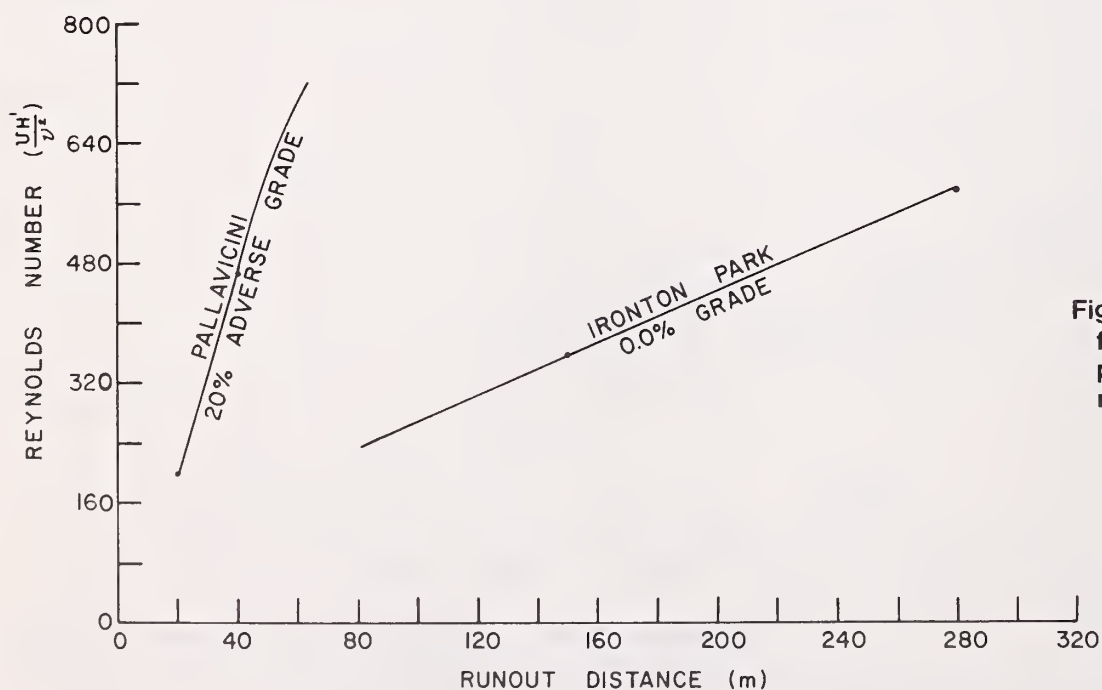


Figure 11.—Reynolds number as a function of runout distance for paths with different grade in the runout zone.

## Hematite Gulch Avalanche Path

**Location:** Highway 110 north of Howardsville, Colo.

**Starting Zone:** South facing bowl-shaped basin.

**Track:** Vertical drop approximately 915 m; length, approximately 670 m. In upper reach, flow is open sheet flow, which changes to gully flow over 55% of total path.

**Runout Zone:** Broad valley of bare ground and rocks cut by the Animas River.

**Avalanche:** A wet slab avalanche occurred on May 7, 1975. Fracture thickness was between 1 and 1.5 m and tapered off at the flanks to about 0.5 m. Approximately one-fourth of the snow in the starting zone was released. The flow emerged from the gully and flowed into the Animas River.

**Profile:** Howardsville Quadrangle, Colorado (7.5'). A centerline profile of the path is shown in figure 12. Three bends of 45, 30, and 35 degrees, starting with the uppermost, are indicated on the profile. Extent of the gully is indicated also.

The slope-parallel cell dimension is taken as 20 m in this case, resulting in a total of 112 cells to represent the entire path. An embankment occurs upslope from both the road and the river which can not be duplicated accurately in AVALNCH, since actual modeling would require depositing snow in the depressions formed by the banks.<sup>7</sup> Instead the road is shown one cell wider than actual, with these cells level ( $g_x = 0$ ), and the friction set at  $f = 0.9$ , a large value. The wet snow of this avalanche is assumed to have high viscosity ( $\nu = 0.55$ ). Friction is also assumed large, at  $f = 0.55$ , over the entire path, with local increases at the bends ( $f = 0.65$ ), and in the runout zone where the flow crosses bare, rocky ground ( $f = 0.9$ ). Initial slab thickness is 1.5 m over a downslope span of 40 m (two cells).

The leading edge of the avalanche stopped in the Animas River (cell 110), the debris extended 80 m upslope from the river, with a maximum height of 0.8 m. Maximum velocity of the flow after leaving the steep starting-zone was 26 m/s in cell 15. The flow encountered bare ground at cell 89, just below the lowest bend of the path. The velocity of the leading edge at this point was 10 m/s.

<sup>7</sup>Recent research with the computer code SMAC, a more elaborate version of SOLASURF, indicates that it will handle this condition.

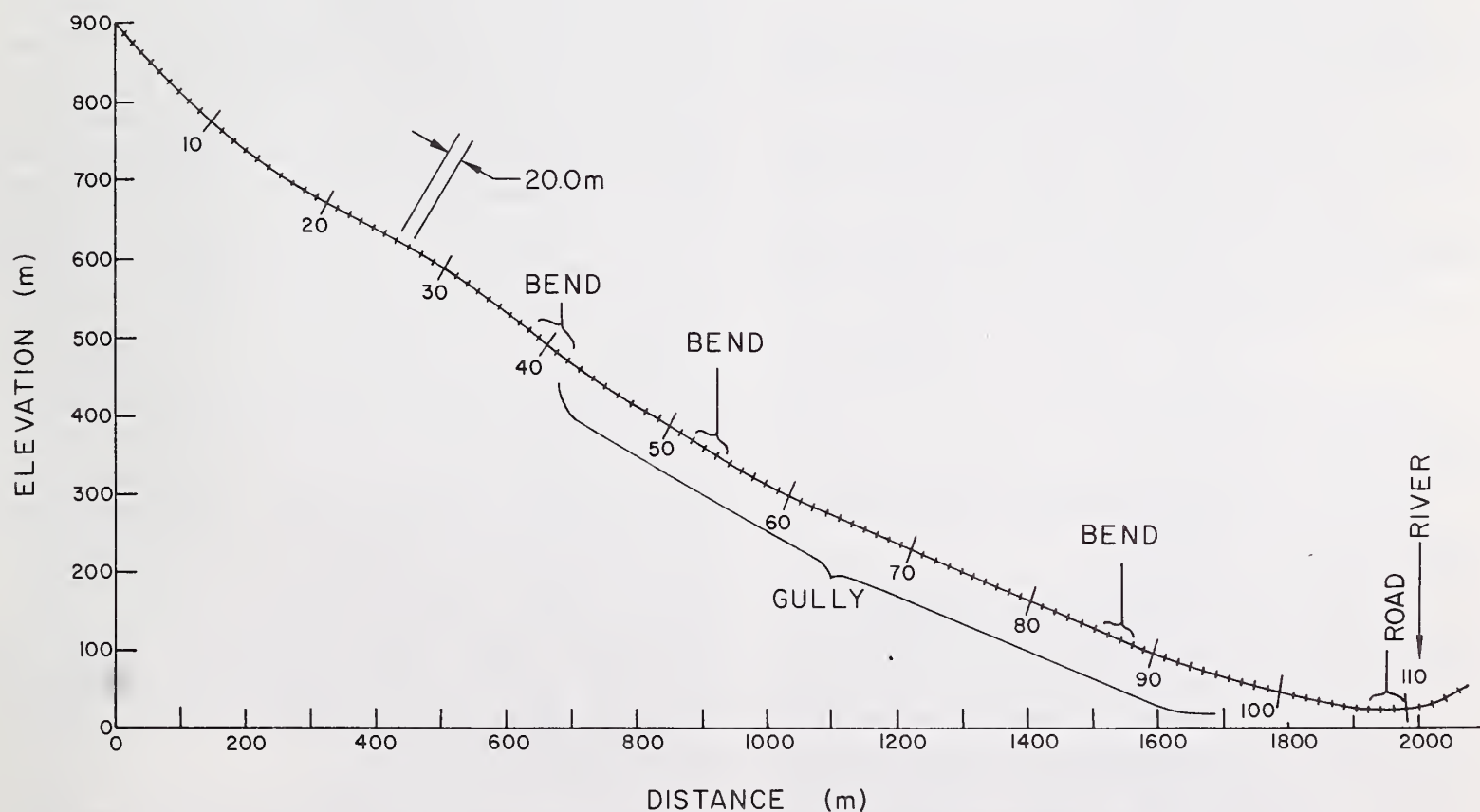


Figure 12.—Longitudinal profile of Hematite Gulch avalanche path.

At Hematite Gulch avalanches are known to cross the road and river and flow across the valley. Increasing initial slab thickness to 2 m and dropping  $\nu$  and  $f$  values of 0.5 and 0.4 approximately models the worst case avalanche condition. However, specific data on the worst case event is lacking for this path, so no attempt is made at computer simulation.

Conclusions drawn from this analysis are:

1. Viscosity and friction coefficient values on the order of 0.55 appear to model wet spring snow of the high viscosity type.
2. Friction set at 0.9 for bare ground with rocks appears to be consistent with the nominal value of 0.55 for the remainder of the profile in stopping the avalanche as was observed.
3. For the volume of snow set in motion, the river and road represent an imposing barrier for stopping the flow.
4. Some mechanism should be incorporated in AVALNCH to account for contracting and spreading of the flow when local geometry dictates three-dimensional flow conditions.

### Stanley Avalanche Path

Location:	Front range Colorado; south of Berthoud Pass; southeast slope of the east shoulder of Stanley Mountain.
Starting Zone:	No. 1. A bowl-shaped depression on the slope above timberline; elevation 3,540 to 3,780 m. No. 2. Wind blown snow slab along a treeline extending upward from 3,470 m elevation.
Track:	Vertical drop 730 m; length 1,700 m. U.S. Highway 40 crosses at two elevations. One crossing is at about 1,300 m, the second at about 1,700 m, in the valley bottom.
Runout Zone:	Lower section of the track with a gentle slope and the valley of Clear Creek.
Avalanches:	Stanley frequently blocks the upper highway. Most avalanches do not reach the valley bottom; however, a few of the larger avalanches have been known to overrun the lower highway and come to rest at the foot of the opposite slope. Most avalanches releasing at starting zone No. 2 stop at or

above the upper highway. Most large avalanches released in starting zone No. 1 stop between the two highways.

Profile:

Berthoud Pass Quadrangle, Colorado (7.5'). A centerline profile of the eastern most of the three tracks of Stanley is shown in figure 13. The slope above the upper road is uniform except for a small rise at the starting zone.

Major consideration is modeling the upper road to represent the different types of flow adequately. The upper road is three lanes wide with a turnout, which is equivalent to one cell of 20 m. Two additional cells are placed at zero grade to represent the uphill highway cut and the snowplow embankment of the downhill side, so that three zero grade cells ( $g_x = 0$ ) constitute the road intrusion. These three cells, plus one additional on each side of the road, are specified with large friction ( $f = 0.9$ ) to simulate the irregular snow profile in the vicinity of the road. For the remainder of the path, typical midwinter hard pack snow coefficient values are assumed with  $\nu = f = 0.55$ , which are also assumed across the lower road since it offers little resistance to flowing snow.

Results of several "typical" avalanche runs are listed in table 4. We see that 1-m deep avalanches starting in release zone No. 2 are trapped at the road consistent with a number of sightings. A 1.5-m deep avalanche starting in release zone No. 1 barely passes the road, then regains speed and finally stops between the roads. Increasing the avalanche thickness to 2 m and starting in release zone No. 1, the avalanche crosses the lower road. Tapered avalanche slabs 2.5 and 3 m thick at the crown, and 1 m thick at the toe 100 m downslope, behave similarly to the 2-m avalanche. The 3-m avalanche flows out of the grid but is slowing rapidly on the adverse grade past the creek. Comparing runs Nos. 1 and 3, and Nos. 5 and 6, we conclude that length of the starting slab does not change flow limits significantly. Flow length could be important when the leading part of the flow fills a recess (road cut, creek recess, etc.) and the flow is long enough so that the trailing part flows over the snow-filled recess. This phenomenon cannot be modeled exactly by AVALNCH except to fill the recess by changing the profile of the path prior to making the computer run.

A field observation on March 4, 1977, showed that an avalanche released by explosives in starting zone

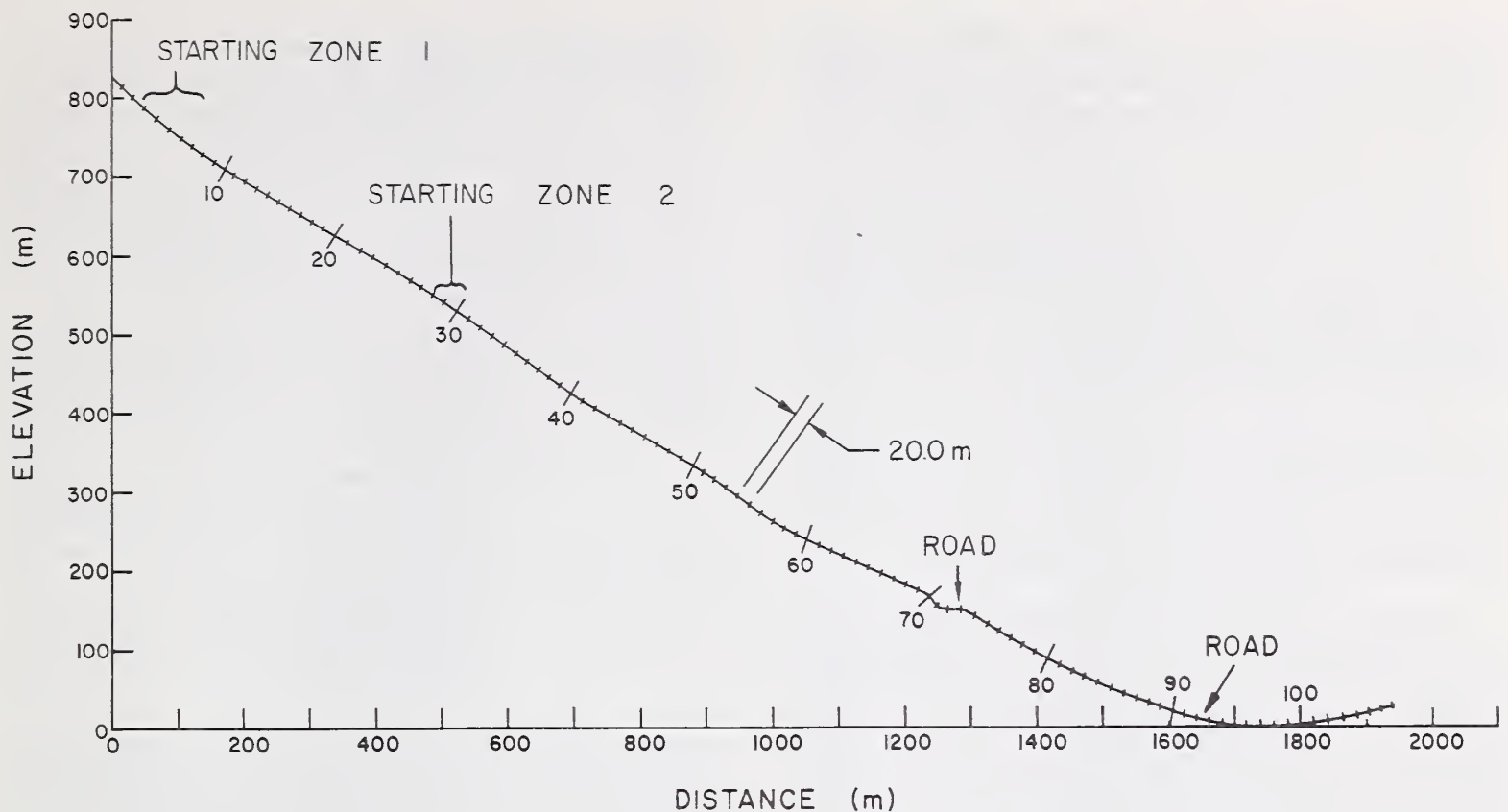


Figure 13.—Longitudinal profile of Stanley avalanche path.

Table 4.—Travel distance and maximum velocity for the Stanley Avalanche for specified flow conditions

Run No.	Starting Zone No.	Viscosity ( $m^2/s$ )	Friction Coeff.	Initial Thickness of slab (m)	Maximum Velocity m/s	Cell No.	Travel Distance (m)	Cell No.	Comments
1	1	0.55	0.55	1.0	9	35	1,300	74	Initial 40-m slab stops in upper road; 1.3 m max. depth; extent 100 m; upper road $f = 0.55$ .
2	2	0.60	0.60	1.0	8	34	770	73	Initial 40-m slab stops in upper road; 1.1 m max. depth; extent 160 m; upper road $f = 0.6$ .
3	2	0.55	0.55	1.0	10	34	800	74	Initial 100-m slab stops in upper road; 1.8 max. depth; extent 280 m; upper road $f = 0.55$ .
4	1	0.55	0.55	1.5	22	10	1,600	90	Initial 60-m slab stops between roads; 0.5 m max. depth; extent 320 m; upper road $f = 0.9$ velocity across road $V = 5$ m/s, then to $V = 13$ m/s.
5	1	0.55	0.55	2.0	28	10	1,780	99	Initial 60-m slab stops past second road; 7.3 m max. depth; extent 20 m; upper road $f = 0.9$ ; velocity across road $V = 23$ m/s.
6	1	0.55	0.55	2.0 tapered to 1.0	28	74	1,780	99	Initial 100-m slab stops past second road; 8.6 m max. depth; extent 20 m; upper road $f = 0.55$ ; velocity across road $V = 23$ m/s.
7	1	0.55	0.55	2.0	28	74	1,780	99	Initial 60-m slab stops past second road; 8.6 m max. depth; extent 20 m; upper road $f = 0.55$ ; velocity across road $V = 26$ m/s.
8	1	0.55	0.55	2.5 tapered to 1.0	45	75	1,820	101	Initial 100-m slab stops past second road; 9.0 m max depth; extent 20 m; upper road $f = 0.55$ , velocity across road $V = 45$ m/s.
9	1	0.55	0.55	3.0	60	78	Flows out of grid		Initial 100-m slab flows out of grid at $V = 37$ m/s, upper road $f = 0.55$ ; velocity across road $V = 59$ m/s.

No. 1 reached a speed of 33 m/s above the upper road. Most debris stopped in the upper road (cell 70-73) with a small amount extending to cell No. 85. Average fracture face thickness was 1.51 m, and average slab thickness in the starting zone was 1.19 m. The case that best matches this occurrence is Run 4 in table 4. The greatest discrepancy is in the two velocity values, which is probably due to the difference between the slab thickness used in the calculations and the flow height actually attained in the field.

The upper road intrusion modeled for Stanley is apparently sufficient to stop the smaller avalanches, and yet, permit the larger ones to flow beyond. User judgment is warranted in setting up these intrusion models for each case that is encountered.

Finally, it is noted that on the near uniform slope in release zones Nos. 1 and 2, avalanche velocity for the 1- and 1.5-m avalanches approximates the quoted condition that flow velocity reaches 80% of maximum speed after the avalanche has covered a distance equal to 25 times the initial slab thickness (Voellmy 1964). An alternate statement that is less precise is that the avalanche accelerates rapidly at the start, then flows on at a near equilibrium flow rate if the slope is constant. This physical condition is generally observed in the AVALNCH results.

General conclusions derived from the Stanley avalanche study include:

1. Heavy midwinter dry snowpack of 1- to 2-m thick slabs may be modeled with  $\nu = f = 0.55$ .
2. Slab length has secondary effect on avalanche flow, under restrictions of modeling by AVALNCH.
3. Individual road cut modeling must be subject to user judgment. The specific modeling of the upper road on Stanley as outlined herein has yielded physically reasonable results.

### **Number 3 East Avalanche off Max's Mountain, Alyeska Ski Area, Girdwood, Alaska**

**Location:** Northwest slope of Baumann Bump (Max's Mountain); 5 km east of Girdwood, Alaska, or 64 km southeast of Anchorage, Alaska, on the north side of Turnagain Arm.

**Starting Zone:** One of a series of narrow rocky slots at an elevation of about 760 m.

**Track:** Open slope with two benches: one at about 400 m, the other at about 230 m.

**Runout Zone:** Deeply incised stream valley.

**Avalanche:** Avalanches often start in cold, dry snow at the top of the mountain and encounter damp or wet snow on the lower slopes. Debris stops in the stream channel with only airborne particles crossing the canyon.

**Profile:** Seward (D-6) Quadrangle, Alaska (15' x 22.5'). A centerline profile of the No. 3 East, Max's Mountain path is shown in figure 14. The several rapid changes in elevation on the profile were not modified in order to see if AVALNCH could handle them, even though such rapid changes are physically unlikely because of snow cover smoothing.

The avalanche path is modeled by 129 slope parallel cells, each 10 m long. A frequent condition on this path is dry snow down to an elevation of approximately 400 m and wet, viscous snow below this elevation. All avalanches observed in the past several years have stopped on the slope or in the gully at cell 116 with no flow onto the bench of the gun tower.

Three runs were made to model different conditions known to occur on this slope. In two runs the initial slab was taken as 1.5 m thick and 40 m in extent. In the third run slab thickness was reduced to 1 m.

**Run No. 1:** High viscosity ( $\nu=0.7$ ) is assigned the slab to simulate wet snow in the starting zone. Friction is set at  $f=0.7$  to cell 80 and  $f=0.9$  to cell 129, to model moderate friction on the upper path and large friction on the lower path.

Results show maximum velocity attained is 20 m/s at cell 12, and the avalanche enters cell 115 at a speed of 10 m/s and stops in cell 116. The debris is scattered over 120 m to a depth of 0.94 m in cell 116.

**Run No. 2:** Midwinter deep snowpack viscosity is assumed with  $\nu = 0.55 \text{ m}^2/\text{s}$ . Friction is set at  $f=0.5$  to cell 72,  $f=0.7$  from cell 73 through 80, and  $f=0.9$  for the remainder of the path. This is intended to simulate dry snow running on a dry upper path and onto wet snow on the lower path. The avalanche attains a

maximum speed of 27 m/s at cell 33, enters cell 115 at 10 m/s, and stops at cell 116. Debris covers 90 m, to a maximum depth of 1.4 m in cell 116.

Run No. 3: The same viscosity and friction conditions as in Run No. 2 are assumed. The only difference is that the thickness of the initially released slab is set at 1 m. Under these conditions, the flow does not reach the creek, but stops at cell 100. As noted from figure 14, cell 100 is in the middle of a flatter part of the slope that starts at cell 92.

This reduction in slope coupled with the assigned viscosity and friction for this region are apparently sufficient to halt the avalanche.

Conclusions drawn from this example are:

1. Friction values in the range of 0.7 to 0.9 are large, and seldom should values larger than this be used for clear slopes.
2. Program AVALNCH remains stable for rapid variations in  $g_x$  when the slope changes significantly between the adjacent cells. Sign changes for  $g_x$  in the case of adverse slopes are readily handled by AVALNCH.

3. No. 3 East Max's Mountain path is a good example that there is a physical basis for treating friction as a variable quantity over the path.

### Imogene Avalanche Path

**Location:** Second unnamed drainage north of middle fork of Mineral Creek; top elevation 3,780 m; east facing slope.

**Starting Zone:** Broad basin with large rock outcrops; lower portion has small rock outcrops and grass.

**Track:** Narrowing V-shaped depression, grass, and willows.

**Runout Zone:** Broad fan, grass and willows.

**Avalanches:** Runout is into the Mineral Creek valley. An avalanche has crossed the highway twice since 1951. Both runs were full-track. Total vertical drop is 670 m; length of path is 1,730 m.

**Profile:** Silverton Quadrangle, Colorado (7.5'). This path is characterized by a constricted region from 520 to 880 m distance along the path as

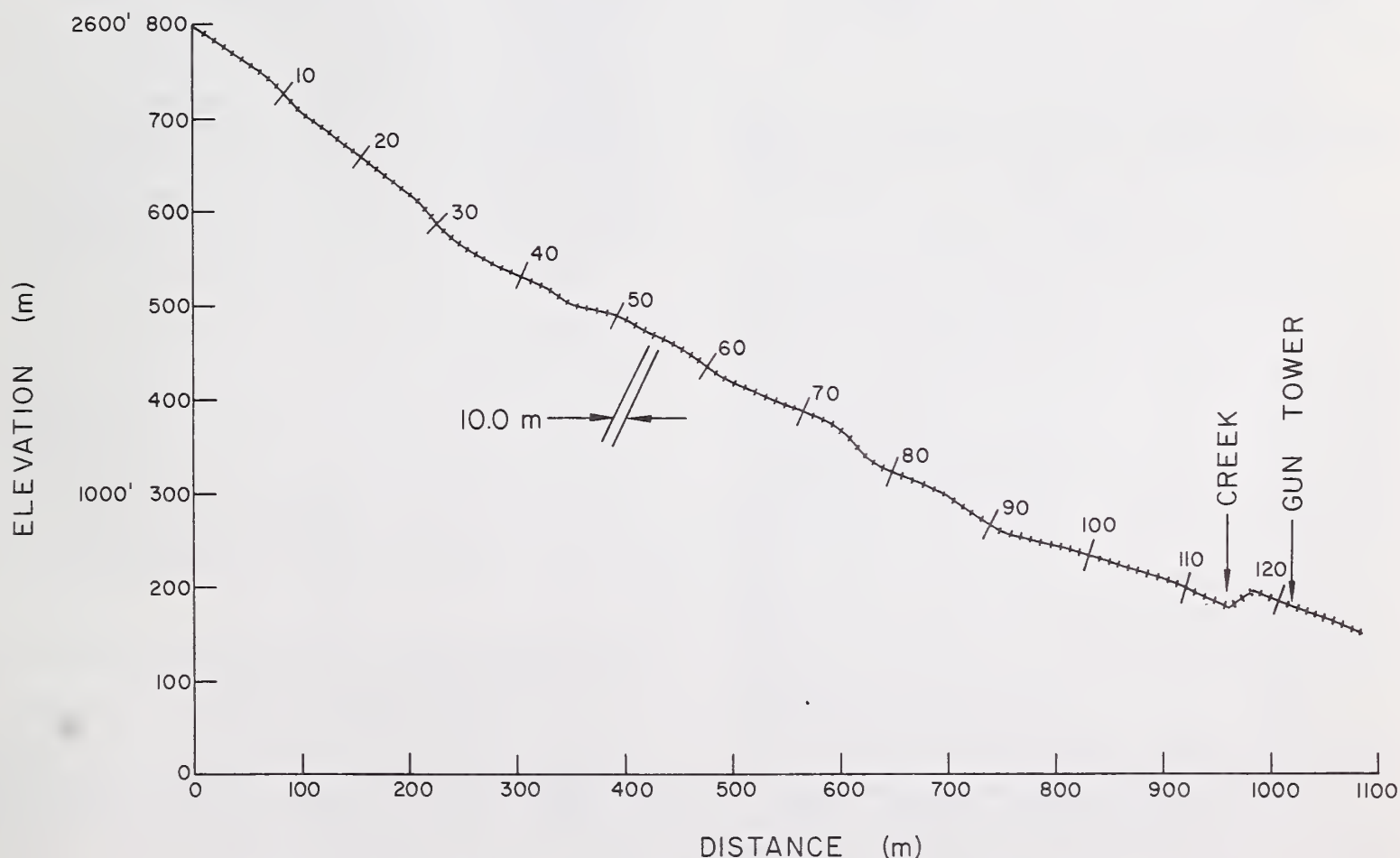


Figure 14.—Longitudinal profile of Number 3 East avalanche path (Max's Mountain).

noted in figure 15. After flow crosses the creek and road, the avalanche encounters adverse grade.

The path is modeled by 91 cells each 20 m long. Initial flow height is set at 1.5 m, and the extent of the starting slab along the fall line is 100 m. Viscosity is set at a nominal midwinter value of 0.5. The friction coefficient is varied in three ways in the constricted region of the flow, for the three computer runs carried out.

Run No. 1: Friction coefficient at 0.5 over the entire path. Flow velocity is maximum at 26 m/s (cell 16) and decreases until flow stops at cell 85 midway between the creek and the road. Debris height reaches a maximum of 5.5 m for a distance of 140 m. The leading edge velocity at exit from the constricted region is 20 m/s.

Run No. 2: The friction coefficient is increased to 0.6 for cells in the constricted region. Flow stops, as in run No. 1, at cell 85. Debris depth is 5.5 m maximum over 160-m extent. Although stopping dis-

tance is equal for the two cases, the velocity of the leading edge emerging from the constricted region in this case is 17 m/s, a decrease of 15% from run No. 1.

Run No. 3: The friction coefficient is decreased to 0.4 for cells in the constricted region. Flow again stops in cell 85 with maximum debris depth of 5.6 m, extending for 140 m. Flow velocity coming out of the constricted region is about 24 m/s, an increase of 20% over that of run No. 1.

Conclusions drawn from the study of this avalanche path are:

1. Varying the friction coefficient in the constricted zone of the avalanche track had no effect on total runout distance. This implies that travel distance on the Imogene path is dominantly controlled by the geometry of the runout zone itself. Generally, the dynamics of constrictions suggests that the surface friction decreases in importance because flow depth increases, and viscosity increases in importance because circulation increases. However, little information exists on flow of snow, so that we have no basis

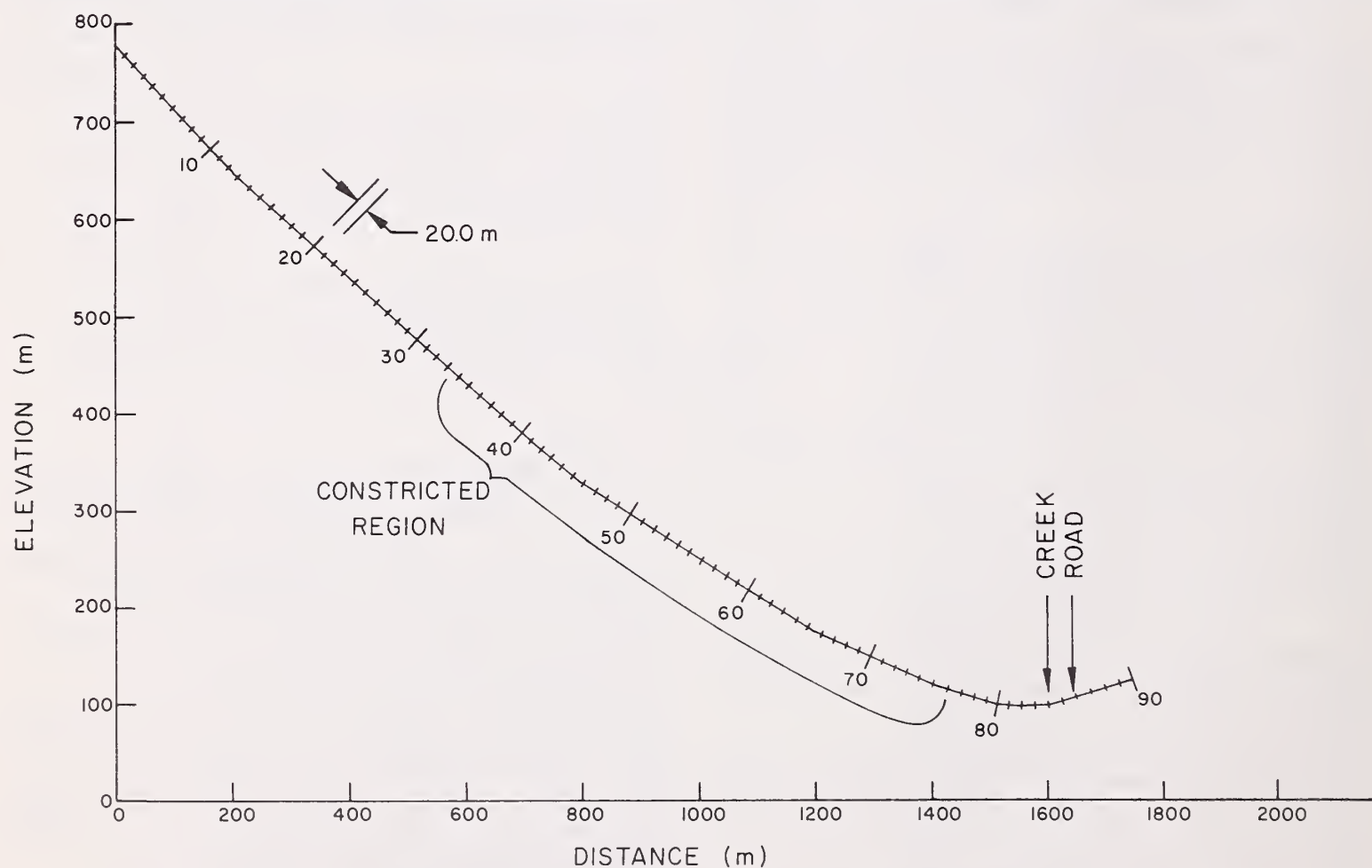


Figure 15.—Longitudinal profile of Imogene avalanche path.

for selecting any one criterion over another. Our previous conclusions that  $\nu$  and  $f$  have approximately equal influence suggests that, in the case of a constriction, no adjustment should be made.

2. Little information is known on flow properties of snow, and further research is warranted in this area.

## Numerical Studies with Program AVALNCH

### Equilibrium Flow Calculation

To establish upper limits on the flow velocity that can be attained as a function of slope steepness, equilibrium flow calculations were carried out for 30-, 40-, and 50-degree slopes. Surface friction and viscosity coefficients were assigned values from 0.4 to 0.6, which is representative of the range of these parameters in avalanche cases considered previously. To obtain steady-state flow, continuity in-flow and out-flow boundary conditions were imposed at the upper and lower boundaries, respectively. A single cell depth of flow over the entire domain was then specified and iteration to steady flow was carried out. Results of these calculations are shown in figure 16, in which equilibrium velocity is plotted versus flow height of the core material with slope angle, friction, and viscosity as parameters. In actual avalanche runout cases, the flow is rotational because continuous geometry changes cause local circulation. For a flow to achieve the velocities shown in figure 16, it is necessary for the geometry to be constant and continuous, a condition that is unlikely in actual cases. Thus, the velocities shown in figure 16 can be considered upper limits, which are reported only for reference when interpreting actual flow results.

It is noted that in AVALNCH when computing equilibrium flow, the use of noninteger heights (e.g. 1.5 m) results in an unstable condition that is attributable to numerical round-off in certain instructions in the code. By recoding, the problem can be averted; however, since only transient conditions will be seen in all avalanche evaluations, this recoding is not attempted in the unmodified version of AVALNCH.

### Variable Width Option for Program AVALNCH

The width of many avalanche paths vary. The version of AVALNCH used previously in this report does not account for variable width. The interpretation given previously in the results section should be per-unit-width, down the centerline of the flow as represented by the longitudinal profile with no provi-

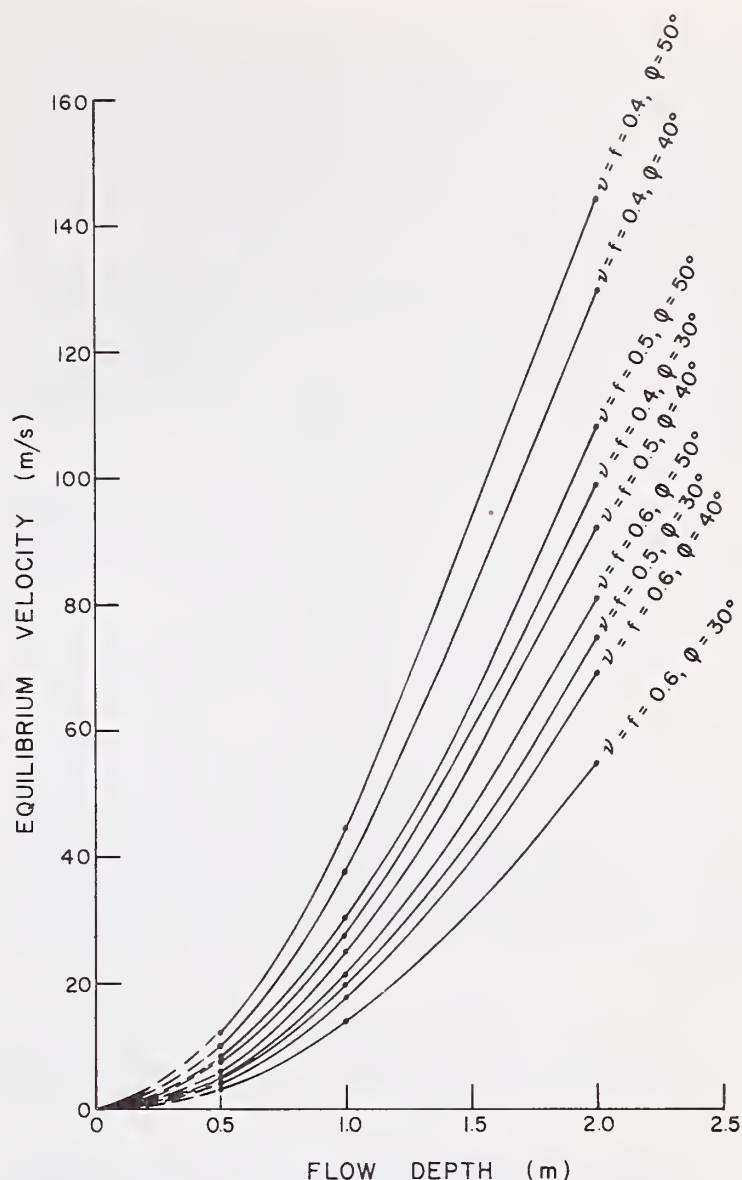


Figure 16.—Equilibrium velocity as a function of flow depth for different values of surface friction,  $f$ , viscosity,  $\nu$ , and slope angle,  $\phi$ .

sions made for spreading or narrowing of the flow (two-dimensional version of code). For avalanche paths with only small variations in the flow width, the two-dimensional formulation is adequate. However, in this section we report the findings of a pseudo simulation of three-dimensional flow in which the two-dimensional flow height of each cell is adjusted each CYCLE of iteration to account for local changes in flow width. This approximation is not a complete three-dimensional formulation, for which height variation along a contour would be admitted. However, it will account for large variations in width consistent with the accuracy to be expected based upon the nominal slope and material properties we are able to establish for flowing snow.

The version of AVALNCH including the variable width option is listed in Appendix D. Arrows are used to identify changes and additions from the nonvariable width version listed in Appendix B. The specific type of change or addition can be determined by

comparing the two listings. For the variable width program, additional input includes a width factor,  $W(I)$ , for each cell that can be read directly from a topographic map. The width factors are an array of numbers that follow card 4 in Appendix A, and have the same format as card 4. One approach to setting values for  $W(I)$  is to select a value of 1 for cells in the starting zone of the avalanche and adjusting this value for downslope cells as the width changes. In representing width change, even abrupt changes, the factors should vary gradually, since snow entrapment will smooth any irregular boundary.

For AVALNCH to accommodate increases in height of the flow due to a constriction, it is necessary to include more than one row of cells above the row in which the avalanche initially flows.

Appendix D provides a grid five cells high for a flow that was initially only one cell high. This requires a total of seven cells high (five active and two boundary), in place of four cells of the non-variable height code. This change increases the storage allocation of the code, and computer running time. For the Imogene path, described below, computer time is more than doubled to account for variable width.

The Imogene avalanche path is used as an example of a path with variable width. The outline of this path is depicted by the solid lines in figures 17 and 18. The

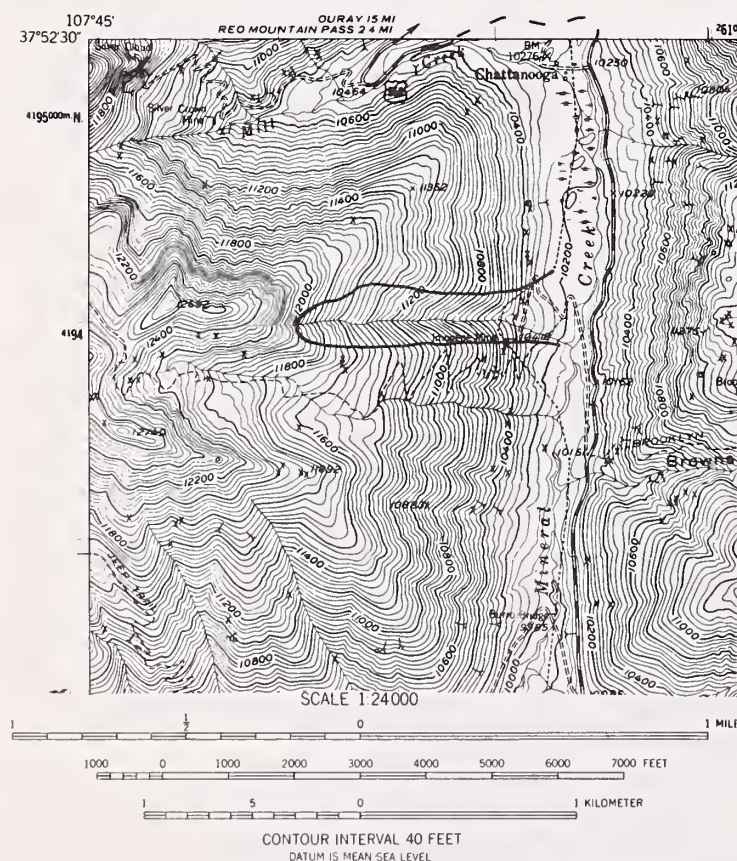


Figure 17.—Topography map of Imogene avalanche path, from which geometric path data was taken.



Figure 18.—Photograph of Imogene and adjacent avalanche paths (Miller, Armstrong and Armstrong 1976).

shaded region in figure 17 is the assumed extent of the starting zone. The dashed lines are the assumed boundaries of the flow after release. Under these assumptions, the width factor read directly from figure 17 is plotted in figure 19, from which individual cell values are interpolated.

Results of the variable flow calculations show that the flowing snow emerges from the constricted region of the path at a speed of approximately 23 m/s and comes to rest in cell 85. Thus, Run No. 3 of the Imogene path is roughly duplicated, indicating that by decreasing the friction coefficient in the constricted area, the overall effect of flow constriction is modeled. We note that the variable width flow stops in cell 85, the same as reported in the section on the Imogene path for constant width flows. Cell 85 is the

first cell of adverse grade (20%) after the flow crosses the creek bed. This amount of adverse grade is significant in stopping snow flow over a broad range of entering velocities. Thus, a meaningful number for comparison of the different runs is the velocity of the leading edge of the flow entering cell 85. The leading edge velocity and the final maximum debris height are listed in table 5 for the variable width runs of this section and the three constant-width runs of the Imogene path section. The reported velocity is the average of the velocities computed for cells 80 through 84, which, by averaging, reduces total computational variations.

We conclude from these results that the various assumptions made in modeling the constricted zone, bring about an overall effect on terminal flow that is small compared to the influence of terminal zone geometry. Significant variation in snow debris height is noted from table 5. For the constant flow-width cases, two active cells are used to represent vertical motion. By comparing the two-cell-high runs with the variable-width runs having three, four and five cells vertically, we note apparent numerical instability in height prediction when flow enters the upper boundary cell layer. The same effect occurs also in

the variable-width runs in the constricted zone where flow height increases by a factor of 2.5. With this increase in height, flow is in the cell next to the upper boundary cell for the three-cell-height case, and still one cell or more below the boundary cell in the four and five cell cases. The subsequent differences arising from interpolating with a boundary cell in one case, and with an active cell in the other, is the source for the differences in terminal speeds between the three- and four-cell cases. For consistent results one cell height should be maintained between the cell of maximum flow height and the upper boundary cell, at all points along the path. It appears that if accurate prediction of debris height is not required, all models predict terminal velocities within the limits of accuracy encountered on selecting values for  $v$  and  $f$  (to represent material and surface conditions).

Based upon these results, we conclude that we have a choice of ways to account for moderate constriction (or expansion) of factors up to 2 or 3. One approach is to use the variable-width code at a cost more than double that for the constant-width code. Alternatively, we can use the constant-width code and reduce friction in the constricted region.

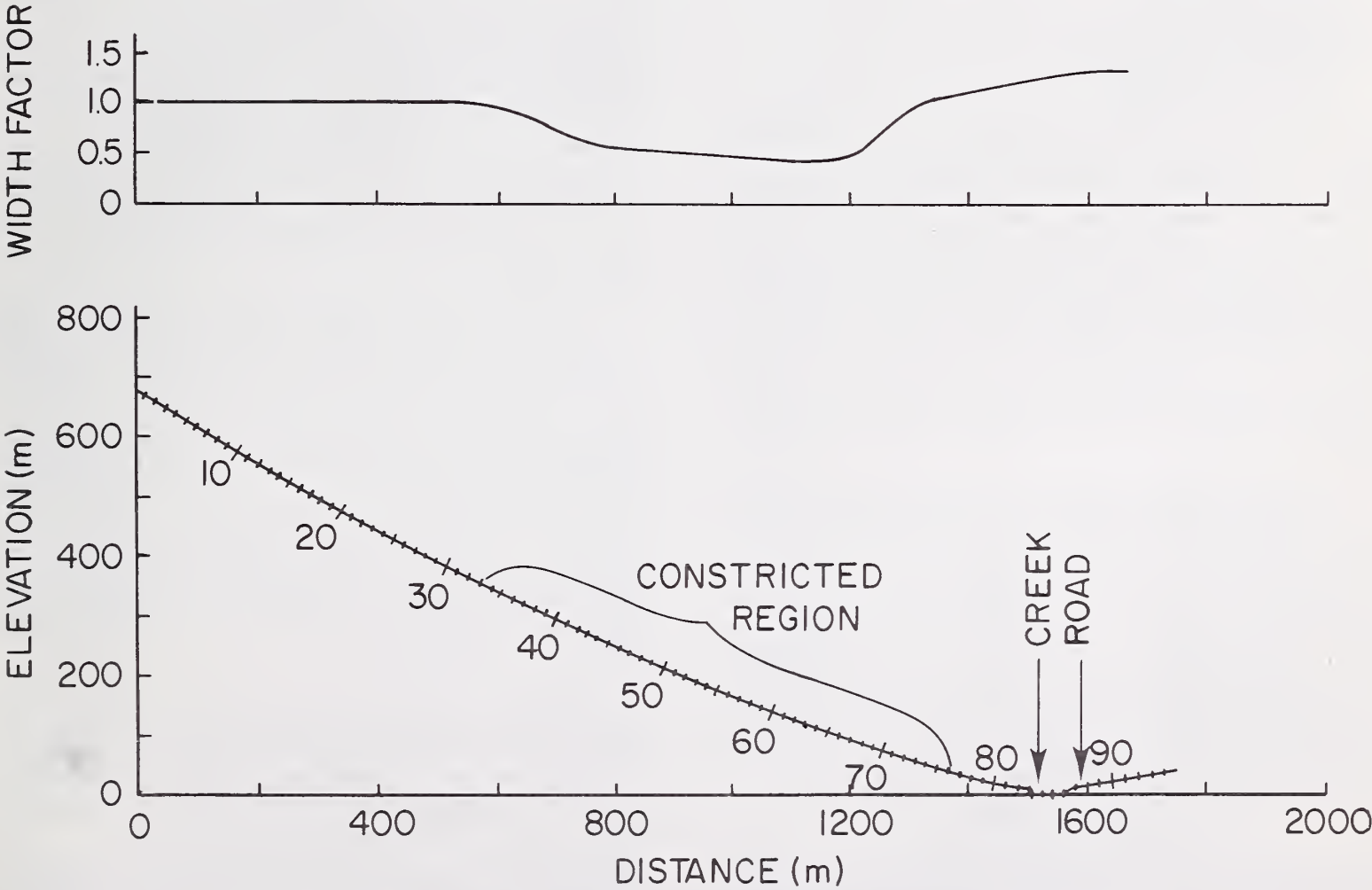


Figure 19.—Longitudinal profile of Imogene avalanche path and width fraction.

Table 5.—Summary of leading edge terminal velocity and maximum debris height for the Imogene Avalanche path.

Run No.	Description of numerical simulation in computer run	Average flow velocity into cell 85 (m/s)	Maximum height of snow debris (m)
1	Constant width flow. Friction $f = 0.5$ over path, and $f = 0.4$ in constriction region. Two-cell-height model of flow regime.	10.98	5.6
2	Constant width flow. Friction $F = 0.5$ over entire path. Two-cell-height model of flow regime.	10.74	5.5
3	Constant width flow. Friction $f = 0.5$ over path, and $f = 0.6$ in constriction region. Two-cell-height model of flow regime.	10.68	5.5
4	Variable width flow. Friction $f = 0.5$ over entire path. Three-cell-height model of flow regime.	11.9	2.9
5	Variable width flow. Friction $f = 0.5$ over entire path. Four-cell-height model of flow regime.	12.9	3.1
6	Variable width flow. Friction $f = 0.5$ over entire path. Five-cell-height model of flow regime.	12.9	3.2

This is physically incorrect because it does not account for proper mass distribution but it gives acceptable results. If prediction of the distribution of terminal debris in cases of pile-up on adverse grade is required, then cost differences between the two methods is removed. This occurs because a height of more than two active cells is then needed in the constant-width code also, which is the factor that increases cost.

A possible application of the variable-width code is in modeling avalanche flow in which flow from a tributary comes into that of the main stream. In this case, the tributary inflow is estimated in terms of the fractional increase it introduces over mainstream flow height. Denoting this factor by  $\eta_j$  and main stream flow width fraction by  $w_j$  for cell  $j$  on the path, then the adjustment of flow height, accounting for both width variation and tributary inflow, is

$$h_{j_{\text{new}}} = \eta_j \frac{w_{j-1}}{w_j} h_j.$$

In actual application of this equation, account must also be taken of the time sequencing between main

and tributary flows. This feature has not been programmed into the variable-width code, but it warrants consideration in order to evaluate the worst-case occurrence for some types of avalanche paths.

### Sensitivity of Runout Distance to Various Parameters

Results are reported from numerical experimentation carried out with the Iron-ton Park avalanche path. Runout of this path is onto a flat frozen lake surface. Because of the simple geometry of this path, alteration of the path was introduced into the computer model to assess the sensitivity of the flow to different parameters. Among parameters considered were average thickness of the initially released slab, friction and viscosity of the flow, adverse grade in the runout zone, and spreading angle of the flow in the runout zone. The thickness, friction, and viscosity parameters have already been evaluated and are reported in table 2. The adverse grade and terminal flow spreading angle parameters remain to be assessed. These were introduced separately into the Iron-ton Park runout by artificially representing their effect. For example, although an actual avalanche would not spread appreciably on the flat surface, numerical spreading was introduced in the computer model. Thus, the effect of spreading on runout distance was appraised without introducing the attendant slope rolloff, which must actually produce the phenomenon. The effect of adverse grade was likewise modeled by simple specification of gravity components in place of those corresponding to the lake surface.

In the modeling of flow spreading, angle  $\phi$  was introduced starting at cell 73 (fig. 8), which is the first cell on the surface of the lake. Angle  $\phi/2$  is then the angle between the centerline of the flow and one of the flow boundaries. Results are presented in figure 20 of spreading angle,  $\phi$ , versus runout distance for  $v = f = 0.5$  and an initial release slab thickness of 2 m. Spreading begins at 615 m distance (cell 73). An angle change from 0 to 45 degrees, holding all other parameters constant, decreased travel distance by 21%.

Results of various adverse slopes in the runout zone of the Iron-ton Park path are shown in figure 21. As expected, travel distance continues to shorten as the adverse grade steepens, finally becoming asymptotic at 615 m for an infinitely steep slope.

Using the data in figures 20 and 21 and table 2, a measure of the sensitivity of runout distance to the

various parameters can be formulated for the Ironton Park avalanche path. For example, by selecting a nominal set of values for the different parameters, we can then vary a specific parameter by a given amount and note the change in runout distance. Spreading angle was nominally set at  $\phi = 10$  degrees, and 20% and 40% increases in angle were introduced to evaluate change in runout distance. Adverse slope was nominally set at 10 degrees, and 20% and 40% increases were evaluated. The same procedure was followed using nominal values of viscosity and friction at 0.5, and slab thickness at 2 m. Results of these computations are shown in figure 22. It should be noted that most of the variations of parameters with runout distance are nonlinear (figs. 9, 20, and 21), and the selection of a nominal value was arbitrary. An attempt was made to select values that did not lie in either a flat or a steep portion of any curve.

The intent, then, was to establish order-of-magnitude estimates of the relative importance of the parameters for a simple avalanche path. The extent to which this goal was achieved is indicated in figure 22. Runout distance is most sensitive to the thickness of slab with a mean effect that a 30% variation in slab thickness results in a 70% change in runout distance.

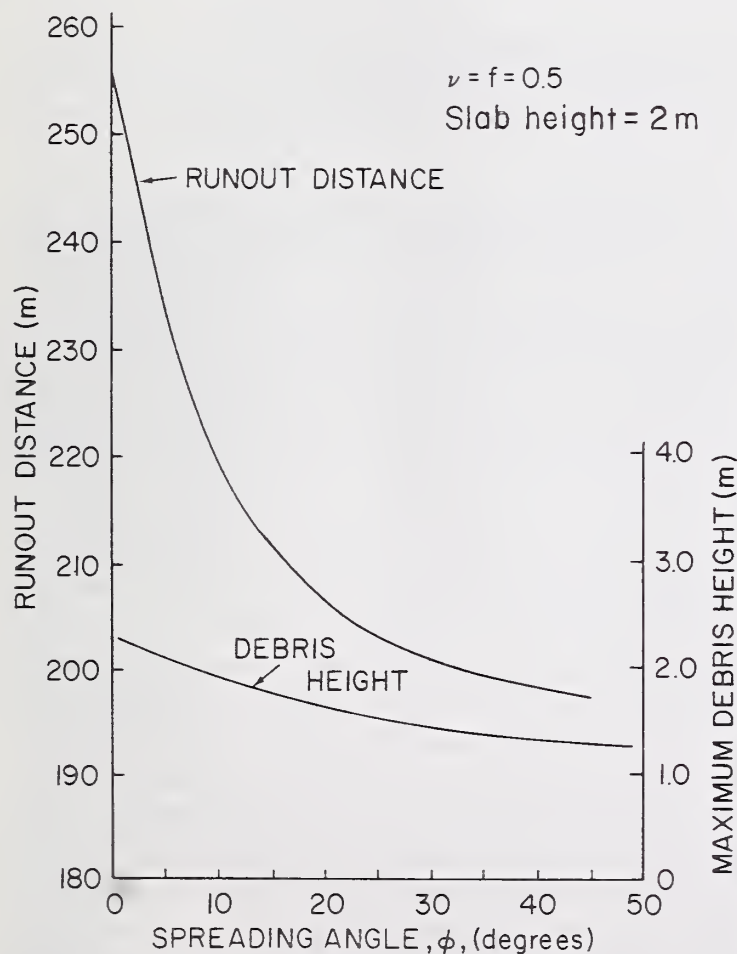


Figure 20.—Avalanche runout distance and maximum terminal debris height as a function of flow spreading angle for the Ironton Park avalanche path.

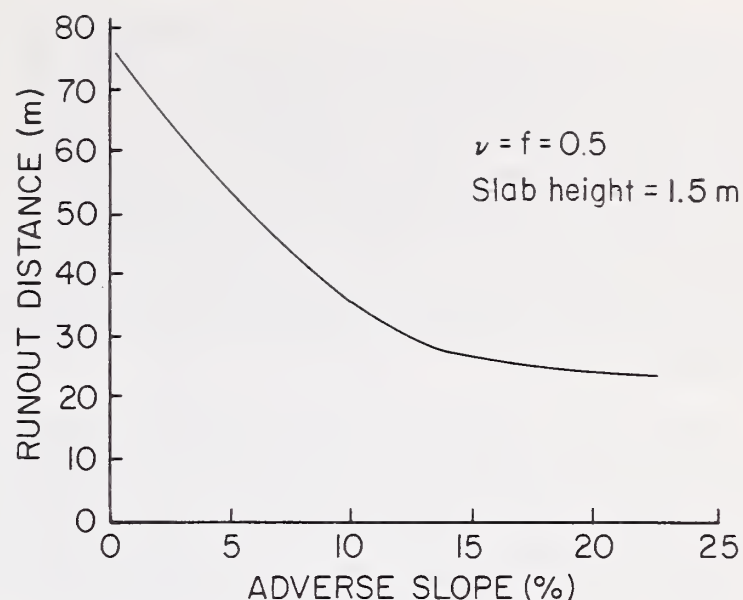


Figure 21.—Avalanche runout distance as a function of adverse slope angle for the Ironton Park avalanche path.

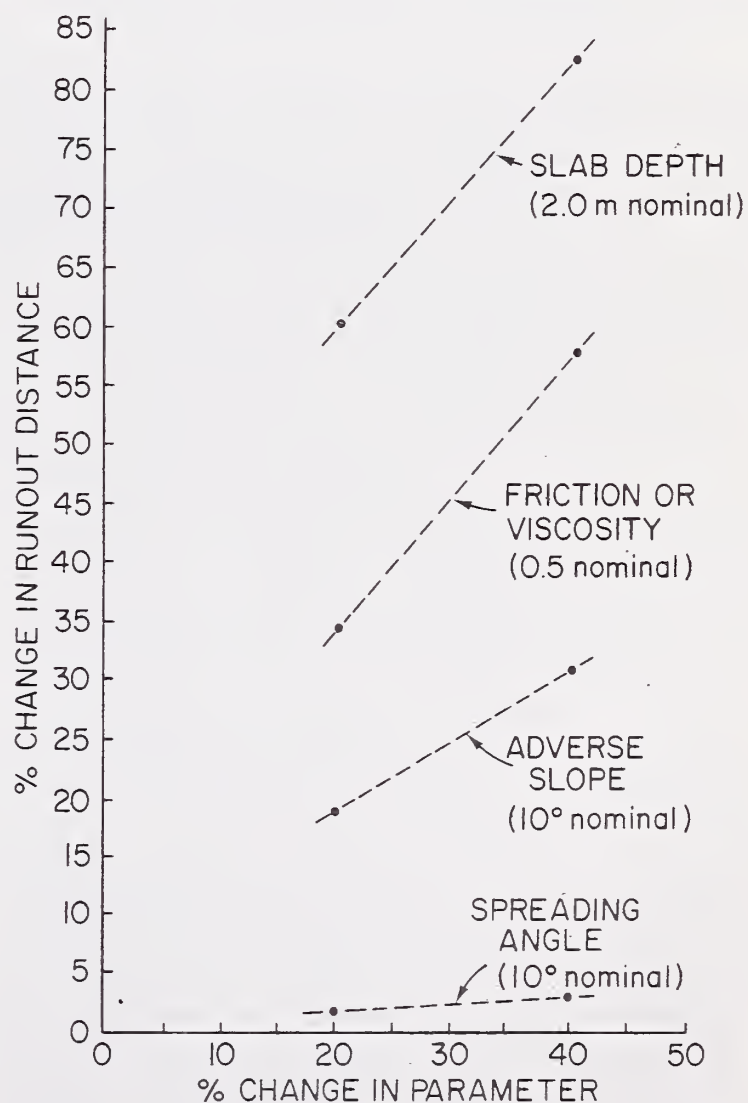


Figure 22.—Change in avalanche runout distance as a function of change in various flow parameters for the Ironton Park avalanche path.

This is followed by viscosity or friction in which a 30% change in parameter results in a 45% change in runout distance. Adverse slope change of 30% corresponds to 25% change in runout distance, and 30% change in spreading angle amounts to only about a 2% change in runout distance. One parameter not reported in figure 22 is the slope-parallel length of snow slab released, but it is determined to have negligible effect on runout distance (see the section on Stanley path.)

The primary conclusion we draw from these results is that the parameters of adverse grade and spreading angle, which can most readily be evaluated from topography maps, have the least effect on runout distance. The parameters of slab thickness and friction and viscosity of the flow, have the greatest effect on runout distance. These are much more difficult to evaluate, and certainly deserve special attention in future avalanche research.

### Leading Edge Snow Entrainment Modeling

Many avalanches entrain additional snow as they move down the slope. Generally, the entrained snow is loose and lightweight—the result of recent snowfall. Thus, we envision two possible influences on flow. First, the volume of the moving mass increases; since more mass is being accelerated, flow velocity at any point on the path should be lower than what it would be in the absence of entrainment. Second, the loose snow at the leading edge may reduce friction by air entrainment at the flow boundary interface. This would speed up the flow. To model the case of reduced friction in AVALNCH, we simply decrease the value of the friction coefficient,  $f$ . We noted previously that reducing friction to  $f = 0.4$  on the Pallavicini path results in snow runout that duplicated avalanches with a significant airborne component.

To model the effect of an increase in mass due to entrainment requires modifications to AVALNCH. As currently written, program AVALNCH converts elevation change of each finite difference cell along the path to components of gravity,  $g_x$  and  $g_y$ . Hence, gravity components along the entire path are specified initially. Thus, if we attempt to simply represent the snow mass at the leading edge by specifying a non-zero height of snow in all cells, then all snow on the sloping path will accelerate since  $g_x$  and  $g_y$  are specified. This is not the desired result. We want the avalanche to encounter stationary snow, which is then brought up to the speed of the advancing volume. To model this, consistent with the finite

difference representation used, we simply introduce one cell of stationary snow at the leading edge of the avalanche each time the flow enters a new cell. The momentum balancing the ITER phase of the numerical methodology in AVALNCH accelerates this new snow and assimilates it into the mass of flowing snow, with a corresponding increase in volume.

The following changes are necessary to introduce constant-depth leading-edge snow entrainment over the entire length of an avalanche path:

1. Specify thickness of entrained snow by parameter HNT, and insert instruction of the form HNT = 0.05 (units of meters) following instruction 55 in Appendix B.
2. Insert the following statements after instruction 264 in Appendix B:

$$\begin{aligned} \text{HIT} &= \text{H(LDEG)} \\ \text{H(LDEG)} &= \text{HIT} + \text{HNT} \\ \text{U(LDEG, 2)} &= \text{HIT} * \text{U(LDEG, 2)} / \text{H(LDEG)} \\ \text{U(LDEG, 1)} &= \text{U(LDEG, 2)} * (1.0 - 2.0 * \\ &\quad \text{FRC(LDEG)}) \\ \text{V(LDEG, 2)} &= \text{HIT} * \text{V(LDEG, 2)} / \text{H(LDEG)} \\ \text{FV}\phi\text{L} &= \text{FV}\phi\text{L} + \text{HNT} * \text{DELX} \\ \text{FV}\phi\text{L1} &= \text{FV}\phi\text{L1} + \text{HNT} * \text{DELX} \end{aligned}$$

If a variable entrainment thickness is to be modeled, then a one-dimensional array must be specified and the thickness values read into AVALNCH as part of the input data.

As a simple example, the Ironton Park avalanche path described previously is used to evaluate the effect of mass entrainment. Additional mass, expressed as a fraction of the maximum avalanche slab thickness of 2 m, is assumed over the entire path (fig. 8). Based upon snow entrainment thickness of 0.02 m (1% of slab thickness), 0.05 and 0.1 m, the nominal leading edge velocity versus cell number along the path, is shown in figure 23 for each case. It is seen that slowdown occurs as entrainment thickness is increased. However, as the flow comes off the sloping part of the path, the total momentum of the moving mass must increase with an increase in entrainment thickness, because more snow is accelerated by gravity than when entrainment is absent. Thus, if entrainment were eliminated in the runout zone, the enlarged avalanche mass (due to entrainment on the slope) entering the runout zone should flow farther than in the case of no entrainment. The imposed continued entrainment in the runout zone acts to resist the continued motion of the mass. For Ironton Park the two effects apparently cancel, and runout distances of the different cases do not vary signifi-

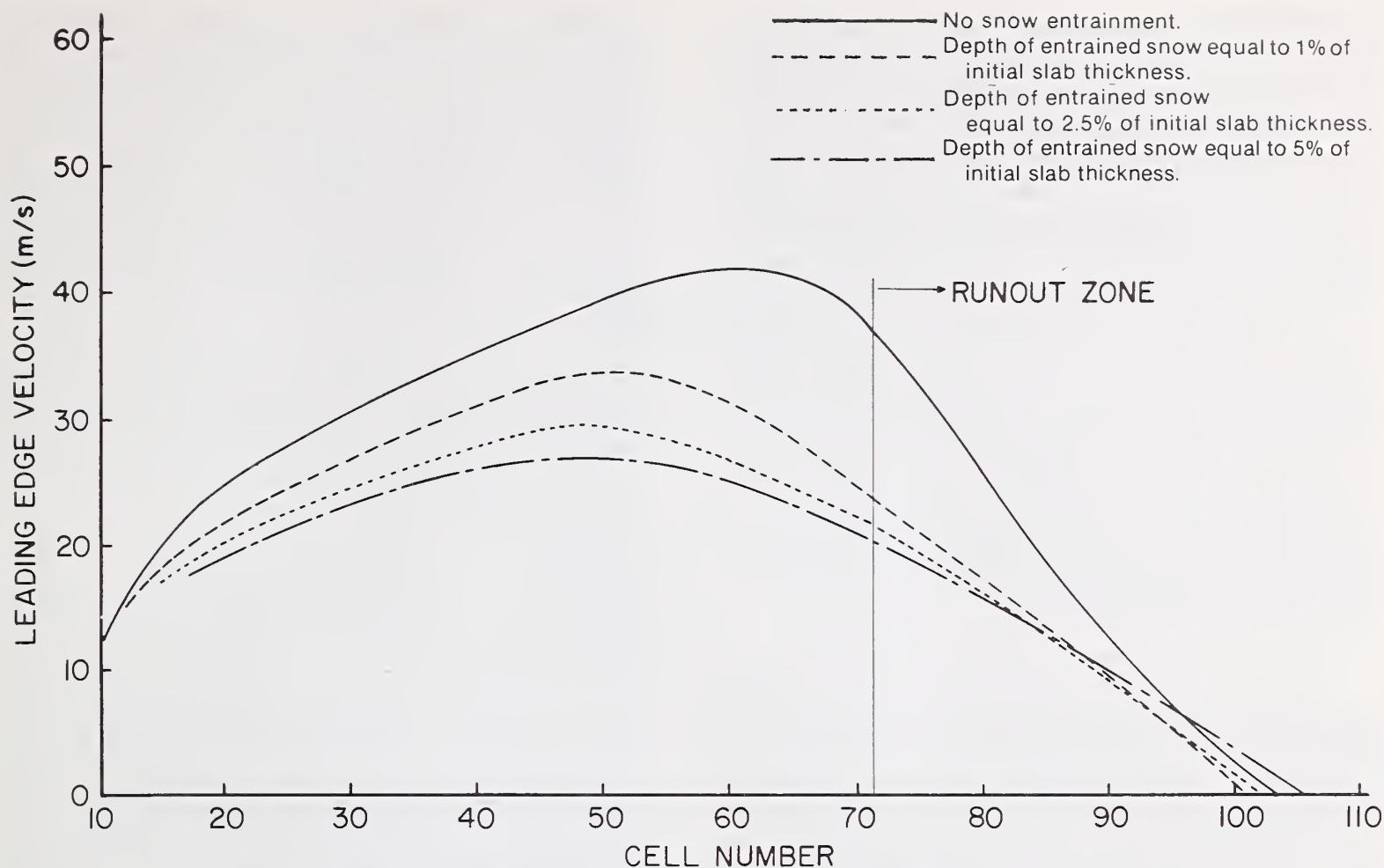


Figure 23.—Leading edge velocity variation with cell number along the Ironton Park avalanche path for different leading edge mass entrainment heights.

cantly. It is expected, however, that for paths with short runout zones, such as the Pallavacini, avalanches with entrained snow would run further than those without.

The results of figure 23 are based upon a two-cell vertical grid, for which flow heights of the snow entrainment cases exceeded values that correspond to accurate prediction of snow distribution. Thus, it is not possible from the data obtained to compute momentum values for the different cases. However, based upon the findings in the section headed "Variable Width Option for Program AVALNCH," we can expect the predicted velocities and travel distances to be realistic and slow down in the runout zone to be more uniform and gradual than for the zero entrainment case. A more accurate five-cell vertical model was run for the 5% entrainment case and showed that momentum of the entrainment case does not exceed that of the zero entrainment case. It also showed runout to be one or two cells farther than is reported for the two-cell vertical case. All of the entrainment cases could be rerun using a more refined vertical scale (with increase in computer expense); however, the results presented demonstrate that there is no fundamental difficulty in

representing the entrainment problem. More rational evaluation can be carried out when more actual avalanche events are available for reference.

### Discussion and Summary

A computer code applicable for predicting snow avalanche runout distance has been developed based upon two-dimensional, viscous fluid dynamic equations. Basic parameters of surface friction, fluid viscosity, and local terrain variations are accounted for separately by empirical evaluations based on known avalanche occurrences. The primary objective in developing the code was to model gross avalanche response and limiting-case events. Only gross response was modeled because of lack of knowledge about the properties of flowing snow. In particular, specification of internal viscosity and surface friction as functions of distance along the avalanche path are related in some, as yet unknown, manner to particle size in the flow, surface conditions, air entrainment, density distribution, and other factors that make each avalanche distinct.

In modeling gross response, local variations or gradual changes in parameter values with travel

along the path are assumed to be averaged out, provided the dominant characteristics of the flow are represented. Empirical evaluations are based on specific avalanche events in order to successively develop technology in modeling. A simple avalanche slope (see section on Ironton Park Avalanche Path) was used to establish nominal, total-path values for the coefficients of surface friction and internal viscosity based upon known early winter avalanches. It was established that, with the units of measure used, friction and viscosity coefficients of approximately equal value and of the order  $f = \nu = 0.5$  model the flow. In addition, some technique is needed to duplicate the slowdown dynamics of avalanches. An exponential dependence of surface friction on avalanche velocity at the time of terminal flow was selected based on numerous observations, although rare exceptions are noted where avalanches have flowed inordinate distance for reasons unknown.

The second avalanche path studied is the Pallavicini, where a terminal adverse grade is effective in stopping the larger avalanches. On this path, it is known that only avalanches having a significant airborne fraction reach the road (fig. 10). To match this occurrence, friction and viscosity were reduced to  $\nu = f = 0.4$ . It should be emphasized that only the more consolidated central core of the avalanche, not the turbulent airborne dust cloud, is modeled. Data are scarce concerning airborne avalanches or the airborne component of mixed motion avalanches. There is even a lack of information on the distribution of terminal debris from such avalanches which would help define the amount and distribution of snow in the snow dust cloud.

The third and fourth examples reported are the Hematite Gulch and Stanley avalanche paths, which are considered because of their local terrain anomalies. Hematite Gulch has three bends in the path, and the avalanche modeled ran out onto rocky, bare ground (fig. 12). Gross modeling of this spring, wet snow avalanche was achieved by letting  $f = \nu = 0.55$ , for most of the path, with values of  $f = \nu = 0.65$  at the bends. For runout onto the rocky ground, friction was set at  $f = 0.9$  and viscosity left at  $\nu = 0.55$ . For these values the model showed the avalanche flowing to the recorded terminal debris zone. Lacking sufficient field data, further evaluation of local terrain effects, as depicted by the Hematite Gulch path, is not warranted. Flow velocities along the path as the avalanche advances are additional basic data needed to see how well the model duplicates the actual event. This type of data would result in more accurate specifications of  $f$  and  $\nu$ .

The Stanley path (fig. 13) is a rather uniform slope interrupted by two highway cuts. Small to moderate size avalanches are known to be trapped by the upper road cut, and large avalanches to flow to the lower road cut. Predicted response was obtained using midwinter snowpack conditions  $\nu = f = 0.55$  over the entire path. At the road cuts, friction was increased to  $f = 0.9$  to represent, in some sense, the resistance of the road bed and snow embankments to flow.

The fifth avalanche path analyzed is at Alyeska, Alaska, very close to the ocean (see section on Number 3 East Avalanche). The typical effect of the maritime climate is a wet, viscous snowpack on the lower part of the slope and drier snow farther up the mountain. Thus, the initially released slab is often relatively dry ( $\nu = 0.55$ ) and flows over a similar snowpack ( $f = 0.5$ ). Farther along the path, friction is increased to  $f = 0.7$  to  $0.9$  to account for the viscous effects of the wet snow in the lower part of the path. Based upon this modeling, a slab 1 m deep and 40 m long in the slope-parallel direction stopped short of the gully at the foot of the slope (fig. 14), whereas a similar slab 1.5 m deep flowed into the gully. Data from the area are rather general, however, and about all we can say is that  $\nu$  and  $f$  values are consistent with those found satisfactory for other evaluations.

The final example reported is the Imogene path which depicts the classic "dog bone" or contraction-expansion flow common to many paths. The first attempt to model this variable width characteristic involved adjustment of the friction coefficient,  $f$ . However, evidence is lacking as to whether  $f$  should be increased or decreased particularly for a viscous material like snow. Later a pseudo-variable-width option added to program AVALNCH verified that  $f$  should be increased. This result, the outcome of a numerical analysis, warrants further verification from field measurements.

Having established a basis for selection of values for  $\nu$  and  $f$  to model "typical" cases of avalanche flow, we next studied particular aspects of avalanche flow to which our numerical model is applicable. This is not to suggest that specification of  $\nu$  and  $f$  is automatic for different avalanche cases. Each avalanche evaluation must be considered separately, but as experience is gained in specifying  $\nu$  and  $f$  and assessing the results of analysis, credibility of the methodology should improve. One factor that aids in establishing credibility is the small range of  $\nu$  and  $f$  needed to model a wide variety of avalanches from the large airborne avalanche to the wet, viscous, spring ava-

lanche. This advantage over other previously developed analysis schemes is the direct result of separating flow properties from local geometry effects. An additional feature of program AVALNCH is that the basic numerical approach of subdividing the flow domain into an array of cells permits the user to incorporate additional information later.

Since open channel equilibrium flow has been used in most dynamic evaluations of avalanches, one numerical study using program AVALNCH was to establish equilibrium flow velocity as functions of  $v$ ,  $f$ , flow height, and slope angle. It is not anticipated that this data will be extremely useful in the future; however, it is included for completeness.

As mentioned above, a variable width option of program AVALNCH is reported that permits evaluation of snow flow as the width of the flow changes. This phenomenon occurs when snow flows into a constricting region such as a gully, or into an expanding region such as an alluvial fan. The three-dimensional effect is represented by maintaining continuity of flow, not by a more accurate accounting which would require the introduction of a three-dimensional grid. This is another example where a numerical capability was developed, but cannot be verified until better field data, including flow velocities, are available. The variable width runs on the Imogene path establish the friction,  $f$ , should be increased in constricting flow when the constant width version of the code is used.

Perhaps the most significant numerical study reported is the sensitivity or error analysis of the basic parameters in avalanche flow. These parameters are the friction and kinematic viscosity, slab thickness, adverse grade, and flow spreading angle. By establishing nominal values for these parameters, then allowing one parameter to vary, the change in avalanche runout distance can be computed. For nominal 30% changes in each of these parameters, imposed separately, runout distance is found to change by 70% for slab thickness, 45% for friction or viscosity, 25% for adverse grade, and 2% for spreading angle. Thus, a scale of the relative importance of different types of field measurements and observations needed for a better definition of snow avalanche dynamics is set.

The final study involves evaluation of the effect on avalanche dynamics when loose snow is entrained into the flow at the leading edge of the avalanche. Leading edge entrainment can result in change of the surface friction, as well as gradual increase of the volume of

snow in motion. In the study reported, only the effect of volume increase is considered for a particular path. For the Ironton Park path, snow entrainment did not result in appreciable change in runout distance. The additional momentum due to increased mass moving down the slope was apparently cancelled by the resistance of the snow that was entrained during flow over the level runout zone. The primary benefit of this study was to set up a mechanism in AVALNCH for treating snow entrainment.

There are several notes of caution that should be mentioned concerning the use of program AVALNCH

1. The program predicts only the flow characteristics of the core material—not the snow dust cloud. In cases where avalanches run beneath structures such as bridges, the failure to account for the snow dust cloud could lead to underdesign of the structure.
2. Limited field observations indicate that long runout distances are not necessarily associated with extra thick slabs as indicated by the program. In Colorado, thick slabs are usually in wind deposition areas and are usually hard slabs. Such snow is strongly bonded and resists disintegration as it moves downslope. As a result, flow height is roughly equal to initial slab thickness, runout distance is not great, and the debris tends to mound up in the runout zone. Fresh soft slab, on the other hand, is weakly bonded and quickly fluidized after fracture. This leads to greater flow heights, longer runout distances, greater speeds, and a uniform, shallow layer of debris in the runout zone. Hence, more field data are needed to establish better estimates of kinematic viscosity and surface friction for various types of snow. The current program can handle this situation if given proper input.

In summary, a computer code has been developed based upon transient fluid dynamic equations to model snow avalanche flow. In test cases the program has predicted results consistent with known field observations for a number of avalanche events. Capability to modify the program to treat special conditions such as variable width flow, variable friction, snow entrainment, and other features has been demonstrated. Further refinement and application of the program to more complex flow conditions are basically limited by a lack of field data on avalanche flow which can be used for verification.

### Literature Cited

- Amsden, Anthony A., and Francis H. Harlow. 1970. The SMAC method: A numerical technique for calculating incompressible fluid flows. Los Alamos Sci. Lab., Los Alamos, N. Mex., LA 4370. 85p.
- Hirt, C.W., B.D. Nichols, and N.C. Romero. 1975. SOLA: A numerical solution algorithm for transient fluid flows. Los Alamos Sci. Lab., Los Alamos, N. Mex., LA 5852. 50p.
- Miller, Len, Betsy R. Armstrong, and Richard L. Armstrong. 1976. Avalanche Atlas San Juan County, Colorado. Univ. Colo. Inst. Arctic and Alpine Res. Occas. Pap. 17, 232p.
- Perla, Ronald I., and M. Martinelli, Jr. 1976. Avalanche Handbook. U.S. Dep. Agric., Agric. Handb. 489, 238p.
- Voellmy, A. 1964. On the destructive force of avalanches. 64p. USDA For. Serv., Alta Avalanche Stud. Cent., Transl. No. 2 [Available from Rocky Mt. For. and Range Exp. Stn., Fort Collins, Colo.]
- Welch, J.E., F.H. Harlow, J.P. Shannon, and B.J. Daly. 1966. The MAC method: A computing technique for solving viscous, incompressible, transient fluid-flow problem involving free surfaces. Los Alamos Sci. Lab., Los Alamos, N. Mex., LA 3425. 50p.

## Appendix A

### Input Data Format

The following input data is needed for program AVALNCH:

Card 1: FORMAT (20A4)

Columns 1 through 80: title and identification information.

Card 2: FORMAT (8F 10.0)

Columns 1 through 10: IBAR\* — number of cells in x direction.

Columns 11 through 20: JBAR\* — number of cells in y direction.

Columns 21 through 30: DELX — cell dimension in meters, x direction.

Columns 31 through 40: DELY — cell dimension in meters, y direction.

Columns 41 through 50: NU — kinematic viscosity ( $\text{m}^2/\text{s}$ ).

Columns 51 through 60: FRK\*\* — surface friction coefficient.

Columns 61 through 70: TWFIN — avalanche flow time in seconds.

Columns 71 through 80: CWPRT — cycles between extended printouts.

\*Using version of AVALNCH listed in Appendix B,  $\text{IBAR} \leq 200$ , and  $\text{JBAR} = 2$ .

These limits can be changed by changing the dimension statement in the code.

\*\*FRK = 0.0 if different values are to be used for different cells of the path.

\*\*FRK  $\neq$  0.0 if a constant value is to be used over the entire path (in this case list value to be used).

Card 3: FORMAT (8F 10.0)

Columns 1 through 10: thickness of avalanche slab in cell 1 in meters.

Columns 11 through 20: thickness of avalanche slab in cell 2 in meters.

Columns 21 through 30: thickness of avalanche slab in cell 3 in meters.

Columns 31 through 40: thickness of avalanche slab in cell 4 in meters.

Columns 41 through 50: thickness of avalanche slab in cell 5 in meters.

Columns 51 through 60: thickness of avalanche slab in cell 6 in meters.

Columns 61 through 70: thickness of avalanche slab in cell 7 in meters.

Columns 71 through 80: thickness of avalanche slab in cell 8 in meters.

(Continue on succeeding cards for IBAR entrees, including zero-thickness cells.)

Card 4: FORMAT (8F 10.0)

(Take these data from longitudinal profile of slope)

Columns 1 through 10: change of height from cell 1 to cell 2 in meters.

Columns 11 through 20: change of height from cell 2 to cell 3 in meters.

Columns 21 through 30: change of height from cell 3 to cell 4 in meters.

Columns 31 through 40: change of height from cell 4 to cell 5 in meters.

Columns 41 through 50: change of height from cell 5 to cell 6 in meters.

Columns 51 through 60: change of height from cell 6 to cell 7 in meters.

Columns 61 through 70: change of height from cell 7 to cell 8 in meters.

Columns 71 through 80: change of height from cell 8 to cell 9 in meters.

(continue on succeeding cards for IBAR entrees)

Card 5: FORMAT (8F 10.0)

(This set of data required if  $\text{FRK} = 0.0$  on card 4)

Columns 1 through 10: friction coefficient in cell 1.

Columns 11 through 20: friction coefficient in cell 2.

Columns 21 through 30: friction coefficient in cell 3.

Columns 31 through 40: friction coefficient in cell 4.

Columns 41 through 50: friction coefficient in cell 5.

Columns 51 through 60: friction coefficient in cell 6.

Columns 61 through 70: friction coefficient in cell 7.

Columns 71 through 80: friction coefficient in cell 8.

(continue on succeeding cards for IBAR entrees)

Two example data decks are shown following the first for friction specified in an array, and the second for friction constant over the flow domain.

EXAMPLE NO. 1: INPUT OF INDIVIDUAL CELL FRICTION VALUES

IRON TON PARK AVALANCHE: CØLØRADO									
TITLE	PARAMETERS	13	2	10	1.5	0.4	0.0	500	1000
SNOW	1.5	1.5	1.5	0.0	0.0	0.0	0.0	0.0	0.0
THICKNESS	0.0	0.0	0.0	0.0	0.0	0.0	6	5	5
HEIGHT CHANGE	6	5	7	7.2	6*	-1.2	0.6	0.7	0.7
PER CELL	4	2	1	0	0	0	0.6	0.7	0.7
CELL	0.6	0.6	0.6	0.6	0.6	0.6	0.6	0.7	0.7
FRICTION	0.7	0.7	0.7	0.7	0.7	0.7	0.7	0.7	0.7

\*Negative sign denotes adverse grade.

EXAMPLE NO. 2: INPUT OF CONSTANT FRICTION OVER PATH

NO. 3 EAST MAX'S MOUNTAIN: ALYESKA ALASKA									
TITLE	PARAMETERS	25	2	10	2	0.4	0.4	500	1000
SNOW	2.0	2.0	2.0	2.0	0.0	0.0	0.0	0.0	0.0
THICKNESS	0.0	0.0	0.0	0.0	0.0	0.0	0.0	0.0	0.0
HEIGHT CHANGE	7	7	7	7	6	6	6	7	6
PER CELL	6	5	5	5	5	5	4	4	3
	3	2	2	1	0	0	0	0	0
	0								

## Appendix B

### Fortran Listing of AVALNCH—Unit Width Version

```

1.  C  PROGRAM AVALNCH.
2.  *
3.  C  EQUIVALENT HORIZONTAL GRID OPTION
4.  *
5.  C  THIS PROGRAM HAS BEEN DEVELOPED TO NUMERICALLY SOLVE (USING
6.  C  FINITE DIFFERENCE TECHNIQUES) THE NAVIER - STOKES EQUATIONS
7.  C  FOR TRANSIENT FLUID FLOW PROBLEMS. IT WILL BE USED TO SIMULATE
8.  C  THE PROBLEM OF SNOW AND ICE AVALANCHES ON SLOPES OF VARYING SLOPE.
9.  C  DIMENSION U(202,4),V(202,4),UN(202,4),VN(202,4),P(202,4),FR(202),
10.  C  1XPUT( 8),H(202),HN(202),JT(202),NAME(20),GX(202),GY(202),FRC(202)
11.  REAL NU
12.  INTEGER CYCLE
13.  READ (105,45) NAME
14.  WRITE (108,35)
15.  WRITE (108,45) NAME
16.  *
17.  C * * READ AND PRINT INITIAL INPUT DATA
18.  *
19.  READ(105,25) (XPUT(I),I=1,8)
20.  IBAR=XPUT(1) ; JBAR=XPUT(2) ; DELX=XPUT(3) ; DELY=XPUT(4)
21.  NU=XPUT(5) ; FRK=XPUT(6) ; TWFIN=XPUT(7) ; CWPRT=XPUT(8)
22.  WRITE (108,50) (XPUT(I),I=1,8)
23.  25 FORMAT(8F10.0)
24.  35 FORMAT(1H1)
25.  45 FORMAT(20A4)
26.  47 FORMAT(6X'I'7X'J'8X'U'13X'V'13X'P'13X'H'9X,'SUR CELL')
27.  48 FORMAT(4X,I3,5X,I3,4(4X,1PE10.3),6X,I2)
28.  49 FORMAT(2X'CYCLE='I3,2X'ITER='I3,2X'DELT='1PE9.2,2X'TIME='E9.2,2X,
29.  1'FVOL='E9.2,2X'UMAX='E9.2,2X'UEDG='E9.2,2X'LDEG='I3)
30.  50 FORMAT(1H ,1X'IBAR='F4.0,2X'JBAR='F3.0,2X'DELX='F6.2,2X'DELY='F5.2
31.  1,2X'NU='F4.2,2X'FRK='F4.2,2X'TWFIN='F5.0,2X'CWPRT='F5.0)
32.  60 FORMAT(8F10.0)
33.  61 FORMAT(8F10.3)
34.  70 FORMAT(1H0,35X,'FLOW HEIGHT')
35.  71 FORMAT(1H0,25X'ELEVATION CHANGE FOR EACH CELL')
36.  72 FORMAT(1H0,25X,'BOUNDARY FRICTION COEFFICIENTS')
37.  73 FORMAT(1H0,25X,'SLOPE-PARALLEL GRAVITY COMPONENT')
38.  74 FORMAT(1H0,25X,'SLOPE-NORMAL GRAVITY COMPONENT')
39.  75 FORMAT(1H0,30X,'END OF INPUT DATA'//)
40.  82 FORMAT(5X,'PROBLEM RUNNING TIME EXCEEDED-CALCULATIONS TERMINATED')
41.  83 FORMAT(5X,'AVALANCHE AT END OF GRID-CALCULATIONS TERMINATED')
42.  84 FORMAT(5X,'FLOW VELOCITY NEGLIGIBLE-CALCULATIONS TERMINATED')
43.  *
44.  C * * COMPUTE CONSTANT TERMS AND INITIALIZE NECESSARY VARIABLES
45.  *
46.  IMAX=IBAR+2 ; JMAX=JBAR+2
47.  IM1=IMAX-1 ; JM1=JMAX-1
48.  RDX=1.0/DELX
49.  RDY=1.0/DELY
50.  DELM=DELY/100.
51.  DELT=1.0
52.  IM2=IMAX-2
53.  JM2=JMAX-2
54.  T=FLG=UEDG1=0.0
55.  CYCLE=ITER=IND=LDEG=0
56.  G=9.8 ; DMG=1.7 ; EPSI=.001 ; ALPHA=0.1 ; GAMMA=0.1 ; DZRO=1.0
57.  G=9.8 ; DMG=1.7 ; EPSI=.05 ; ALPHA=0.1 ; GAMMA=0.1 ; DZRO=1.0
58.  BETA= DMG/(2.*DELT*(RDX**2+RDY**2))
59.  ICPRT=INT(CWPRT)
60.  IF(ICPRT.EQ.1) ICPRT=2
61.  DO 100 I=1,IMAX

```

```

62.      H(I)=HN(I)=JT(I)=GX(I)=GY(I)=FRC(I)=0.0
63.      DO 100 J=1,JMAX
64.      100 U(I,J)=V(I,J)=UN(I,J)=VN(I,J)=P(I,J)=0.0
65.      *
66.      C * * SPECIAL INPUT DATA
67.      *
68.      READ(105,60)(H(I),I=2,IM1)
69.      READ(105,60)(HN(I),I=2,IM1)
70.      IF(FRK.GT.0.0) GO TO 120
71.      READ(105,60) (FRC(I),I=2,IM1)
72.      GO TO 130
73.      120 DO 125 I=2,IM1
74.      125 FRC(I)=FRK
75.      130 CONTINUE
76.      DO 150 I=2,IM1
77.      FR(I)=FRC(I)
78.      SP=HN(I)/DELX
79.      CP=SQRT(1.0-SP*SP)
80.      GX(I)=G*SP
81.      150 GY(I)=-G*CP
82.      WRITE(108,70)
83.      WRITE(108,61)(H(I),I=2,IM1)
84.      WRITE(108,71)
85.      WRITE(108,61)(HN(I),I=2,IM1)
86.      WRITE(108,72)
87.      WRITE(108,61) (FRC(I),I=2,IM1)
88.      WRITE(108,73)
89.      WRITE(108,61)(GX(I),I=2,IM1)
90.      WRITE(108,74)
91.      WRITE(108,61)(GY(I),I=2,IM1)
92.      WRITE(108,75)
93.      DO 240 I=2,IM1
94.      JT(I)=INT(H(I)*RDY+1.E-6)+2
95.      IF(JT(I).GT.JM1) JT(I)=JM1
96.      240 HN(I)=0.0
97.      H(1)= H(2)
98.      H(IMAX)= H(IM1)
99.      JT(1)= JT(2)
100.     JT(IMAX)= JT(IM1)
101.     *
102.     C * * CALCULATE HYDROSTATIC PRESSURE
103.     *
104.     DO 280 I=2,IM1
105.     JT1=JT(I)
106.     DO 280 J=2,JT1
107.     280 P(I,J)=-GY(I)*(H(I)-(FLOAT(J)-1.5)*DELY)
108.     ASSIGN 4280 TO KRET
109.     GO TO 2000
110.     *
111.     C * * START CYCLE
112.     *
113.     1000 CONTINUE
114.     ITER=0
115.     FLG=1.
116.     ASSIGN 3000 TO KRET
117.     *
118.     C * * COMPUTE TEMPORARY U AND V
119.     *
120.     DO 1100 I=2,IM1
121.     JT1=JT(I)
122.     DO 1100 J=2,JT1
123.     FUX=((UN(I,J)+UN(I+1,J))*(UN(I,J)+UN(I+1,J))+ALPHA*ABS(UN(I,J)+UN(
124.     1I+1,J))*(UN(I,J)-UN(I+1,J))-(UN(I-1,J)+UN(I,J))*(UN(I-1,J)+UN(I,J)
125.     2)-ALPHA*ABS(UN(I-1,J)+UN(I,J))*(UN(I-1,J)-UN(I,J)))/(4.*DELX)
126.     FUY=((VN(I,J)+VN(I+1,J))*(UN(I,J)+UN(I,J+1))

```

```

127.      1+ALPHA*ABS(VN(I,J)+VN(I+1,J))*(UN(I,J)-UN(I,J+1))
128.      2-(VN(I,J-1)+VN(I+1,J-1))*(UN(I,J-1)+UN(I,J))
129.      3-ALPHA*ABS(VN(I,J-1)+VN(I+1,J-1))*(UN(I,J-1)-UN(I,J))/(4.*DELY)
130.      FVX=((UN(I,J)+UN(I,J+1))*(VN(I,J)+VN(I+1,J))+ALPHA*ABS(UN(I,J)+UN(
131.      1I,J+1))*(VN(I,J)-VN(I+1,J))-(UN(I-1,J)+UN(I-1,J+1))*(VN(I-1,J)+VN(
132.      2I,J))-ALPHA*ABS(UN(I-1,J)+UN(I-1,J+1))*(VN(I-1,J)-VN(I,J))/(4.*DE
133.      3LX)
134.      FVY=((VN(I,J)+VN(I,J+1))*(VN(I,J)+VN(I,J+1))+ALPHA*ABS(VN(I,J)+VN
135.      1(I,J+1))*(VN(I,J)-VN(I,J+1))-(VN(I,J-1)+VN(I,J))*(VN(I,J-1)+VN(I,J
136.      2))-ALPHA*ABS(VN(I,J-1)+VN(I,J))*(VN(I,J-1)-VN(I,J))/(4.*DELY)
137.      VISX= NU*((UN(I+1,J)-2.*UN(I,J)+UN(I-1,J))/DELX**2+
138.      1      (UN(I,J+1)-2.*UN(I,J)+UN(I,J-1))/DELY**2)
139.      VISY= NU*((VN(I+1,J)-2.*VN(I,J)+VN(I-1,J))/DELX**2+
140.      1      (VN(I,J+1)-2.*VN(I,J)+VN(I,J-1))/DELY**2)
141.      U(I,J)= UN(I,J)+DELT*((P(I,J)-P(I+1,J))*RDX + GX(I)-FUX-FUY+VISX)
142.      1100 V(I,J)= VN(I,J)+DELT*((P(I,J)-P(I,J+1))*RDY + GY(I)-FVX-FVY+VISY)
143.      *
144. C * * SET BOUNDARY CONDITIONS
145.      *
146.      2000 CONTINUE
147.      HN(1)= HN(2)
148.      HN(IMAX)=HN(IM1)
149.      JT(1)=JT(2)
150.      JT(IMAX)=JT(IM1)
151. C   LEFT WALL RIGID AND SLIP FREE.
152. C   RIGHT WALL CONTINUOUS OUTFLOW.
153.      DO 2200 J=1,JMAX
154.      U(1,J)=0.0
155.      V(1,J)=V(2,J)
156.      IF(ITER.GT.0) GO TO 2200
157.      U(IM1,J)=U(IM2,J)
158.      V(IMAX,J)=V(IM1,J)
159.      2200 CONTINUE
160. C   TOP WALL CONTINUOUS OUTFLOW.
161. C   BOTTOM WALL RIGID - WITH FRICTION
162.      DO 2500 I=1,IMAX
163.      IF(ITER.GT.0) GO TO 2400
164.      V(I,JM1)=V(I,JM2)
165.      U(I,JMAX)=U(I,JM1)
166.      2400 V(I,1)=0.0
167.      2500 U(I,1)=U(I,2)*(1.0-2.0*FRC(I))
168.      *
169. C * * FREE SURFACE BOUNDARY CONDITIONS
170.      *
171.      DO 2650 I=2,IM1
172.      JT1=JT(I)
173.      IF(JT(I+1).LT.JT(I)) U(I,JT1)=U(I,JT1-1)
174.      V(I,JT1)= V(I,JT1-1)-DELY*RDX*(U(I,JT1)-U(I-1,JT1))
175.      2650 U(I,JT1+1)= U(I,JT1)
176.      GO TO KRET,(3000,4280)
177.      3000 CONTINUE
178.      *
179. C * * HAS CONVERGENCE BEEN REACHED
180.      *
181.      IF(FLG.EQ.0.) GO TO 4000
182.      ITER=ITER+1
183.      IF(ITER.LT.500) GO TO 3050
184.      IF(CYCLE.LT.10) GO TO 4000
185.      T=1.E+10
186.      GO TO 4000
187.      3050 FLG=0.0
188.      *
189. C * * COMPUTE UPDATED CELL PRESSURE AND VELOCITIES
190.      *
191.      JB1=2

```

```

192.      DO 3500 I=2,IM1
193.      JT1=JT(I)
194.      DO 3500 J=2,JT1
195.      IF(JT1.EQ.JB1) GO TO 3060
196.      IF(J.NE.JB1 .AND. J.NE.JT1) GO TO 3200
197.      IF(J.EQ.JT1) GO TO 3100
198.      GO TO 3200
199. 3060 CONTINUE
200.      F=V(I,J)+DELY*RDY*(U(I,J)-U(I-1,J))
201.      DFDP=DELT*RDY*(1.0+2.0*DELY**2*RDY**2)
202.      DELP1=-F/DFDP
203. 3100 ETA=DELY/(HN(I)-(FLOAT(JT1)-2.5)*DELY)
204.      DELP=(1.0-ETA)*P(I,JT1-1)-P(I,JT1)
205.      IF(JB1.EQ.JT1) DELP=0.5*(DELP+DELP1)
206.      GO TO 3300
207. 3200 D=RDY*(U(I,J)-U(I-1,J))+RDY*(V(I,J)-V(I,J-1))
208.      IF(ABS(D/DZRO).GE.EPSI) FLG=1.0
209.      DELP= -BETA*D
210. 3300 P(I,J)=P(I,J)+DELP
211.      U(I,J)=U(I,J)+DELT*RDY*DELP
212.      U(I-1,J)=U(I-1,J)-DELT*RDY*DELP
213.      V(I,J)=V(I,J)+DELT*RDY*DELP
214. 3500 V(I,J-1)=V(I,J-1)-DELT*RDY*DELP
215.      GO TO 2000
216. 4000 CONTINUE
217. *
218. C * * COMPUTE NEW POSITION FOR TOP SURFACE
219. *
220.      DO 4100 I=2,IM1
221.      JT1=JT(I)
222.      HV= RDY*(HN(I)-FLOAT(JT1-2)*DELY)
223.      UAV= 0.5*(U(I-1,JT1) + U(I,JT1))
224.      H(I)=HN(I)*FVOL1/FVOL+DELT*(HV*V(I,JT1)+(1.0-HV)*V(I,JT1
225. 1-1)-0.5*RDY*(UAV*HN(I+1)+GAMMA*ABS(UAV)*(HN(I)-HN(I+1))
226. 2 -UAV*HN(I-1)-GAMMA*ABS(UAV)*(HN(I-1)-HN(I))))
227. 4100 CONTINUE
228. *
229. C * * CALCULATE CELL IN WHICH SURFACE IS LOCATED AND UPDATE ARRAY
230. *
231.      DO 4250 I=2,IM1
232.      IF(H(I).LT.DELM) H(I)=0.0
233.      JT(I)=INT(H(I)*RDY+1.0E-6)+2
234.      IF(JT(I).GT.JM1) JT(I)=JM1
235. 4250 CONTINUE
236.      ASSIGN 4280 TO KRET
237.      GO TO 2000
238. 4280 CONTINUE
239. *
240. C * * CALCULATE TOTAL FLUID VOLUME
241. *
242.      FVOL=0.0
243.      DO 4300 I=2,IM1
244. 4300 FVOL=FVOL+H(I)*DELY
245.      IF(CYCLE.EQ.0) FVOL1=FVOL
246. *
247. C * * FIND LEADING AND TRAILING EDGES OF AVALANCHE AND LD. EDGE VELOCITY
248. *
249.      LDEG1=LDEG
250.      I=IM2
251. 4400 IF(H(I).GT.DELM) GO TO 4500
252.      I=I-1
253.      GO TO 4400
254. 4500 LDEG=I
255.      I=2
256. 4600 IF(H(I).GT.DELM) GO TO 4700

```

```

257.      I=I+1
258.      GO TO 4600
259.      4700 KTEG=I
260.      IF(LDEG.EQ.LDEG1) GO TO 4800
261.      IF(CYCLE.GT.0) UEDG=DELX/TC
262.      IF(CYCLE.EQ.0) UEDG=5.0
263.      TC=DELT
264.      INFLO=1
265.      IF(UEDG.GT.UEDG1) UEDG1=UEDG
266.      GO TO 4910
267.      4800 TC=TC+DELT
268.      INFLO=INFLO+1
269.      *
270.      C * * ADVANCE U,V,H ARRAYS.
271.      *
272.      4910 UMAX=VMAX=0.0
273.      DO 4900 I=1,IMAX
274.      DO 4900 J=1,JMAX
275.      IF(ABS(U(I,J)).GT.1.0E+04) U(I,J)=0.0
276.      UN(I,J)=U(I,J)
277.      IF(ABS(V(I,J)).GT.1.0E+04) V(I,J)=0.0
278.      VN(I,J)=V(I,J)
279.      IF(ABS(P(I,J)).LT.1.0E-16) P(I,J)=0.0
280.      4900 HN(I)=H(I)
281.      DO 4950 I=KTEG,LDEG
282.      DO 4950 J=2,JM1
283.      UT=ABS(UN(I,J))
284.      VT=ABS(VN(I,J))
285.      IF(UT.GT.UMAX) UMAX=UT
286.      4950 IF(VT.GT.VMAX) VMAX=VT
287.      *
288.      C * * LIST VELOCITY, PRESSURE, AND SURFACE POSITION
289.      *
290.      5000 WRITE(108,49) CYCLE,ITER,DELT,T,FVOL,UMAX,UEDG,LDEG
291.      IF(CYCLE.EQ.ICPRT) GO TO 5030
292.      IF(CYCLE.NE.ICPRT) GO TO 6000
293.      5030 ICPRT= ICPRT + INT(CWPRT)
294.      5060 CONTINUE
295.      WRITE(108,47)
296.      DO 5250 I=1,IMAX
297.      JT1= JT(I)
298.      JT2=JT1+1
299.      DO 5250 J=1,JT2
300.      WRITE(108,48) I,J,U(I,J),V(I,J),P(I,J),H(I),JT1
301.      5250 CONTINUE
302.      IF(IND.EQ.2) GO TO 6520
303.      IF(IND.EQ.3) GO TO 6530
304.      IF(IND.EQ.4) GO TO 6540
305.      *
306.      C * * RECOMPUTE CONTROL PARAMETERS.
307.      *
308.      6000 IF(CYCLE.EQ.0) GO TO 6300
309.      DTX=DELX/UMAX
310.      DTY=DELY/VMAX
311.      DELT=AMIN1(DTX,DTY)/3.0
312.      IF(ITER.LT.10) DELT=1.5*DELT
313.      IF(NU-1.E-6.LT.0.0) GO TO 6300
314.      DET=(DELX*DELY)**2/(2.*NU*(DELX**2+DELY**2))
315.      IF(DELT.LT.DET) GO TO 6300
316.      DELT=0.9*DET
317.      6300 T=T+DELT
318.      IF(CYCLE.EQ.0) GO TO 6400
319.      DAX=UMAX*DELT/DELX
320.      DAY=VMAX*DELT/DELY
321.      ALPHA=1.35*AMAX1(DAX,DAY)

```

```

322.      IF(ALPHA.GT.1.0) ALPHA=0.95
323.      GAMMA=ALPHA
324.      BETA=OMG/(2.*DELT*(RDX**2+RDY**2))
325.      *
326.      C * * TEST FOR PROGRAM TERMINATION.
327.      *
328.      6400 IF(T.GT.TWFIN) IND=2
329.      IF(H(IM2).GT.DELM) IND=3
330.      IF(UEDG.LT.0.05*UEDG1) IND=4
331.      IF(INFLO.EQ.50) IND=4
332.      IF(IND.GT.1) GO TO 6500
333.      IF(CYCLE.LT.3) GO TO 6440
334.      AA=1.0+20.0*EXP(-1.25*UEDG)
335.      DO 6430 I=2,IM1
336.      6430 FRC(I)=AA*FR(I)
337.      6440 CYCLE=CYCLE+1
338.      GO TO 1000
339.      6500 T=T-DELT
340.      GO TO 5060
341.      6520 WRITE(108,82)
342.      GO TO 6600
343.      6530 WRITE(108,83)
344.      GO TO 6600
345.      6540 WRITE(108,84)
346.      6600 STOP
347.      END

```

## Appendix C

### Listing of Output Data from AVALNCH for Ironton Park Avalanche

IRONTON PARK AVALANCHE PATH - HORIZONTAL GRID OPTION.  
IBAR=100. JBAR=2. DELX=10.00 DELY=2.00 NU=.50 FRK=.50 TWFIA=750. CWPRT=1000.

[illegible]

ELEVATION CHANGE FOR EACH CELL							
6.500	6.200	6.200	6.200	6.500	6.200	6.200	6.200
6.500	6.500	6.200	5.800	6.000	5.800	5.600	5.600
5.200	4.600	4.200	4.200	4.600	5.200	4.600	4.800
5.000	5.200	5.400	5.600	5.800	6.200	6.200	6.200
6.200	6.500	6.800	7.400	7.200	7.200	7.100	7.000
7.000	7.000	6.600	6.200	6.200	6.000	6.000	5.600
5.200	5.200	5.000	4.600	4.200	4.200	4.000	4.000
3.600	3.600	3.400	3.400	3.000	2.800	2.500	2.200
1.800	1.600	1.400	1.200	.900	.700	.500	.400
.300	.100	.000	.000	.000	.000	.000	.000
.000	.000	.000	.000	.000	.000	.000	.000
.000	.000	.000	.000	.000	.000	.000	.000
.000	.000	.000	.000				

[illegible]

SLOPE-PARALLEL GRAVITY COMPONENT							
6.370	6.076	6.076	6.076	6.370	6.076	6.076	6.076
6.370	6.370	6.076	5.684	5.880	5.684	5.488	5.488
5.096	4.508	4.116	4.116	4.508	5.096	4.508	4.704
4.900	5.096	5.292	5.488	5.684	6.076	6.076	6.076
6.076	6.370	6.664	7.252	7.056	7.056	6.958	6.860
6.860	6.860	6.468	6.076	6.076	5.880	5.880	5.488
5.096	5.096	4.900	4.508	4.116	4.116	3.920	3.920
3.528	3.528	3.332	3.332	2.940	2.744	2.450	2.156
1.764	1.568	1.372	1.176	.882	.686	.490	.392
.294	.098	.000	.000	.000	.000	.000	.000
.000	.000	.000	.000	.000	.000	.000	.000
.000	.000	.000	.000	.000	.000	.000	.000
.000	.000	.000	.000				

[illegible]

END OF INPUT DATA





CYCLE=176	ITER= 1	DELT= 2.39E-01	TIME= 2.81E 01	FVOL= 1.29E 02	UMAX= 2.12E 01	UECG= 1.04E 01	LCEG= 87
CYCLE=177	ITER= 5	DELT= 2.36E-01	TIME= 2.84E 01	FVOL= 1.29E 02	UMAX= 2.13E 01	UECG= 1.04E 01	LCEG= 87
CYCLE=178	ITER= 4	DELT= 2.35E-01	TIME= 2.86E 01	FVOL= 1.28E 02	UMAX= 1.97E 01	UECG= 1.04E 01	LCEG= 87
CYCLE=179	ITER= 1	DELT= 2.54E-01	TIME= 2.88E 01	FVOL= 1.29E 02	UMAX= 2.00E 01	UECG= 8.65E 00	LCEG= 88
CYCLE=180	ITER= 4	DELT= 2.50E-01	TIME= 2.91E 01	FVOL= 1.29E 02	UMAX= 2.01E 01	UECG= 8.65E 00	LCEG= 88
CYCLE=181	ITER= 5	DELT= 2.49E-01	TIME= 2.93E 01	FVOL= 1.29E 02	UMAX= 1.84E 01	UECG= 8.65E 00	LCEG= 88
CYCLE=182	ITER= 4	DELT= 2.72E-01	TIME= 2.96E 01	FVOL= 1.28E 02	UMAX= 1.87E 01	UECG= 8.65E 00	LCEG= 88
CYCLE=183	ITER= 4	DELT= 2.67E-01	TIME= 2.99E 01	FVOL= 1.28E 02	UMAX= 1.73E 01	UECG= 9.75E 00	LCEG= 89
CYCLE=184	ITER= 1	DELT= 2.89E-01	TIME= 3.02E 01	FVOL= 1.31E 02	UMAX= 1.68E 01	UECG= 9.75E 00	LCEG= 89
CYCLE=185	ITER= 5	DELT= 2.73E-01	TIME= 3.04E 01	FVOL= 1.29E 02	UMAX= 1.72E 01	UECG= 9.75E 00	LCEG= 89
CYCLE=186	ITER= 5	DELT= 2.90E-01	TIME= 3.07E 01	FVOL= 1.28E 02	UMAX= 1.75E 01	UECG= 9.75E 00	LCEG= 89
CYCLE=187	ITER= 4	DELT= 2.86E-01	TIME= 3.10E 01	FVOL= 1.28E 02	UMAX= 1.55E 01	UECG= 8.93E 00	LCEG= 90
CYCLE=188	ITER= 1	DELT= 2.96E-01	TIME= 3.13E 01	FVOL= 1.30E 02	UMAX= 1.60E 01	UECG= 8.93E 00	LCEG= 90
CYCLE=189	ITER= 4	DELT= 2.94E-01	TIME= 3.16E 01	FVOL= 1.28E 02	UMAX= 1.62E 01	UECG= 8.93E 00	LCEG= 90
CYCLE=190	ITER= 5	DELT= 3.08E-01	TIME= 3.19E 01	FVOL= 1.28E 02	UMAX= 1.41E 01	UECG= 8.93E 00	LCEG= 90
CYCLE=191	ITER= 5	DELT= 3.53E-01	TIME= 3.23E 01	FVOL= 1.28E 02	UMAX= 1.48E 01	UECG= 8.45E 00	LCEG= 91
CYCLE=192	ITER= 1	DELT= 2.14E-01	TIME= 3.25E 01	FVOL= 1.30E 02	UMAX= 1.50E 01	UECG= 8.45E 00	LCEG= 91
CYCLE=193	ITER= 4	DELT= 3.16E-01	TIME= 3.28E 01	FVOL= 1.28E 02	UMAX= 1.22E 01	UECG= 8.45E 00	LCEG= 91
CYCLE=194	ITER= 4	DELT= 3.28E-01	TIME= 3.31E 01	FVOL= 1.29E 02	UMAX= 1.26E 01	UECG= 8.45E 00	LCEG= 91
CYCLE=195	ITER= 5	DELT= 3.49E-01	TIME= 3.35E 01	FVOL= 1.28E 02	UMAX= 1.33E 01	UECG= 8.45E 00	LCEG= 91
CYCLE=196	ITER= 1	DELT= 3.76E-01	TIME= 3.39E 01	FVOL= 1.30E 02	UMAX= 1.38E 01	UECG= 6.41E 00	LCEG= 92
CYCLE=197	ITER= 8	DELT= 1.80E-01	TIME= 3.40E 01	FVOL= 1.29E 02	UMAX= 1.05E 01	UECG= 6.41E 00	LCEG= 92
CYCLE=198	ITER= 4	DELT= 3.74E-01	TIME= 3.44E 01	FVOL= 1.29E 02	UMAX= 1.10E 01	UECG= 6.41E 00	LCEG= 92
CYCLE=199	ITER= 4	DELT= 2.77E-01	TIME= 3.47E 01	FVOL= 1.29E 02	UMAX= 1.13E 01	UECG= 6.41E 00	LCEG= 92
CYCLE=200	ITER= 1	DELT= 3.99E-01	TIME= 3.51E 01	FVOL= 1.31E 02	UMAX= 1.16E 01	UECG= 6.41E 00	LCEG= 92
CYCLE=201	ITER= 4	DELT= 3.09E-01	TIME= 3.54E 01	FVOL= 1.28E 02	UMAX= 1.21E 01	UECG= 6.23E 00	LCEG= 93
CYCLE=202	ITER= 3	DELT= 2.06E-01	TIME= 3.56E 01	FVOL= 1.29E 02	UMAX= 8.96E 00	UECG= 6.23E 00	LCEG= 93
CYCLE=203	ITER= 6	DELT= 3.61E-01	TIME= 3.60E 01	FVOL= 1.30E 02	UMAX= 9.39E 00	UECG= 6.23E 00	LCEG= 93
CYCLE=204	ITER= 1	DELT= 2.70E-01	TIME= 3.62E 01	FVOL= 1.28E 02	UMAX= 9.40E 00	UECG= 6.23E 00	LCEG= 93
CYCLE=205	ITER= 4	DELT= 3.73E-01	TIME= 3.66E 01	FVOL= 1.29E 02	UMAX= 9.44E 00	UECG= 6.23E 00	LCEG= 93
CYCLE=206	ITER= 4	DELT= 2.92E-01	TIME= 3.69E 01	FVOL= 1.29E 02	UMAX= 9.75E 00	UECG= 6.23E 00	LCEG= 93
CYCLE=207	ITER= 1	DELT= 4.42E-01	TIME= 3.73E 01	FVOL= 1.29E 02	UMAX= 1.04E 01	UECG= 5.52E 00	LCEG= 94
CYCLE=208	ITER= 3	DELT= 1.65E-01	TIME= 3.75E 01	FVOL= 1.30E 02	UMAX= 1.06E 01	UECG= 5.52E 00	LCEG= 94
CYCLE=209	ITER= 5	DELT= 3.96E-01	TIME= 3.79E 01	FVOL= 1.30E 02	UMAX= 8.70E 00	UECG= 5.52E 00	LCEG= 94
CYCLE=210	ITER= 1	DELT= 2.55E-01	TIME= 3.82E 01	FVOL= 1.29E 02	UMAX= 8.56E 00	UECG= 5.52E 00	LCEG= 94
CYCLE=211	ITER= 3	DELT= 3.99E-01	TIME= 3.86E 01	FVOL= 1.29E 02	UMAX= 8.26E 00	UECG= 5.52E 00	LCEG= 94
CYCLE=212	ITER= 3	DELT= 2.76E-01	TIME= 3.88E 01	FVOL= 1.29E 02	UMAX= 7.87E 00	UECG= 5.52E 00	LCEG= 94
CYCLE=213	ITER= 1	DELT= 4.50E-01	TIME= 3.93E 01	FVOL= 1.32E 02	UMAX= 8.18E 00	UECG= 5.17E 00	LCEG= 95
CYCLE=214	ITER= 3	DELT= 1.64E-01	TIME= 3.94E 01	FVOL= 1.30E 02	UMAX= 8.23E 00	UECG= 5.17E 00	LCEG= 95
CYCLE=215	ITER= 6	DELT= 3.95E-01	TIME= 3.98E 01	FVOL= 1.29E 02	UMAX= 8.59E 00	UECG= 5.17E 00	LCEG= 95
CYCLE=216	ITER= 1	DELT= 2.53E-01	TIME= 4.01E 01	FVOL= 1.29E 02	UMAX= 8.87E 00	UECG= 5.17E 00	LCEG= 95
CYCLE=217	ITER= 3	DELT= 3.86E-01	TIME= 4.05E 01	FVOL= 1.29E 02	UMAX= 7.56E 00	UECG= 5.17E 00	LCEG= 95
CYCLE=218	ITER= 3	DELT= 2.78E-01	TIME= 4.08E 01	FVOL= 1.30E 02	UMAX= 7.25E 00	UECG= 5.17E 00	LCEG= 95
CYCLE=219	ITER= 1	DELT= 4.18E-01	TIME= 4.12E 01	FVOL= 1.31E 02	UMAX= 6.76E 00	UECG= 5.19E 00	LCEG= 96
CYCLE=220	ITER= 3	DELT= 1.77E-01	TIME= 4.14E 01	FVOL= 1.30E 02	UMAX= 6.69E 00	UECG= 5.19E 00	LCEG= 96
CYCLE=221	ITER= 3	DELT= 3.74E-01	TIME= 4.17E 01	FVOL= 1.30E 02	UMAX= 6.80E 00	UECG= 5.19E 00	LCEG= 96
CYCLE=222	ITER= 5	DELT= 2.56E-01	TIME= 4.20E 01	FVOL= 1.30E 02	UMAX= 6.91E 00	UECG= 5.19E 00	LCEG= 96
CYCLE=223	ITER= 4	DELT= 3.48E-01	TIME= 4.23E 01	FVOL= 1.30E 02	UMAX= 6.83E 00	UECG= 5.19E 00	LCEG= 96
CYCLE=224	ITER= 1	DELT= 2.95E-01	TIME= 4.26E 01	FVOL= 1.31E 02	UMAX= 6.90E 00	UECG= 5.19E 00	LCEG= 96
CYCLE=225	ITER= 5	DELT= 3.53E-01	TIME= 4.30E 01	FVOL= 1.29E 02	UMAX= 6.93E 00	UECG= 5.19E 00	LCEG= 96
CYCLE=226	ITER= 4	DELT= 3.05E-01	TIME= 4.33E 01	FVOL= 1.29E 02	UMAX= 7.39E 00	UECG= 5.19E 00	LCEG= 96
CYCLE=227	ITER= 1	DELT= 3.64E-01	TIME= 4.37E 01	FVOL= 1.31E 02	UMAX= 7.85E 00	UECG= 3.96E 00	LCEG= 97
CYCLE=228	ITER= 3	DELT= 2.00E-01	TIME= 4.39E 01	FVOL= 1.30E 02	UMAX= 8.03E 00	UECG= 3.96E 00	LCEG= 97
CYCLE=229	ITER= 3	DELT= 3.61E-01	TIME= 4.42E 01	FVOL= 1.31E 02	UMAX= 5.90E 00	UECG= 3.96E 00	LCEG= 97
CYCLE=230	ITER= 8	DELT= 2.62E-01	TIME= 4.45E 01	FVOL= 1.31E 02	UMAX= 5.98E 00	UECG= 3.96E 00	LCEG= 97
CYCLE=231	ITER= 1	DELT= 3.36E-01	TIME= 4.48E 01	FVOL= 1.31E 02	UMAX= 5.87E 00	UECG= 3.96E 00	LCEG= 97
CYCLE=232	ITER= 4	DELT= 2.93E-01	TIME= 4.51E 01	FVOL= 1.31E 02	UMAX= 5.86E 00	UECG= 3.96E 00	LCEG= 97
CYCLE=233	ITER= 5	DELT= 3.32E-01	TIME= 4.54E 01	FVOL= 1.30E 02	UMAX= 5.69E 00	UECG= 3.96E 00	LCEG= 97
CYCLE=234	ITER= 1	DELT= 3.16E-01	TIME= 4.58E 01	FVOL= 1.31E 02	UMAX= 5.48E 00	UECG= 3.96E 00	LCEG= 97
CYCLE=235	ITER= 3	DELT= 3.33E-01	TIME= 4.61E 01	FVOL= 1.30E 02	UMAX= 5.32E 00	UECG= 3.96E 00	LCEG= 97
CYCLE=236	ITER= 5	DELT= 3.17E-01	TIME= 4.64E 01	FVOL= 1.30E 02	UMAX= 5.15E 00	UECG= 3.96E 00	LCEG= 97
CYCLE=237	ITER= 4	DELT= 3.30E-01	TIME= 4.67E 01	FVOL= 1.30E 02	UMAX= 5.03E 00	UECG= 3.21E 00	LCEG= 98

I	J	U	V	P	H	SUR CELL
1	1	.000E 00	.000E 00	.000E 00	2.000E 00	2
1	2	.000E 00	-2.009E 00	.000E 00	2.000E 00	2
1	3	.000E 00	-5.531E 00	.000E 00	2.000E 00	2
2	1	-1.423E 00	.000E 00	.000E 00	.000E 00	2
2	2	1.004E 01	-2.009E 00	.000E 00	.000E 00	2
2	3	1.004E 01	-5.531E 00	-6.251E 00	.000E 00	2
3	1	-1.926E 00	.000E 00	.000E 00	.000E 00	2
3	2	1.359E 01	-7.097E 01	.000E 00	.000E 00	2
3	3	1.359E 01	-3.288E 00	-7.286E 00	.000E 00	2
4	1	-2.291E 00	.000E 00	.000E 00	.000E 00	2
4	2	1.617E 01	-5.152E 01	.000E 00	.000E 00	2
4	3	1.617E 01	-2.329E 00	-7.607E 00	.000E 00	2
5	1	-2.577E 00	.000E 00	.000E 00	.000E 00	2
5	2	1.819E 01	-4.042E 01	.000E 00	.000E 00	2
5	3	1.819E 01	-2.129E 00	-7.575E 00	.000E 00	2
6	1	-2.845E 00	.000E 00	.000E 00	.000E 00	2
6	2	2.008E 01	-3.783E 01	.000E 00	.000E 00	2
6	3	2.008E 01	-2.005E 00	-7.257E 00	.000E 00	2
7	1	-3.054E 00	.000E 00	.000E 00	.000E 00	2
7	2	2.155E 01	-2.947E 01	.000E 00	.000E 00	2
7	3	2.155E 01	-2.026E 00	-7.351E 00	.000E 00	2
8	1	-3.239E 00	.000E 00	.000E 00	.000E 00	2
8	2	2.286E 01	-2.614E 01	.000E 00	.000E 00	2
8	3	2.286E 01	-4.194E 00	.000E 00	.000E 00	2

9	1	-3.402E 00	.000E 00	.000E 00	.000E 00	2
9	2	2.401E 01	-2.296E-01	.000E 00	.000E 00	2
9	3	2.401E 01	-4.094E 00	.000E 00	.000E 00	2
10	1	-3.567E 00	.000E 00	.000E 00	.000E 00	2
10	2	2.518E 01	-2.339E-01	.000E 00	.000E 00	2
10	3	2.518E 01	-3.870E 00	.000E 00	.000E 00	2
11	1	-3.720E 00	.000E 00	.000E 00	.000E 00	2
11	2	2.626E 01	-2.162E-01	.000E 00	.000E 00	2
11	3	2.626E 01	-3.865E 00	.000E 00	.000E 00	2
12	1	-3.848E 00	.000E 00	.000E 00	.000E 00	2
12	2	2.716E 01	-1.802E-01	.000E 00	.000E 00	2
12	3	2.716E 01	-3.988E 00	.000E 00	.000E 00	2
13	1	-3.941E 00	.000E 00	.000E 00	.000E 00	2
13	2	2.782E 01	-1.317E-01	.000E 00	.000E 00	2
13	3	2.782E 01	-4.086E 00	.000E 00	.000E 00	2
14	1	-4.041E 00	.000E 00	.000E 00	.000E 00	2
14	2	2.852E 01	-1.412E-01	.000E 00	.000E 00	2
14	3	2.852E 01	-3.911E 00	.000E 00	.000E 00	2
15	1	-4.126E 00	.000E 00	.000E 00	.000E 00	2
15	2	2.912E 01	-1.197E-01	.000E 00	.000E 00	2
15	3	2.912E 01	-4.017E 00	.000E 00	.000E 00	2
16	1	-4.195E 00	.000E 00	.000E 00	.000E 00	2
16	2	2.961E 01	-9.672E-02	.000E 00	.000E 00	2
16	3	2.961E 01	-4.053E 00	.000E 00	.000E 00	2
17	1	-4.263E 00	.000E 00	.000E 00	.000E 00	2
17	2	3.009E 01	-9.571E-02	.000E 00	.000E 00	2
17	3	3.009E 01	-4.019E 00	.000E 00	.000E 00	2
18	1	-4.311E 00	.000E 00	.000E 00	.000E 00	2
18	2	3.043E 01	-6.871E-02	.000E 00	.000E 00	2
18	3	3.043E 01	-4.194E 00	.000E 00	.000E 00	2
19	1	-4.331E 00	.000E 00	.000E 00	.000E 00	2
19	2	3.057E 01	-2.737E-02	.000E 00	.000E 00	2
19	3	3.057E 01	-4.361E 00	.000E 00	.000E 00	2
20	1	-4.329E 00	.000E 00	.000E 00	.000E 00	2
20	2	3.056E 01	1.599E-03	.000E 00	.000E 00	2
20	3	3.056E 01	-4.391E 00	.000E 00	.000E 00	2
21	1	-4.326E 00	.000E 00	.000E 00	.000E 00	2
21	2	3.054E 01	4.300E-03	.000E 00	.000E 00	2
21	3	3.054E 01	-4.317E 00	.000E 00	.000E 00	2
22	1	-4.338E 00	.000E 00	.000E 00	.000E 00	2
22	2	3.062E 01	-1.624E-02	.000E 00	.000E 00	2
22	3	3.062E 01	-4.166E 00	.000E 00	.000E 00	2
23	1	-4.386E 00	.000E 00	.000E 00	.000E 00	2
23	2	3.096E 01	-6.769E-02	.000E 00	.000E 00	2
23	3	3.096E 01	-4.036E 00	.000E 00	.000E 00	2
24	1	-4.400E 00	.000E 00	.000E 00	.000E 00	2
24	2	3.105E 01	-1.947E-02	.000E 00	.000E 00	2
24	3	3.105E 01	-4.334E 00	.000E 00	.000E 00	2
25	1	-4.422E 00	.000E 00	.000E 00	.000E 00	2
25	2	3.121E 01	-3.152E-02	.000E 00	.000E 00	2
25	3	3.121E 01	-4.161E 00	.000E 00	.000E 00	2
26	1	-4.452E 00	.000E 00	.000E 00	.000E 00	2
26	2	3.142E 01	-4.278E-02	.000E 00	.000E 00	2
26	3	3.142E 01	-4.108E 00	.000E 00	.000E 00	2
27	1	-4.490E 00	.000E 00	.000E 00	.000E 00	2
27	2	3.169E 01	-5.281E-02	.000E 00	.000E 00	2
27	3	3.169E 01	-4.048E 00	.000E 00	.000E 00	2
28	1	-4.533E 00	.000E 00	.000E 00	.000E 00	2
28	2	3.200E 01	-6.150E-02	.000E 00	.000E 00	2
28	3	3.200E 01	-3.982E 00	.000E 00	.000E 00	2
29	1	-4.583E 00	.000E 00	.000E 00	.000E 00	2
29	2	3.235E 01	-7.023E-02	.000E 00	.000E 00	2
29	3	3.235E 01	-3.912E 00	.000E 00	.000E 00	2
30	1	-4.626E 00	.000E 00	.000E 00	.000E 00	2
30	2	3.272E 01	-7.532E-02	.000E 00	.000E 00	2
30	3	3.272E 01	-3.827E 00	.000E 00	.000E 00	2
31	1	-4.706E 00	.000E 00	.000E 00	.000E 00	2
31	2	3.322E 01	-9.850E-02	.000E 00	.000E 00	2
31	3	3.322E 01	-3.654E 00	.000E 00	.000E 00	2
32	1	-4.772E 00	.000E 00	.000E 00	.000E 00	2
32	2	3.368E 01	-9.293E-02	.000E 00	.000E 00	2
32	3	3.368E 01	-3.694E 00	.000E 00	.000E 00	2
33	1	-4.835E 00	.000E 00	.000E 00	.000E 00	2
33	2	3.412E 01	-8.851E-02	.000E 00	.000E 00	2
33	3	3.412E 01	-3.683E 00	.000E 00	.000E 00	2
34	1	-4.892E 00	.000E 00	.000E 00	.000E 00	2
34	2	3.453E 01	-8.079E-02	.000E 00	.000E 00	2
34	3	3.453E 01	-3.662E 00	.000E 00	.000E 00	2
35	1	-4.958E 00	.000E 00	.000E 00	.000E 00	2
35	2	3.500E 01	-9.378E-02	.000E 00	.000E 00	2
35	3	3.500E 01	-3.492E 00	.000E 00	.000E 00	2
36	1	-5.029E 00	.000E 00	.000E 00	.000E 00	2
36	2	3.550E 01	-1.003E-01	.000E 00	.000E 00	2
36	3	3.550E 01	-3.337E 00	.000E 00	.000E 00	2
37	1	-5.125E 00	.000E 00	.000E 00	.000E 00	2
37	2	3.617E 01	-1.345E-01	.000E 00	.000E 00	2
37	3	3.617E 01	-3.012E 00	.000E 00	.000E 00	2

38	1	-5.206E 00	.000E 00	.000E 00	.000E 00	2
38	2	3.674E 01	-1.146E-01	.000E 00	.000E 00	2
38	3	3.674E 01	-3.192E 00	.000E 00	.000E 00	2
39	1	-5.284E 00	.000E 00	.000E 00	.000E 00	2
39	2	3.729E 01	-1.101E-01	.000E 00	.000E 00	2
39	3	3.729E 01	-3.157E 00	.000E 00	.000E 00	2
40	1	-5.355E 00	.000E 00	.000E 00	.000E 00	2
40	2	3.780E 01	-1.002E-01	.000E 00	.000E 00	2
40	3	3.780E 01	-3.208E 00	.000E 00	.000E 00	2
41	1	-5.418E 00	.000E 00	.000E 00	.000E 00	2
41	2	3.824E 01	-8.955E-02	.000E 00	.000E 00	2
41	3	3.824E 01	-3.244E 00	.000E 00	.000E 00	2
42	1	-5.478E 00	.000E 00	.000E 00	.000E 00	2
42	2	3.867E 01	-8.441E-02	.000E 00	.000E 00	2
42	3	3.867E 01	-3.220E 00	.000E 00	.000E 00	2
43	1	-5.538E 00	.000E 00	.000E 00	.000E 00	2
43	2	3.909E 01	-8.475E-02	.000E 00	.000E 00	2
43	3	3.909E 01	-3.220E 00	.000E 00	.000E 00	2
44	1	-5.584E 00	.000E 00	.000E 00	.000E 00	2
44	2	3.941E 01	-6.448E-02	.000E 00	.000E 00	2
44	3	3.941E 01	-3.450E 00	.000E 00	.000E 00	2
45	1	-5.611E 00	.000E 00	.000E 00	.000E 00	2
45	2	3.960E 01	-3.823E-02	.000E 00	.000E 00	2
45	3	3.960E 01	-3.599E 00	.000E 00	.000E 00	2
46	1	-5.633E 00	.000E 00	.000E 00	.000E 00	2
46	2	3.976E 01	-3.168E-02	.000E 00	.000E 00	2
46	3	3.976E 01	-3.542E 00	.000E 00	.000E 00	2
47	1	-5.640E 00	.000E 00	.000E 00	.000E 00	2
47	2	3.981E 01	-9.665E-03	.000E 00	.000E 00	2
47	3	3.981E 01	-3.639E 00	.000E 00	.000E 00	2
48	1	-5.654E 00	.000E 00	.000E 00	.000E 00	2
48	2	3.991E 01	-1.945E-02	.000E 00	.000E 00	2
48	3	3.991E 01	-3.642E 00	.000E 00	.000E 00	2
49	1	-5.679E 00	.000E 00	.000E 00	.000E 00	2
49	2	4.008E 01	-3.525E-02	.000E 00	.000E 00	2
49	3	4.008E 01	-3.871E 00	.000E 00	.000E 00	2
50	1	-5.716E 00	.000E 00	.000E 00	.000E 00	2
50	2	4.034E 01	-5.193E-02	.000E 00	.000E 00	2
50	3	4.034E 01	-3.980E 00	.000E 00	.000E 00	2
51	1	-5.737E 00	.000E 00	.000E 00	.000E 00	2
51	2	4.049E 01	-2.971E-02	.000E 00	.000E 00	2
51	3	4.049E 01	-3.839E 00	.000E 00	.000E 00	2
52	1	-5.649E 00	.000E 00	.000E 00	.000E 00	2
52	2	3.987E 01	1.234E-01	.000E 00	.000E 00	2
52	3	3.987E 01	-3.793E 00	.000E 00	.000E 00	2
53	1	-5.417E 00	.000E 00	.000E 00	.000E 00	2
53	2	3.823E 01	3.282E-01	.000E 00	.000E 00	2
53	3	3.823E 01	-3.976E 00	.000E 00	.000E 00	2
54	1	-5.254E 00	.000E 00	.000E 00	.000E 00	2
54	2	3.703E 01	2.302E-01	.000E 00	.000E 00	2
54	3	3.703E 01	-4.537E 00	.000E 00	.000E 00	2
55	1	-5.654E 00	.000E 00	.000E 00	.000E 00	2
55	2	3.990E 01	-5.645E-01	.000E 00	.000E 00	2
55	3	3.990E 01	-5.043E 00	.000E 00	.000E 00	2
56	1	-6.430E 00	.000E 00	.000E 00	.000E 00	2
56	2	4.538E 01	-1.095E 00	.000E 00	.000E 00	2
56	3	4.538E 01	-4.641E 00	.000E 00	.000E 00	2
57	1	-5.829E 00	.000E 00	.000E 00	.000E 00	2
57	2	4.114E 01	8.484E-01	.000E 00	.000E 00	2
57	3	4.114E 01	-2.205E 00	.000E 00	.000E 00	2
58	1	-3.841E 00	.000E 00	.000E 00	.000E 00	2
58	2	2.711E 01	2.806E 00	.000E 00	.000E 00	2
58	3	2.711E 01	-3.699E 00	.000E 00	.000E 00	2
59	1	-2.874E 00	.000E 00	.000E 00	.000E 00	2
59	2	2.028E 01	1.365E 00	.000E 00	.000E 00	2
59	3	2.028E 01	-9.730E 00	.000E 00	.000E 00	2
60	1	-5.405E 00	.000E 00	.000E 00	.000E 00	2
60	2	3.815E 01	-3.573E 00	.000E 00	.000E 00	2
60	3	3.815E 01	-1.214E 01	.000E 00	.000E 00	2
61	1	-1.038E 01	.000E 00	.000E 00	.000E 00	2
61	2	7.328E 01	-7.026E 00	.000E 00	.000E 00	2
61	3	7.328E 01	-8.137E 00	.000E 00	.000E 00	2
62	1	-2.666E 00	.000E 00	.000E 00	.000E 00	2
62	2	1.881E 01	1.089E 01	.000E 00	.000E 00	2
62	3	1.881E 01	-2.558E 01	.000E 00	.000E 00	2
63	1	-6.887E-01	.000E 00	.000E 00	.000E 00	2
63	2	4.861E 00	2.790E 00	.000E 00	.000E 00	2
63	3	4.861E 00	-1.535E 01	.000E 00	.000E 00	2
64	1	2.080E 00	.000E 00	.000E 00	.000E 00	2
64	2	-1.468E 01	3.908E 00	.000E 00	.000E 00	2
64	3	-1.468E 01	-1.236E 01	.000E 00	.000E 00	2
65	1	3.369E 00	.000E 00	.000E 00	.000E 00	2
65	2	-2.378E 01	1.820E 00	.000E 00	.000E 00	2
65	3	-2.378E 01	.000E 00	.000E 00	.000E 00	2
66	1	1.056E 01	.000E 00	.000E 00	.000E 00	2
66	2	-7.450E 01	1.014E 01	.000E 00	.000E 00	2
66	3	-7.450E 01	-2.740E 03	.000E 00	.000E 00	2

67	1	1.544E 02	.000E 00	.000E 00	.000E 00	2
67	2	-1.090E 03	2.030E 02	.000E 00	.000E 00	2
67	3	-1.090E 03	2.925E 01	.000E 00	.000E 00	2
68	1	3.940E 02	.000E 00	.000E 00	.000E 00	2
68	2	-2.781E 03	3.383E 02	.000E 00	.000E 00	2
68	3	-2.781E 03	-1.815E 03	.000E 00	.000E 00	2
69	1	4.929E 02	.000E 00	.000E 00	.000E 00	2
69	2	-3.479E 03	1.396E 02	.000E 00	.000E 00	2
69	3	-3.479E 03	-6.194E 03	.000E 00	.000E 00	2
70	1	1.260E 03	.000E 00	.000E 00	.000E 00	2
70	2	-8.891E 03	1.082E 03	.000E 00	.000E 00	2
70	3	-8.891E 03	.000E 00	.000E 00	.000E 00	2
71	1	-2.357E 03	.000E 00	.000E 00	.000E 00	2
71	2	.000E 00	-5.106E 03	.000E 00	.000E 00	2
71	3	.000E 00	.000E 00	.000E 00	.000E 00	2
72	1	2.421E-01	.000E 00	.000E 00	.000E 00	2
72	2	-1.709E 00	3.328E 03	.000E 00	.000E 00	2
72	3	-1.709E 00	3.904E 01	.000E 00	.000E 00	2
73	1	2.039E 00	.000E 00	.000E 00	.000E 00	2
73	2	-1.439E 01	2.537E 00	.000E 00	.000E 00	2
73	3	-1.439E 01	-2.543E 00	.000E 00	.000E 00	2
74	1	9.794E 00	.000E 00	.000E 00	.000E 00	2
74	2	-6.913E 01	1.095E 01	.000E 00	.000E 00	2
74	3	-6.913E 01	-2.468E 01	.000E 00	.000E 00	2
75	1	1.436E 01	.000E 00	.000E 00	.000E 00	2
75	2	-1.014E 02	6.448E 00	.000E 00	.000E 00	2
75	3	-1.014E 02	-1.367E 02	-8.413E 00	.000E 00	2
76	1	-4.431E 01	.000E 00	.000E 00	.000E 00	2
76	2	3.128E 02	-8.282E 01	.000E 00	.000E 00	2
76	3	3.128E 02	-1.421E 02	-9.824E 00	.000E 00	2
77	1	-2.413E 00	.000E 00	.000E 00	.000E 00	2
77	2	1.703E 01	5.915E 01	.000E 00	.000E 00	2
77	3	1.703E 01	6.673E 00	-8.744E 00	.000E 00	2
78	1	-3.533E 00	.000E 00	.000E 00	.000E 00	2
78	2	2.494E 01	-1.582E 00	.000E 00	.000E 00	2
78	3	2.494E 01	-4.751E 00	-8.764E 00	.000E 00	2
79	1	-4.172E 00	.000E 00	.000E 00	.000E 00	2
79	2	2.945E 01	-9.023E-01	.000E 00	.000E 00	2
79	3	2.945E 01	-2.832E 00	-8.946E 00	.000E 00	2
80	1	-3.068E 00	.000E 00	.000E 00	.000E 00	2
80	2	2.166E 01	1.558E 00	.000E 00	.000E 00	2
80	3	2.166E 01	-3.199E-01	-8.960E 00	.000E 00	2
81	1	-2.656E 00	.000E 00	.000E 00	.000E 00	2
81	2	1.875E 01	5.816E-01	.000E 00	.000E 00	2
81	3	1.875E 01	-1.477E 00	-3.650E 00	.000E 00	2
82	1	-2.589E 00	.000E 00	.000E 00	.000E 00	2
82	2	1.827E 01	9.567E-02	.000E 00	.000E 00	2
82	3	1.827E 01	-1.820E 00	-9.035E 00	.000E 00	2
83	1	-2.316E 00	.000E 00	.000E 00	.000E 00	2
83	2	1.635E 01	3.844E-01	.000E 00	.000E 00	2
83	3	1.635E 01	-1.287E 00	-1.028E 01	.000E 00	2
84	1	-2.101E 00	.000E 00	.000E 00	.000E 00	2
84	2	1.483E 01	3.039E-01	.000E 00	.000E 00	2
84	3	1.483E 01	-1.622E 00	-9.358E 00	.000E 00	2
85	1	-1.939E 00	.000E 00	.000E 00	.000E 00	2
85	2	1.369E 01	2.285E-01	.000E 00	.000E 00	2
85	3	1.369E 01	-1.672E 00	-9.406E 00	.000E 00	2
86	1	-1.767E 00	.000E 00	.000E 00	.000E 00	2
86	2	1.247E 01	2.436E-01	.000E 00	.000E 00	2
86	3	1.247E 01	-1.709E 00	-9.152E 00	.000E 00	2
87	1	-1.599E 00	.000E 00	.000E 00	.000E 00	2
87	2	1.128E 01	2.372E-01	.000E 00	.000E 00	2
87	3	1.128E 01	-1.883E 00	-8.439E 00	.000E 00	2
88	1	-1.439E 00	.000E 00	.000E 00	.000E 00	2
88	2	1.015E 01	2.260E-01	.000E 00	.000E 00	2
88	3	1.015E 01	-1.308E 00	-1.118E 01	.000E 00	2
89	1	-1.279E 00	.000E 00	.000E 00	.000E 00	2
89	2	9.027E 00	2.254E-01	.000E 00	.000E 00	2
89	3	9.027E 00	-2.089E 00	-7.609E 00	.000E 00	2
90	1	-1.165E 00	.000E 00	.000E 00	.000E 00	2
90	2	8.223E 00	1.606E-01	.000E 00	.000E 00	2
90	3	8.223E 00	-1.916E 00	-8.828E 00	.000E 00	2
91	1	-7.098E-01	.000E 00	.000E 00	7.938E-01	2
91	2	5.010E 00	6.427E-01	2.193E-12	7.938E-01	2
91	3	5.010E 00	-1.321E 00	-8.574E 00	7.938E-01	2
92	1	-4.757E-01	.000E 00	.000E 00	2.046E 00	3
92	2	3.357E 00	3.176E-01	1.060E 01	2.046E 00	3
92	3	4.191E 00	4.813E-01	-8.719E 00	2.046E 00	3
92	4	4.191E 00	.000E 00	.000E 00	2.046E 00	3
93	1	-4.359E-01	.000E 00	.000E 00	2.226E 00	3
93	2	3.077E 00	5.680E-02	1.199E 01	2.226E 00	3
93	3	4.438E 00	7.499E-03	-7.533E 00	2.226E 00	3
93	4	4.438E 00	.000E 00	.000E 00	2.226E 00	3
94	1	-4.635E-01	.000E 00	.000E 00	2.204E 00	3
94	2	3.271E 00	-4.633E-02	1.194E 01	2.204E 00	3
94	3	5.016E 00	-1.620E-01	-7.596E 00	2.204E 00	3
94	4	5.016E 00	.000E 00	.000E 00	2.204E 00	3

95	1	-4.838E-01	.000E 00	.000E 00	2.063E 00	3
95	2	3.415E 00	1.834E-02	1.026E 01	2.063E 00	3
95	3	5.027E 00	1.620E-02	-9.468E 00	2.063E 00	3
95	4	5.027E 00	.000E 00	.000E 00	2.063E 00	3
96	1	-7.060E-01	.000E 00	.000E 00	2.107E 00	3
96	2	4.983E 00	-3.261E-01	1.163E 01	2.107E 00	3
96	3	4.983E 00	-3.173E-01	-7.458E 00	2.107E 00	3
96	4	4.983E 00	.000E 00	.000E 00	2.107E 00	3
97	1	-2.186E-01	.000E 00	.000E 00	1.561E 00	2
97	2	1.543E 00	6.880E-01	-4.201E-03	1.561E 00	2
97	3	1.543E 00	-3.184E 00	.000E 00	1.561E 00	2
98	1	-7.898E-03	.000E 00	.000E 00	2.891E-02	2
98	2	5.575E-02	2.974E-01	5.575E-05	2.891E-02	2
98	3	5.575E-02	-4.429E 00	.000E 00	2.891E-02	2
99	1	-1.757E-05	.000E 00	.000E 00	.000E 00	2
99	2	1.240E-04	1.112E-02	8.604E-07	.000E 00	2
99	3	1.240E-04	-5.141E 00	.000E 00	.000E 00	2
100	1	5.890E-08	.000E 00	.000E 00	.000E 00	2
100	2	-4.157E-07	2.488E-05	-8.514E-09	.000E 00	2
100	3	-4.157E-07	-5.156E 00	.000E 00	.000E 00	2
101	1	5.888E-08	.000E 00	.000E 00	.000E 00	2
101	2	-4.156E-07	-1.811E-11	-1.031E-09	.000E 00	2
101	3	-4.156E-07	-5.182E 00	.000E 00	.000E 00	2
102	1	.000E 00	.000E 00	.000E 00	.000E 00	2
102	2	.000E 00	-5.182E 00	.000E 00	.000E 00	2
102	3	.000E 00	-5.182E 00	.000E 00	.000E 00	2

FLOW VELOCITY NEGLIGIBLE-CALCULATIONS TERMINATED

# Appendix D

## Listing of Program AVALNCH— Variable Width Option

```

1.  C  PROGRAM AVALNCH.
2.  *
3.  C  EQUIVALENT HORIZONTAL GRID OPTION : VARIABLE WIDTH OPTION
4.  *
5.  C  THIS PROGRAM HAS BEEN DEVELOPED TO NUMERICALLY SOLVE (USING
6.  C  FINITE DIFFERENCE TECHNIQUES) THE NAVIER - STOKES EQUATIONS
7.  C  FOR TRANSIENT FLUID FLOW PROBLEMS. IT WILL BE USED TO SIMULATE
8.  C  THE PROBLEM OF SNOW AND ICE AVALANCHES ON SLOPES OF VARYING SLOPE.
9.  C  DIMENSION U(202,7),V(202,7),UN(202,7),VN(202,7),P(202,7),FR(202),
10. 1XPUT( 8),H(202),HN(202),JT(202),NAME(20),GX(202),GY(202),FRC(202),
11. 2W(202)
12.  REAL NU
13.  INTEGER CYCLE
14.  READ (105,45) NAME
15.  WRITE (108,35)
16.  WRITE (108,45) NAME
17.  *
18.  C * * READ AND PRINT INITIAL INPUT DATA
19.  *
20.  READ(105,25) (XPUT(I),I=1,8)
21.  IBAR=XPUT(1) ; JBAR=XPUT(2) ; DELX=XPUT(3) ; DELY=XPUT(4)
22.  NU=XPUT(5) ; FRK=XPUT(6) ; TWFIN=XPUT(7) ; CWPRT=XPUT(8)
23.  WRITE (108,50) (XPUT(I),I=1,8)
24.  25 FORMAT(8F10.0)
25.  35 FORMAT(1H1)
26.  45 FORMAT(20A4)
27.  47 FORMAT(6X'I'7X'J'8X'U'13X'V'13X'P'13X'H'9X,'SUR CELL')
28.  48 FORMAT(4X,I3,5X,I3,4(4X,1PE10.3),6X,I2)
29.  49 FORMAT(2X'CYCLE='I3,2X'ITER='I3,2X'DELT='1PE9.2,2X'TIME='E9.2,2X,
30. 1'FVOL='E9.2,2X'UMAX='E9.2,2X'UEDG='E9.2,2X'LDEG='I3)
31.  50 FORMAT(1H ,1X'IBAR='F4.0,2X'JBAR='F3.0,2X'DELX='F6.2,2X'DELY='F5.2
32. 1,2X'NU='F4.2,2X'FRK='F4.2,2X'TWFIN='F5.0,2X'CWPRT='F5.0)
33.  60 FORMAT(8F10.0)
34.  61 FORMAT(8F10.3)
35.  70 FORMAT(1H0,35X,'FLOW HEIGHT')
36.  71 FORMAT(1H0,25X'ELEVATION CHANGE FOR EACH CELL')
37.  72 FORMAT(1H0,25X,'BOUNDARY FRICTION COEFFICIENTS')
38.  73 FORMAT(1H0,25X,'SLOPE-PARALLEL GRAVITY COMPONENT')
39.  74 FORMAT(1H0,25X,'SLOPE-NORMAL GRAVITY COMPONENT')
40.  75 FORMAT(1H0,30X,'END OF INPUT DATA'//)
41.  76 FORMAT(1H0,30X,'PER UNIT FLOW WIDTH')
42.  82 FORMAT(5X,'PROBLEM RUNNING TIME EXCEEDED-CALCULATIONS TERMINATED')
43.  83 FORMAT(5X,'AVALANCHE AT END OF GRID-CALCULATIONS TERMINATED')
44.  84 FORMAT(5X,'FLOW VELOCITY NEGLIGIBLE-CALCULATIONS TERMINATED')
45.  *
46.  C * * COMPUTE CONSTANT TERMS AND INITIALIZE NECESSARY VARIABLES
47.  *
48.  IMAX=IBAR+2 ; JMAX=JBAR+2
49.  IM1=IMAX-1 ; JM1=JMAX-1
50.  RDX=1.0/DELX
51.  RDY=1.0/DELY
52.  DELM=DELY/100.
53.  DELT=1.0
54.  IM2=IMAX-2
55.  JM2=JMAX-2
56.  T=FLG=UEDG1=0.0
57.  CYCLE=ITER=IND=LDEG=0
58.  G=9.8 ; OMG=1.7 ; EPSI=.001 ; ALPHA=0.1 ; GAMMA=0.1 ; DZRO=1.0

```

```

59.      BETA= OMG/(2.*DELT*(RDX**2+RDY**2))
60.      ICPRT=INT(CWPRT)
61.      IF(ICPRT.EQ.1) ICPRT=2
62.      DO 100 I=1,IMAX
63.      H(I)=HN(I)=JT(I)=GX(I)=GY(I)=FRC(I)=W(I)=0.0
64.      DO 100 J=1,JMAX
65.      100 U(I,J)=V(I,J)=UN(I,J)=VN(I,J)=P(I,J)=0.0
66.      *
67.      C * * SPECIAL INPUT DATA
68.      *
69.      READ(105,60)(H(I),I=2,IM1)
70.      READ(105,60)(HN(I),I=2,IM1)
71.      READ(105,60)(W(I),I=2,IM1)
72.      IF(FRK.GT.0.0) GO TO 120
73.      READ(105,60) (FRC(I),I=2,IM1)
74.      GO TO 130
75.      120 DO 125 I=2,IM1
76.      125 FRC(I)=FRK
77.      130 CONTINUE
78.      DO 150 I=2,IM1
79.      FR(I)=FRC(I)
80.      SP=HN(I)/DELT
81.      CP=SQRT(1.0-SP*SP)
82.      GX(I)=G*SP
83.      150 GY(I)=-G*CP
84.      WRITE(108,70)
85.      WRITE(108,61)(H(I),I=2,IM1)
86.      WRITE(108,71)
87.      WRITE(108,61)(HN(I),I=2,IM1)
88.      WRITE(108,72)
89.      WRITE(108,61) (FRC(I),I=2,IM1)
90.      WRITE(108,73)
91.      WRITE(108,61)(GX(I),I=2,IM1)
92.      WRITE(108,74)
93.      WRITE(108,61)(GY(I),I=2,IM1)
94.      WRITE(108,76)
95.      WRITE(108,61)(W(I),I=2,IM1)
96.      WRITE(108,75)
97.      DO 240 I=2,IM1
98.      JT(I)=INT(H(I)*RDY+1.E-6)+2
99.      IF(JT(I).GT.JM1) JT(I)=JM1
100.      240 HN(I)=0.0
101.      H(1)= H(2)
102.      W(1)=W(2)
103.      H(IMAX)= H(IM1)
104.      JT(1)= JT(2)
105.      JT(IMAX)= JT(IM1)
106.      *
107.      C * * CALCULATE HYDROSTATIC PRESSURE
108.      *
109.      DO 280 I=2,IM1
110.      JT1=JT(I)
111.      DO 280 J=2,JT1
112.      280 P(I,J)=-GY(I)*(H(I)-(FLOAT(J)-1.5)*DELT)
113.      ASSIGN 4100 TO KRET
114.      GO TO 2000
115.      *
116.      C * * START CYCLE
117.      *
118.      1000 CONTINUE
119.      ITER=0
120.      FLG=1.
121.      ASSIGN 3000 TO KRFT
122.      *

```

```

123. C * * COMPUTE TEMPORARY U AND V
124. *
125. DO 1100 I=2,IM1
126. JT1=JT(I)
127. DO 1100 J=2,JT1
128. FUX=((UN(I,J)+UN(I+1,J))*(UN(I,J)+UN(I+1,J))+ALPHA*ABS(UN(I,J)+UN(
129. 1I+1,J))*(UN(I,J)-UN(I+1,J))-(UN(I-1,J)+UN(I,J))*(UN(I-1,J)+UN(I,J)
130. 2)-ALPHA*ABS(UN(I-1,J)+UN(I,J))*(UN(I-1,J)-UN(I,J)))/(4.*DELX)
131. FUY=((VN(I,J)+VN(I+1,J))*(UN(I,J)+UN(I,J+1))
132. 1+ALPHA*ABS(VN(I,J)+VN(I+1,J))*(UN(I,J)-UN(I,J+1))
133. 2-(VN(I,J-1)+VN(I+1,J-1))*(UN(I,J-1)+UN(I,J))
134. 3-ALPHA*ABS(VN(I,J-1)+VN(I+1,J-1))*(UN(I,J-1)-UN(I,J)))/(4.*DELY)
135. FVX=((UN(I,J)+UN(I,J+1))*(VN(I,J)+VN(I+1,J))+ALPHA*ABS(UN(I,J)+UN(
136. 1I,J+1))*(VN(I,J)-VN(I+1,J))-(UN(I-1,J)+UN(I-1,J+1))*(VN(I-1,J)+VN(
137. 2I,J))-ALPHA*ABS(UN(I-1,J)+UN(I-1,J+1))*(VN(I-1,J)-VN(I,J)))/(4.*DE
138. 3LX)
139. FVY=((VN(I,J)+VN(I,J+1))*(VN(I,J)+VN(I,J+1))+ALPHA*ABS(VN(I,J)+VN
140. 1(I,J+1))*(VN(I,J)-VN(I,J+1))-(VN(I,J-1)+VN(I,J))*(VN(I,J-1)+VN(I,J)
141. 2))-ALPHA*ABS(VN(I,J-1)+VN(I,J))*(VN(I,J-1)-VN(I,J)))/(4.*DELY)
142. VISX= NU*((UN(I+1,J)-2.*UN(I,J)+UN(I-1,J))/DELX**2+
143. 1 (UN(I,J+1)-2.*UN(I,J)+UN(I,J-1))/DELY**2)
144. VISY= NU*((VN(I+1,J)-2.*VN(I,J)+VN(I-1,J))/DELX**2+
145. 1 (VN(I,J+1)-2.*VN(I,J)+VN(I,J-1))/DELY**2)
146. U(I,J)= UN(I,J)+DELT*((P(I,J)-P(I+1,J))*RDX + GX(I)-FUX-FUY+VISX)
147. 1100 V(I,J)= VN(I,J)+DELT*((P(I,J)-P(I,J+1))*RDY + GY(I)-FVX-FVY+VISY)
148. *
149. C * * SET BOUNDARY CONDITIONS
150. *
151. 2000 CONTINUE
152. HN(1)= HN(2)
153. HN(IMAX)=HN(IM1)
154. JT(1)=JT(2)
155. JT(IMAX)=JT(IM1)
156. C LEFT WALL RIGID AND SLIP FREE.
157. C RIGHT WALL CONTINUOUS OUTFLOW.
158. DO 2200 J=1,JMAX
159. U(1,J)=0.0
160. V(1,J)=V(2,J)
161. IF(ITER.GT.0) GO TO 2200
162. U(IM1,J)=U(IM2,J)
163. V(IMAX,J)=V(IM1,J)
164. 2200 CONTINUE
165. C TOP WALL CONTINUOUS OUTFLOW.
166. C BOTTOM WALL RIGID - WITH FRICTION
167. DO 2500 I=1,IMAX
168. IF(ITER.GT.0) GO TO 2400
169. V(I,JM1)=V(I,JM2)
170. U(I,JMAX)=U(I,JM1)
171. 2400 V(I,1)=0.0
172. 2500 U(I,1)=U(I,2)*(1.0-2.0*FRC(I))
173. *
174. C * * FREE SURFACE BOUNDARY CONDITIONS
175. *
176. DO 2650 I=2,IM1
177. JT1=JT(I)
178. IF(JT(I+1).LT.JT(I)) U(I,JT1)=U(I,JT1-1)
179. V(I,JT1)= V(I,JT1-1)-DELY*ROX*(U(I,JT1)-U(I-1,JT1))
180. 2650 U(I,JT1+1)= U(I,JT1)
181. GO TO KRET,(3000,4100,4280)
182. 3000 CONTINUE
183. *
184. C * * HAS CONVERGENCE BEEN REACHED
185. *
186. IF(FLG.EQ.0.) GO TO 4000

```

```

187.      ITER=ITER+1
188.      IF(ITER.LT.500) GO TO 3050
189.      IF(CYCLE.LT.10) GO TO 4000
190.      T=1.E+10
191.      GO TO 4000
192. 3050 FLG=0.0
193. *
194. C * * COMPUTE UPDATED CELL PRESSURE AND VELOCITIES
195. *
196.      JB1=2
197.      DO 3500 I=2,IM1
198.      JT1=JT(I)
199.      DO 3500 J=2,JT1
200.      IF(JT1.EQ.JB1) GO TO 3060
201.      IF(J.NE.JB1 .AND. J.NE.JT1) GO TO 3200
202.      IF(J.EQ.JT1) GO TO 3100
203.      GO TO 3200
204. 3060 CONTINUE
205.      F=V(I,J)+DELY*RDY*(U(I,J)-U(I-1,J))
206.      DFDP=DELT*RDY*(1.0+2.0*DELY**2*RDY**2)
207.      DELP1=-F/DFDP
208. 3100 ETA=DELY/(HN(I)-(FLOAT(JT1)-2.5)*DELY)
209.      DELP=(1.0-ETA)*P(I,JT1-1)-P(I,JT1)
210.      IF(JB1.EQ.JT1) DELP=0.5*(DELP+DELP1)
211.      GO TO 3300
212. 3200 D=RDY*(U(I,J)-U(I-1,J))+RDY*(V(I,J)-V(I,J-1))
213.      IF(ABS(D/DZRO).GE.EPSI) FLG=1.0
214.      DELP= -BETA*D
215. 3300 P(I,J)=P(I,J)+DELP
216.      U(I,J)=U(I,J)+DELT*RDY*DELP
217.      U(I-1,J)=U(I-1,J)-DELT*RDY*DELP
218.      V(I,J)=V(I,J)+DELT*RDY*DELP
219. 3500 V(I,J-1)=V(I,J-1)-DELT*RDY*DELP
220.      GO TO 2000
221. 4000 CONTINUE
222. *
223. C * * COMPUTE NEW POSITION FOR TOP SURFACE
224. *
225.      DO 4100 I=2,IM1
226.      JT1=JT(I)
227.      HV= RDY*(HN(I)-FLOAT(JT1-2)*DELY)
228.      UAV= 0.5*(U(I-1,JT1) + U(I,JT1))
229.      H(I)= HN(I)*FVOL1/FVOL+DELT*(HV*V(I,JT1)+(1.0-HV)*V(I,JT1
230.      1-1)-0.5*RDY*(UAV*HN(I+1)+GAMMA*ABS(UAV)*(HN(I)-HN(I+1))
231.      2 -UAV*HN(I-1)-GAMMA*ABS(UAV)*(HN(I-1)-HN(I))))
232. 4100 CONTINUE
233. *
234. C * * FIND LEADING AND TRAILING EDGES OF AVALANCHE AND LD. EDGE VELOCITY
235. *
236.      LDEG1=LDEG
237.      I=IM2
238. 4400 IF(H(I).GT.DELM) GO TO 4500
239.      I=I-1
240.      GO TO 4400
241. 4500 LDEG=I
242.      I=2
243. 4600 IF(H(I).GT.DELM) GO TO 4700
244.      I=I+1
245.      GO TO 4600
246. 4700 KTEG=I
247.      IF(LDEG.EQ.LDEG1) GO TO 4800
248.      IF(CYCLE.GT.0) UEDG=DELT/TC
249.      IF(CYCLE.EQ.0) UEDG=5.0
250.      TC=DELT

```

```

251.      INFLO=1
252.      IF(UEDG.GT.UEDG1) UEDG1=UEDG
253.      DO 4750 I=KTEG,LDEG
254.      4750 H(I)=H(I)*W(I-1)/W(I)
255.      GO TO 4910
256.      4800 TC=TC+DELT
257.      INFLO=INFLO+1
258.      4910 CONTINUE
259.      *
260.      C * * CALCULATE CELL IN WHICH SURFACE IS LOCATED AND UPDATE ARRAY
261.      *
262.      DO 4250 I=2,IM1
263.      IF(H(I).LT.DELM) H(I)=0.0
264.      JT(I)=INT(H(I)*RDY+1.0E-6)+2
265.      IF(JT(I).GT.JM1) JT(I)=JM1
266.      4250 CONTINUE
267.      ASSIGN 4280 TO KRET
268.      GO TO 2000
269.      4280 CONTINUE
270.      *
271.      C * * CALCULATE TOTAL FLUID VOLUME
272.      *
273.      FVOL=0.0
274.      DO 4300 I=KTEG,LDEG
275.      4300 FVOL=FVOL+H(I)*DELX*W(I)
276.      IF(CYCLE.EQ.0) FVOL1=FVOL
277.      *
278.      C * * ADVANCE U,V,H ARRAYS.
279.      *
280.      UMAX=VMAX=0.0
281.      DO 4900 I=1,IMAX
282.      DO 4900 J=1,JM1
283.      IF(ABS(U(I,J)).GT.1.0E+04) U(I,J)=0.0
284.      UN(I,J)=U(I,J)
285.      IF(ABS(V(I,J)).GT.1.0E+04) V(I,J)=0.0
286.      VN(I,J)=V(I,J)
287.      IF(ABS(P(I,J)).LT.1.0E-16) P(I,J)=0.0
288.      4900 HN(I)=H(I)
289.      DO 4950 I=KTEG,LDEG
290.      DO 4950 J=2,JM1
291.      UT=ABS(UN(I,J))
292.      VT=ABS(VN(I,J))
293.      IF(UT.GT.UMAX) UMAX=UT
294.      4950 IF(VT.GT.VMAX) VMAX=VT
295.      *
296.      C * * LIST VELOCITY, PRESSURE, AND SURFACE POSITION
297.      *
298.      5000 WRITE(108,49) CYCLE,ITER,DELT,T,FVOL,UMAX,UEDG,LDEG
299.      IF(CYCLE.NE.ICPRT) GO TO 6000
300.      IF(CYCLE.EQ.ICPRT) GO TO 5030
301.      5030 ICPRT=ICPRT + INT(CWPRT)
302.      5060 CONTINUE
303.      WRITE(108,47)
304.      DO 5250 I=1,IMAX
305.      JT1= JT(I)
306.      JT2=JT1+1
307.      DO 5250 J=1,JT2
308.      WRITE(108,48) I,J,U(I,J),V(I,J),P(I,J),H(I),JT1
309.      5250 CONTINUE
310.      IF(IND.EQ.2) GO TO 6520
311.      IF(IND.EQ.3) GO TO 6530
312.      IF(IND.EQ.4) GO TO 6540
313.      *
314.      C * * RECOMPUTE CONTROL PARAMETERS.

```

```

315.      *
316.      6000 IF(CYCLE.EQ.0) GO TO 6300
317.          DTX=DELX/UMAX
318.          DTY=DELY/VMAX
319.          DELT=AMIN1(DTX,DTY)/3.0
320.          IF(ITER.LT.10) DELT=1.5*DELT
321.          IF(NU-1.E-6.LT.0.0) GO TO 6300
322.          DET=(DELX*DELY)**2/(2.*NU*(DELX**2+DELY**2))
323.          IF(DELT.LT.DET) GO TO 6300
324.          DELT=0.9*DET
325.      6300 T=T+DELT
326.          IF(CYCLE.EQ.0) GO TO 6400
327.          DAX=UMAX*DELT/DELX
328.          DAY=VMAX*DELT/DELY
329.          ALPHA=1.35*AMAX1(DAX,DAY)
330.          IF(ALPHA.GT.1.0) ALPHA=0.95
331.          GAMMA=ALPHA
332.          BETA=OMG/(2.*DELT*(RDX**2+RDY**2))
333.      *
334.      C * * TEST FOR PROGRAM TERMINATION.
335.      *
336.      6400 IF(T.GT.TWFIN) IND=2
337.          IF(H(IM2).GT.DELM) IND=3
338.          IF(UEDG.LT.0.05*UEDG1) IND=4
339.          IF(INFLO.EQ.50) IND=4
340.          IF(IND.GT.1) GO TO 6500
341.          IF(CYCLE.LT.3) GO TO 6440
342.          AA=1.0+20.0*EXP(-1.25*UEDG)
343.          DO 6430 I=2,IM1
344.      6430 FRC(I)=AA*FR(I)
345.      6440 CYCLE=CYCLE+1
346.          GO TO 1000
347.      6500 T=T-DELT
348.          GO TO 5060
349.      6520 WRITE(108,82)
350.          GO TO 6600
351.      6530 WRITE(108,83)
352.          GO TO 6600
353.      6540 WRITE(108,84)
354.      6600 STOP
355.          END

```

01F0:	LANG8232,543	12/20/77	15:17
01F0:	LANG8232,543	12/20/77	15:17
01F0:	LANG8232,543	12/20/77	15:17
01F0:	LANG8232,543	12/20/77	15:17
01F0:	LANG8232,543	12/20/77	15:17
01F0:	LANG8232,543	12/20/77	15:17
01F0:	LANG8232,543	12/20/77	15:17
01F0:	LANG8232,543	12/20/77	15:17
01F0:	LANG8232,543	12/20/77	15:17
01F0:	LANG8232,543	12/20/77	15:17
01F0:	LANG8232,543	12/20/77	15:17
01F0:	LANG8232,543	12/20/77	15:17
01F0:	LANG8232,543	12/20/77	15:17
01F0:	LANG8232,543	12/20/77	15:17
01F0:	LANG8232,543	12/20/77	15:17
01F0:	LANG8232,543	12/20/77	15:17
01F0:	LANG8232,543	12/20/77	15:17
01F0:	LANG8232,543	12/20/77	15:17
01F0:	LANG8232,543	12/20/77	15:17
01F0:	LANG8232,543	12/20/77	15:17
01F0:	LANG8232,543	12/20/77	15:17

01F0:	LANG8232,543	12/20/77	15:17
01F0:	LANG8232,543	12/20/77	15:17
01F0:	LANG8232,543	12/20/77	15:17
01F0:	LANG8232,543	12/20/77	15:17
01F0:	LANG8232,543	12/20/77	15:17
01F0:	LANG8232,543	12/20/77	15:17
01F0:	LANG8232,543	12/20/77	15:17
01F0:	LANG8232,543	12/20/77	15:17
01F0:	LANG8232,543	12/20/77	15:17
01F0:	LANG8232,543	12/20/77	15:17
01F0:	LANG8232,543	12/20/77	15:17
01F0:	LANG8232,543	12/20/77	15:17
01F0:	LANG8232,543	12/20/77	15:17
01F0:	LANG8232,543	12/20/77	15:17
01F0:	LANG8232,543	12/20/77	15:17
01F0:	LANG8232,543	12/20/77	15:17
01F0:	LANG8232,543	12/20/77	15:17
01F0:	LANG8232,543	12/20/77	15:17
01F0:	LANG8232,543	12/20/77	15:17
01F0:	LANG8232,543	12/20/77	15:17
01F0:	LANG8232,543	12/20/77	15:17



Lang, T. E., K. L. Dawson, and M. Martinelli, Jr. 1978. Numerical simulation of snow avalanche flow. USDA For. Serv., Res. Pap. RM-205, 51 p. Rocky Mt. For. and Range Exp. Stn., For. Serv., U.S. Dep. Agric., Fort Collins, Colo. 80526.

A numerical, finite difference computer program based on the Navier-Stokes equations is modified to give avalanche runout distance, velocity of the leading edge of the avalanche, and depth of debris in the runout zone. The program requires a longitudinal profile of the avalanche path, thickness of the snow in the starting zone, and two friction coefficients. Kineomatic viscosity (or coefficient of internal friction) is expressed as an average for the entire avalanche path. Slope inclinations and coefficient of surface friction can be varied for every 10- to 20-m increment of the avalanche path. The program can be modified to allow for variable width of flow and for snow entrainment during flow. In test cases, the program predicted results consistent with observations for a number of avalanche events.

**Keywords:** Avalanche, avalanche runout distance, simulation modeling, avalanche dynamics.

Lang, T. E., K. L. Dawson, and M. Martinelli, Jr. 1978. Numerical simulation of snow avalanche flow. USDA For. Serv., Res. Pap. RM-205, 51 p. Rocky Mt. For. and Range Exp. Stn., For. Serv., U.S. Dep. Agric., Fort Collins, Colo. 80526.

A numerical, finite difference computer program based on the Navier-Stokes equations is modified to give avalanche runout distance, velocity of the leading edge of the avalanche, and depth of debris in the runout zone. The program requires a longitudinal profile of the avalanche path, thickness of the snow in the starting zone, and two friction coefficients. Kineomatic viscosity (or coefficient of internal friction) is expressed as an average for the entire avalanche path. Slope inclinations and coefficient of surface friction can be varied for every 10- to 20-m increment of the avalanche path. The program can be modified to allow for variable width of flow and for snow entrainment during flow. In test cases, the program predicted results consistent with observations for a number of avalanche events.

**Keywords:** Avalanche, avalanche runout distance, simulation modeling, avalanche dynamics.

Lang, T. E., K. L. Dawson, and M. Martinelli, Jr. 1978. Numerical simulation of snow avalanche flow. USDA For. Serv., Res. Pap. RM-205, 51 p. Rocky Mt. For. and Range Exp. Stn., For. Serv., U.S. Dep. Agric., Fort Collins, Colo. 80526.

A numerical, finite difference computer program based on the Navier-Stokes equations is modified to give avalanche runout distance, velocity of the leading edge of the avalanche, and depth of debris in the runout zone. The program requires a longitudinal profile of the avalanche path, thickness of the snow in the starting zone, and two friction coefficients. Kineomatic viscosity (or coefficient of internal friction) is expressed as an average for the entire avalanche path. Slope inclinations and coefficient of surface friction can be varied for every 10- to 20-m increment of the avalanche path. The program can be modified to allow for variable width of flow and for snow entrainment during flow. In test cases, the program predicted results consistent with observations for a number of avalanche events.

**Keywords:** Avalanche, avalanche runout distance, simulation modeling, avalanche dynamics.

Lang, T. E., K. L. Dawson, and M. Martinelli, Jr. 1978. Numerical simulation of snow avalanche flow. USDA For. Serv., Res. Pap. RM-205, 51 p. Rocky Mt. For. and Range Exp. Stn., For. Serv., U.S. Dep. Agric., Fort Collins, Colo. 80526.

A numerical, finite difference computer program based on the Navier-Stokes equations is modified to give avalanche runout distance, velocity of the leading edge of the avalanche, and depth of debris in the runout zone. The program requires a longitudinal profile of the avalanche path, thickness of the snow in the starting zone, and two friction coefficients. Kineomatic viscosity (or coefficient of internal friction) is expressed as an average for the entire avalanche path. Slope inclinations and coefficient of surface friction can be varied for every 10- to 20-m increment of the avalanche path. The program can be modified to allow for variable width of flow and for snow entrainment during flow. In test cases, the program predicted results consistent with observations for a number of avalanche events.

**Keywords:** Avalanche, avalanche runout distance, simulation modeling, avalanche dynamics.

U.S. DEPT. OF AGRICULTURE  
NATL. AGRIC. LIBRARY  
NATL. BUREAU OF PLANT INDUSTRY

JUN 12 '79

